Impurity Induced States

Studied in the RVB Picture
Using an Extended Gutzwiller Approximation

Rasmus B. Christensen

Master Thesis
Advisor Brian M. Andersen
Theory for Nanosystems
Niels Bohr Institute
Copenhagen University
May 2011

Resumé

Stærke korrelationer er centrale i forståelsen af kobberoxid høj-temperatur superledere. De stærke korrelationer er ansvarlige for den Mott-isolerende, antiferromagnetiske tilstand i de ikke-doterede materialer og formentlig også for den d-bølge superledende tilstand, der opstår ved dotering. Når kobberoxid materialer doteres, vil de uundgåeligt blive uordnede, som følge af de urenheder der indføres i materialet. I denne afhandling undersøges urenhedernes indvirkning på den superledende tilstand. Dels undersøges hvorfor den lokale tilstandstæthed bevarer dens V-form på trods af indførelsen af uorden, og dels undersøges det, hvordan urenhederne kan inducere magnetisk orden. Denne afhandling gør brug af t-J modellen ved hjælp af en udvidet Gutzwiller approksimation. Det viser sig, at inkluderingen af et 'lokalt kemisk potential' μ_i er vigtigt både for bevarelsen af V-formen af den lokale tilstandstæthed og for den inducerede magnetiske orden.

Motivation

Strong correlations are in the heart of the understanding of high-temperature superconductivity in the cuprates [12]. The strong correlations are both responsible for the Mott insulating antiferromagnetic state in the undoped mother compounds and presumably also for the d-wave superconducting state which arise upon doping. One of the experimental facts about the superconducting state is its insensitivity to disorder [28][29]. The insensitivity to disorder is unexpected because, unlike s-wave superconductors where Andersons theorem insures insensitivity to weak potential scattering, d-wave superconductivity has zero superconducting gap in the nodal direction; and furthermore, even weak impurities can be poorly screened by the electrons around them because the cuprates are quasi-two-dimensional metals.

A characteristic feature of d-wave superconductivity is the V shaped local density

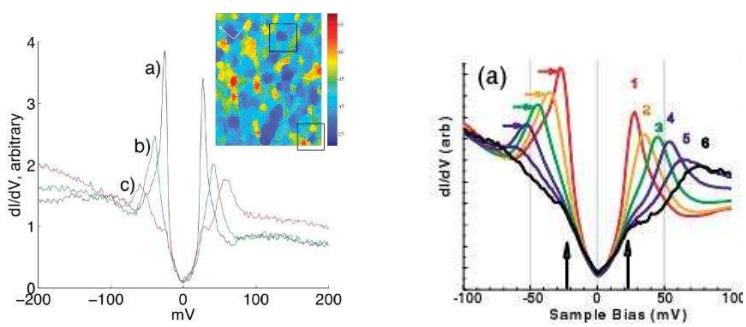

(a) (b)

Figure 1: (a):STM spectra on nearly optimally doped $Bi_2Sr_2CaCu_2O_{8+\delta}$. Spectra in a a) small-, b) average-, and c) large-gap region Adapted from ref. [28]. (b): STM spectra on underdoped $Bi_2Sr_2CaCu_2O_{8+\delta}$, Each curve is obtained by averaging the spectra in the region that exhibit a given local gap value. Adapted from ref. [29].

of states (LDOS). One of the experimental manifestations of the insensitivity to disorder is the robustness of the low energy LDOS. The low energy LDOS probed by STM exhibits a clear V shape, see figure 1. The V shaped LDOS has been treated in the framework of strong correlations by A. Garg et al. [27], Fukushima et al. [26], and B. M. Andersen and P. J. Hirschfeld [30]. In this thesis the central

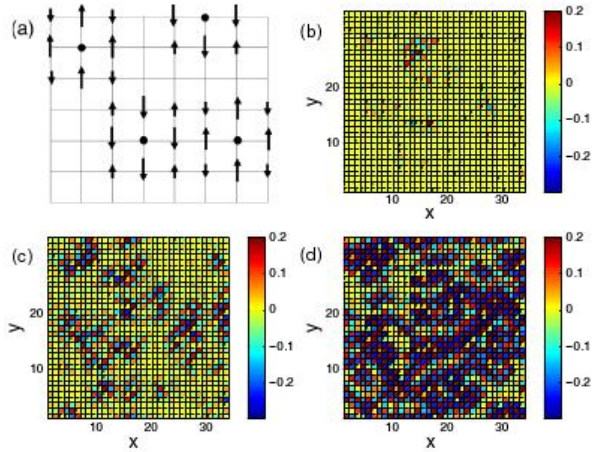

FIG. 2 (color online). (a) Schematic: Stabilization of a single Néel phase by impurities. (b)–(d) Disorder-induced magnetization for a single fixed impurity configuration with $x = 7.5\%$ and (b) $U = 2.8t$, (c) $U = 3.2t$, and (d) $U = 3.6t$. In (a)–(d), the black dots indicate the impurity or dopant positions.

Figure 2: Impurity induced magnetization in a simple mean field treatment of the Hubbard model. The doping dependents of the induced magnetization is simulated by changing U. Adopted from ref. [31]

result of Garg et al. [27] is reproduced; however, the model used by Garg et al. [27] does not take into full account all the effects of the strong correlations[26], and therefore this thesis re-examines the V shaped low energy LDOS in an improved model.

The antiferromagnetic state in the undoped compounds has led to speculations on an intimate relation between superconductivity and magnetism. Neutron scattering experiments have shown evidence of coexistence of superconducting and magnetic order in some of the cuprates but not all; this difference between the different cuprates can be ascribed to the different ways the dopants enter the material. For instance, in $LaSrCuO_4$ (LSCO) the strontium dopants randomly substitute lanthanum giving rise to a weak out-of-plane impurity potential.

Impurity induced magnetism has been studied by the Hubbard model treated in an unrestricted Hartree-Fock approximation [31]. However, a mean field treatment of the Hubbard model does not capture the band narrowing due to the strong correlations near half filling. Therefore, in a simple mean field treatment of the Hubbard model the Hubbard U has to be adjusted by hand when different doping levels are considered. The onset of magnetic order depends heavily on the choice of U, see figure 2.

To move beyond the phenomenological treatment offered by a mean field solution of the Hubbard model and to eliminate the freedom in the choice of U, this

thesis studies impurity induced magnetization in the RVB picture by use of the t-J model using an extended Gutzwiller approximation.

The structure of the thesis is as follows:
In chapter 1 high temperature superconductivity is briefly introduced, then in section 1.1 the structure of one of the simplest cuprates LSCO is discussed.
In chapter 2 the three band model is put forward as a general model to describe the cuprates, and in section 2.2 the connection to the Hubbard model is made. In section 2.3 a simple mean field treatment of the Hubbard model is briefly discussed and the shortcomings of this simple mean field treatment is used as motivation to derive the t-J model.
In chapter 3 the RVB picture is introduced.
In chapter 4 the original Gutzwiller Approximation is introduced to handle the no double occupation constraint in the t-J model, and in section 4.1.2 the weaknesses of the Gutzwiller approximation are discussed.
In order to faithfully treat impurity-induced magnetization the extended Gutzwilller approximation is introduced in chapter 5, and in section 5.6 the extended Gutzwiller approximation is simplified and made site-dependent. In chapter 6 the renormalized mean field Hamiltonian is derived and in section 6.4 a short description of the program, used for calculations, is given.
In chapter 7 the results are presented. In section 7.1 the V shaped LDOS for the overdoped compound is considered. The main result of A. Garg et al. [27], is reproduced and improved. Section 7.2 looks at impurity induced magnetic order near optimal doping. Finally, section 7.3 considers a single impurity for different scattering strengths, at a doping level right before the onset of long range bulk magnetic order.

Contents

Chapter 1

Introduction

This thesis presents results explaining the effect of impurities in High T_c superconducting copper-oxide materials. In 1986 Bednorz and Müller [2] discovered high-temperature superconductivity(HTSC) in Ba-doped La_2CuO_4. After that HTSC has been reported in numerous materials all sharing the characteristics of being layered materials made up of one or more copper-oxygen planes. Many of the HTSC materials have an insulating antiferromagnetic (AF) parent compound that becomes superconducting when doped with holes or electrons. This transition from an antiferromagnetic insulator to a superconductor is fundamentally different from the more conventional superconductivity as for example found in alkaline metals. This difference has stimulated an enormous experimental and theoretical interest in what is the mechanism that drives this transition from an insulating to a supeconducting state of matter. The temperature-doping phase diagram, see figure 1.2, and the d-wave nature of the superconducting pairs are now experimentally well-established. However, there is still no concensus on the theoretical interpretation of these experiments. The proximity to the AF state inspired P. W. Anderson to suggest a resonating-valence-bond (RVB) state as the ground state of the HTSC.
Upon doping, impurities are inevitably introduced in the HTSC compound. The strength and nature of the impurities depend on the dopant and the mother material. Any theory concerning HTSC must be able to acount for the experimentally observed consequences of impurities or in some cases the absence. The most direct method for probing the physics of impurities is application of scanning tunneling microscopy(STM). The advantage of the STM is that it is a local probe, making it possible to measure directly at the impurity site and the neighbouring sites. Thus directly probing how impurities affect the local density of states, makes it possible to perform comparison between experiment and theory. Impurities are also believed to influence the occurrence of magnetic order in the pseudogap- and superconductingphase. This can be probed e.g. by neutron scattering experiments.

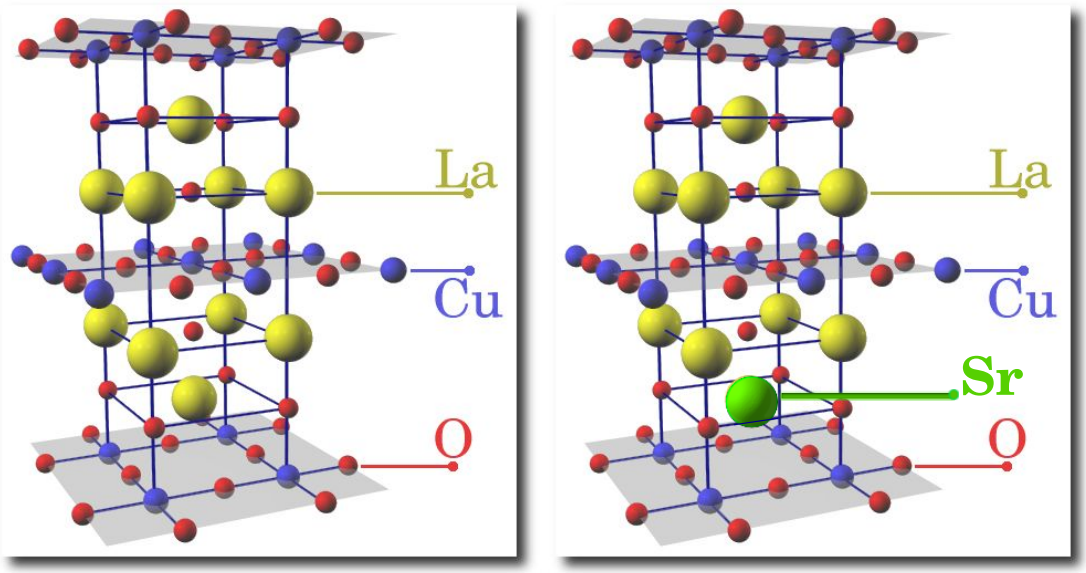

Figure 1.1: Pictures of LSCO [11]. To the left undoped, and doped with strontium to the right. LSCO consists of insulating LaO layers and CuO_2 planes. Upon doping, trivalent La^{3+} is replaced by divalent Sr^{2+}. The added holes go into the oxygen ion, changing these from O^{2-} to the O^{-} configuration.

1.1 Structure

$LaBaCuO_4$ and its close companion $LaSrCuO_4$ (LSCO) were the first materials in which HTSC was discovered. $LaCuO_4$ is a layered material consisting of two types of layers; an insulating LaO plane and a CuO_2 plane, see figure 1.1. All cuprate superconductors have the Cu-O planes in common. In a clean mother compound of La_2CuO_4 the oxygen is in the O^{2-} valence state with a complete p shell; Lanthanum releases 3 electrons to become La^{3+}; and to conserve charge neutrality the copper atoms must deliver two electrons becoming Cu^{2+}, the electrons which are given up is the 4s and one of the 3d electrons, creating a hole in the 3d shell resulting in a unpaired spin 1/2 at each copper site. Each copper ion is surrounded by 6 oxygen ions 4 in the CuO_2 plane and two outside the plane. The distance to the in-plane oxygens is shorter than to the two apical oxygen ions outside the plane, which makes the in-plane Cu-O bonds the dominant ones and breaks rotational symmetry for the copper ions. A consequence of the break of rotational invariance for the Cu^{2+} ions is that the degeneracy of the 3d orbitals is lifted and the $d_{x^2-y^2}$ orbital becomes the one with the highest energy, hence upon hole doping, the hole goes in to this band. The undoped copper-oxides are strongly insulating despite the open shell of the Cu^{2+} ions. The reason that the materials are insulating and not metalic is the strong Coulomb electron-electron

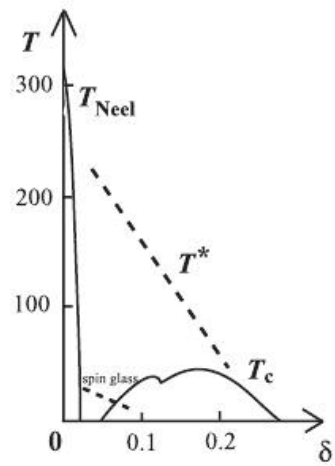

Figure 1.2: Schematic phase diagram for the hole-doped high-T_c cuprates. At zero doping there exists a long range antiferromagnetic order for temperatures less than T_{Neel}. As materials are doped, the AF state is destroyed; for $5\% < \delta < 30\%$ a superconducting state emerges for temperatures less than T_C. The superconducting order parameter has a maximum around 15% of doping. The region where $\delta < 15\%$ is called underdoped, and the region where $\delta > 15\%$ is called overdoped. Between the AF and SC phase and above the SC phase the pseudo-gap appears for temperatures less than T^*. Figure adapted from [5]

correlation, which confines the electrons to the ions in the undoped materials[25].

1.1.1 Doping

The undoped cuprate materials are Mott insulators; however, upon hole doping, mobile charge carriers are introduced into the copper-oxygen planes. La_2CuO_4 can be doped in several ways. One way to hole-dope La_2CuO_4 is to replace a percentage of the trivalent lanthanum ions with divalent strontium ions, see figure 1.1. The strontium ions deliver one electron less to the oxygens in the copper-oxygen planes and thereby introduce holes. The strontium ions sit outside the planes and thus only mildly affect the copper-oxide planes by a small impurity potential. Zinc can also be used as a dopant when zinc ions replace copper ions. Zinc ions are strong impurities because they sit in-plane. For this same reason, only a few percent can be included before superconducting is destroyed.

1.1.2 The Phase Diagram

At zero doping and for temperatures less than $T_{Neel} = 325K$, the system experiences long range antiferromagnetic order. As the material is doped, the AF state

is destroyed. For low temperatures some magnetic order might still be present as a spin glass and can coexist with superconductivity up to around 13% doping (δ). For temperatures less than T_C and for $5\% < \delta < 30\%$ a superconducting state emerges. The superconducting order parameter has a maximum around 15% doping. The region where $\delta < 15\%$ is called underdoped, and the region where $\delta > 15\%$ is called overdoped. Between the AF and SC phases and above the SC phase the pseudo-gap appears for temperatures less than T^*. The pseudo-gap is e.g. apparent in angle resolved photoemission spectroscopy as a almost gaped behaviour of the density of states, and it is one of the great mysteries of HTSC.

Chapter 2

The Model

2.1 The Three Band Model

The problem is not to find a model which in principle describes the HTSCs, but rather to find correct and a sufficiently simple, solvable model, that makes it possible to compute observable quantities. In order to find such a model, aspects of the system which are important needs to be identified; this of course implies a choice that can be disputed. However, a general consensus holds that the copper oxide planes are responsible for the remarkable aspects of the HTSCs, and that the insulating layers between the copper oxide planes primarily work as charge reservoirs. A general model to start with must include the $d_{x^2-y^2}$ electrons of the copper ions and the p electrons of the oxygens, and the hybridization between them.

$$\begin{aligned} H_{dp} = & - t_{dp} \sum_{\langle i,j \rangle \sigma} \left(d^\dagger_{i\sigma} p_{j\sigma} + h.c. \right) - t_p \sum_{\langle j,j' \rangle \sigma} \left(p^\dagger_{j\sigma} p_{j'\sigma} + h.c. \right) \\ & + t'_p \sum_{\langle j,j'' \rangle \sigma} \left(p^\dagger_{j\sigma} p_{j''\sigma} + h.c. \right) + \Delta \sum_{j\sigma} n_{p,j\sigma} \\ & + U_d \sum_i n_{d,i\uparrow} n_{d,i\downarrow} + U_p \sum_i n_{p,i\uparrow} n_{p,i\downarrow} + V \sum_{\langle i,j \rangle} n_{d,i} n_{p,j}. \end{aligned} \tag{2.1}$$

The energy of a single occupied Cu ion is set to zero. $d^\dagger_{i\sigma}(d_{i\sigma})$ creates (annihilates) a $d_{x^2-y^2}$ electron at a Cu site i with spin σ, and $p^\dagger_{j\sigma}(p_{j\sigma})$ creates (annihilates) a p electron at an O site j with spin σ, the p electron is created (annihilated) in the p orbital directed towards the Cu ion. $n_{d,i\sigma} = d^\dagger_{i\sigma} d_{i\sigma} (n_{p,j\sigma} = p^\dagger_{j\sigma} p_{j\sigma})$ is the number operator. $\langle i, j \rangle$ stands for the summation over nearest neighbouing Cu-O bonds, $\langle j, j' \rangle$ stands for the summation over nearest neighbouing O-O bonds and $\langle j, j'' \rangle$ stands for the summation over two oxygen sites across a Cu site.
t_{dp}, t_p, and t'_p are the hopping integrals between the neighbouring copper and oxygen sites, two nearest neighbouring oxygen sites and two next nearest neighbouring oxygen sites respectively, see figure 2.1 on the left.

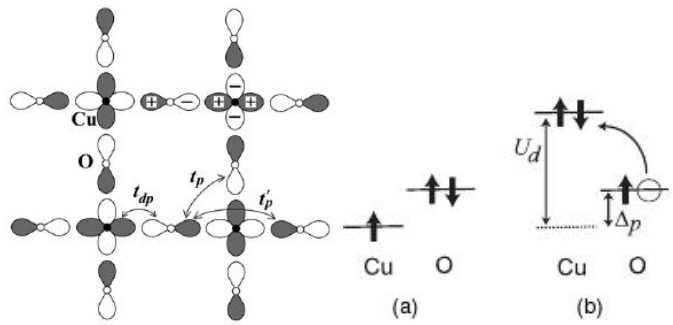

Figure 2.1: To the left: Hopping integrals between the Cu $d_{x^2-y^2}$ and the O 2p orbital. To the right: Schematic picture of the energy levels. Figure adapted from [5]

U_d is the Coulomb energy cost the system pays for having two electrons occupying the same copper site; Δ_p is the energy cost the system pays for having a electron occupying a oxygen site; U_p is the extra energy cost the system pays for having two electrons occupying the same copper site; and V is the energy cost of having two electrons being close by occupying neighbouring copper and oxygen sites.
A first step in simplifying the model in (2.1) is to recognize that the overlap between the O and Cu orbitals is much greater than the overlap between two oxygen orbitals, and that the p orbitals have a much larger radius than the d orbitals. Therefore, t_{dp} is more important than both t_p and t'_p, and U_d is more important than both U_p and V. Thus only keeping the electron-electron repulsion on the copper sites and the Cu-O hopping term gives a two band model:

$$H = -t_{dp} \sum_{\langle i,j \rangle \sigma} \left(d^\dagger_{i\sigma} p_{j\sigma} + h.c. \right) + U_d \sum_i n_{d,i\uparrow} n_{d,i\downarrow} + \Delta \sum_{j\sigma} n_{p,j\sigma}. \tag{2.2}$$

2.2 Connection to the One Band Hubbard Model

One of the most commonly used microscopic Hamiltonians used to describe the HTSCs is the one band Hubbard model.

$$H_{Hub} = \; - \sum_{\langle i,j \rangle \sigma} t_{ij} \left(c^\dagger_{i\sigma} c_{j\sigma} + h.c. \right) + U \sum_i n_{i\uparrow} n_{i\downarrow} \tag{2.3}$$

The Hubbard model builds on the assumption of the existence of a strong one-site Coulomb interaction betwen electrons occupying the same Cu ion, put forward by P. W. Anderson in [12]. However, it is not trivial, That the three band model or even the two band model can be mapped on to the Hubbard model. In the undoped material the oxygen p-shell is filled and the Cu d-shell is haff filled, but because of the strong on-site Coulomb repulsion, no real hopping can occur.

However, virtual hopping between the Cu ions leads to an AF interaction between neighbouring Cu sites. Then both equation (2.1) and (2.3) are reduced to the Heisenberg model:

$$H = J \sum_{\langle ij \rangle} \mathbf{S}_i \cdot \mathbf{S}_j. \tag{2.4}$$

The Heisenberg model in equation (2.4) describes the interaction of the square lattice of AF coupled localized spins on the Cu ions. However, upon doping, mobile charge carriers are introduced into the system in the form of holes. If the lower energy level of the Cu ions had been above the upper energy-level of the O-ions, then the oxygen could just have been ommitted from the model and the connection to the Hubbard Model would have been clear. However, spectroscopic methods have shown [13] that the holes do not form Cu^{3+} ions but mainly occupy the oxygen ions.

2.2.1 The Zhang Rice Singlet

To understand why the one band Hubbard Model is able to describe the cuprates the Zhang Rice singlet is briefly discussed [13]. When a hole is added, the hole will have the energy $E = -\Delta$, according to equation (2.2) to zero-order in t_p. But, because of hybridization the hole can gain energy by spreading out. The four oxygen bands in figure 2.1 surrounding a Cu ion can form a symmetric combination with respect to the Cu ions,

$$P^s_{i\sigma} = \frac{1}{2}(p_{(i+\frac{1}{2}\hat{x})\sigma} + p_{(i+\frac{1}{2}\hat{y})\sigma} + p_{(i-\frac{1}{2}\hat{x})\sigma} + p_{(i-\frac{1}{2}\hat{y})\sigma}) \tag{2.5}$$

or an antisymmetric

$$P^A_{i\sigma} = \frac{1}{2}(-p_{(i+\frac{1}{2}\hat{x})\sigma} - p_{(i+\frac{1}{2}\hat{y})\sigma} + p_{(i-\frac{1}{2}\hat{x})\sigma} + p_{(i-\frac{1}{2}\hat{y})\sigma}). \tag{2.6}$$

($p_{(i+\frac{1}{2}\hat{x})\sigma}$ creates a hole at the nearest neighbour oxygen site in the positive x direction with respect to the Cu site i. The phases of the p orbitals are as in figure 2.1.)
The $P^s_{i\sigma}$s and the $P^A_{i\sigma}$s can be combined with the $d_{x^2-y^2}$ Cu electron to make a singlet $\frac{1}{\sqrt{2}}(P_{i\sigma}d_{i\bar{\sigma}} - P_{i\bar{\sigma}}d_{i\sigma})$, or triplet $\frac{1}{\sqrt{2}}(P_{i\sigma}d_{i\sigma} + P_{i\bar{\sigma}}d_{i\bar{\sigma}})$
To second order the symmetric singlet and triplet states have the energies $E = -8\frac{t^2}{\Delta} - 8\frac{t^2}{U-\Delta}$ and $E = 0$ respectively; while the anti-symmetric state has the energy $E = -4\frac{t^2}{U-\Delta}$.

Thus, in the symmetric singlet state [1], the hole has the lowest energy. For comparison, the energy of one oxygen site making a singlet with a Cu site is $-2\frac{t^2}{\epsilon_p - 2\epsilon_p} - 2\frac{t^2}{\epsilon_p - U}$. Thus, when adding a hole a Zhang-Rice singlet is formed.
What happens when more than two holes are added? The energy for two holes making two separate Zhang-Rice singlets is $-16(\frac{t^2}{\Delta} + \frac{t^2}{U-\Delta})$; however, if the two holes go in to the same Zhang-Rice singlet, they have the energy $E = -6\frac{t^2}{\Delta} - 4\frac{t^2}{U-\Delta}$.

[1] $P_{i\sigma}$ and $P_{j\sigma'}$ are not orthogonal because two Zhang-Rice singlets formed around two neighbouring Cu sites share a oxygen site: $\langle P^s_{i\sigma}|P^{s\dagger}_{j\sigma'}\rangle = \delta_{\sigma\sigma'}(\delta_{ij} - \frac{1}{4}\delta_{\langle ij\rangle})$. However, Wannier functions can be formed, which are orthogonal and complete:

$$\phi_{i\sigma} = \frac{1}{\sqrt{(N_S)}}\sum_k P_{k\sigma}\exp(i\mathbf{k}\cdot\mathbf{R}_i), \tag{2.7}$$

$$P_{k\sigma} = \frac{\beta_k}{\sqrt{(N_S)}}\sum_k P_{k\sigma}\exp(i\mathbf{k}\cdot\mathbf{R}_i), \tag{2.8}$$

where $\beta_k = \frac{1}{\sqrt{1-\frac{1}{2}(cosk_x + cosk_y)}}$. Then $\phi_{i\sigma}$ takes the place of the Zhang-Rich singlet in the above. This changes the energies slightly from the discussion above, but the overall picture remains true [13]

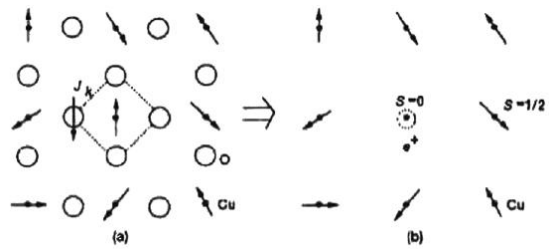

Figure 2.2: The holes are doped into the oxygen orbitals leaving an unpaired spin. The spin forms a singlet with a Cu site. Thus the two band model maps on to the Hubbard Model by considering an electron on a Cu site as a filled site and a Zhang-Rice singlet as a hole. Hole $= \frac{1}{\sqrt{2}}(\uparrow\downarrow - \downarrow\uparrow)$*. Figure adapted from ref. [5]*

Thus a large energy gain is obtained for the holes if the holes do not occupy the same Zhang-Rice singlet; in other words, a strong repulsion exists between holes occupying the same Zang-Rice singlet.

Mapping on to the Hubbard model

To summarize; in the undoped material, the system can be modelled by the antiferromagnetic Heisenberg Hamiltonian, which only takes into account the localized spins on the copper ions. Upon doping, each hole forms a Zang-Rice singlet. This singlet can, as seen in figure 2.2, then be taken as the equivalent of a hole in the Hubbard model; i.e. in equation (2.3) $c^{\dagger}_{i\sigma}$ annihilates a Zhang-Rice singlet and creates a spin σ electron on site i; and $c_{i\sigma}$ annihilates a spin σ electron on site i and creates a Zhang-Rice singlet of the copper ion on site i and the neighbouring oxygens.

2.3 Renormalization to Non Double Occupied Subspace

2.3.1 Mean Field Treatment of the Hubbard Model

To solve the Hubbard model analytically a mean field approximation may be applied

$$H_{mean} = T + U \sum_i n_{i\downarrow}\langle n_{i\uparrow}\rangle + n_{i\uparrow}\langle n_{i\downarrow}\rangle - \langle n_{i\downarrow}\rangle\langle n_{i\uparrow}\rangle. \tag{2.9}$$

The mean field Hamiltonian in equation (2.9) does not include the possibility of superconducting pairing. Therefore, if a mean-field solution of the Hubbard model is to be used to study d-wave HTSC, a postive nearest-neighboring attraction can be included by hand.

$$-V \sum_{\langle ij\rangle} n_{i\downarrow} n_{j\uparrow} \tag{2.10}$$

This positive electron-electron attraction then gives rise to singlet d-wave pairing. Inclusion of equation (2.10) in the mean field solution of the Hubbard model gives:

$$H_{mean} = T + U \sum_i \left(n_{i\downarrow}\langle n_{i\uparrow}\rangle + n_{i\uparrow}\langle n_{i\downarrow}\rangle - \langle n_{i\downarrow}\rangle\langle n_{i\uparrow}\rangle\right) + \sum_{\langle ij\rangle} c^\dagger_{i\downarrow} c^\dagger_{j\uparrow}\Delta_{ij} + c_{j\uparrow} c_{i\downarrow}\Delta^*_{ij} \tag{2.11}$$

where $\Delta_{ij} = V\sigma\langle c_{i\downarrow} c_{j\uparrow}\rangle$.
Eq. (2.11) allows for a phenomenological study of how Coulomb correlations and d-wave superconductivity may compete. However, the mean field solution of the Hubbard model given in (2.11) above has two disadvantages. First of all, it is not satisfying to have to include a positive electron-electron interaction, which do not have a clear origin in the system. Secondly, choosing a unique doping independent U, which gives the right magnitude of the staggered magnetization, is not possible. However, the necessity of the positive electron-electron interaction and the difficulty of choosing a uniqu U are caused by the mean-field treatmen and not the Hubbard model itself.

2.3.2 Inclusion of the Mott Physics

Taking the Mott nature of the HTSCs into account, the two problems mentioned above can be avoided. The system is dominated by a strong onsite Coulomb repulsion, i.e. U is very large compared to t, which means that the system pays a large energy cost for a double occupied site. Thus the ground-state and the low

energy excitations are expected not to have double occupied sites. Therefore, the low energy physics of the system can be described by using a smaller Hilbert-space than the full Hilbert space of the Hubbard model. Thus, looking for an effective Hamiltonian with eigenstates in a Hilbert-space where all the states containing double occupied sites are projected out, simplifies the model.

The Full and Single Occupied Hilbert Space

Every eigenstate ψ of the Hubbard model can be written as a linear combination of Fock states, because Fock states constitute a complete set. The Fock space can be divided into two subspaces S and D contaning none and at least on double occupied site, respectively

$$S = \Big[|n_{1\uparrow}, n_{1\downarrow}, n_{2\uparrow,\ldots}\rangle : \forall i, n_{i\uparrow} + n_{\downarrow} \leq 1\Big] \tag{2.12}$$

$$D = \Big[|n_{1\uparrow}, n_{1\downarrow}, n_{2\uparrow,\ldots}\rangle : \exists i, n_{i\uparrow} + n_{\downarrow} = 2\Big]. \tag{2.13}$$

To find the effective Hamiltonian with eigenstates in S the starting-point is the usual Schrödinger equation:

$$H\psi = E\psi \tag{2.14}$$

where H is the Hubbard Hamiltonian and ψ is an eigenfunctions in $S + D$.

The objective is now to derive a Schrödinger equation of the projected Hilbert space from equation (2.14)

$$H_{eff}\mathbf{P}\psi = E\mathbf{P}\psi \tag{2.15}$$

where H_{eff} is the new effective Hamiltonian and $\mathbf{P}$ is the projection operator, which projects out all states containing at least one double occupied site. The projection operator is given by:

$$\mathbf{P} = \prod_l (1 - n_{l\uparrow} n_{l\downarrow}), \tag{2.16}$$

so if $\psi \in (S + D)$ then $\mathbf{P}\psi \in (S)$. From $\mathbf{P}$ the projection operator $\mathbf{Q}$ can be defined as:

$$\mathbf{Q} = 1 - \mathbf{P}. \tag{2.17}$$

$\mathbf{Q}$ projects out all states that do not contain double occupied sites, so if $\psi \in (S + D)$ then $\mathbf{Q}\psi \in (D)$. Four obvious facts apply to $\mathbf{P}$ and $\mathbf{Q}$:

$$\mathbf{PP} = \mathbf{P} \tag{2.18}$$

$$\mathbf{QQ} = \mathbf{Q} \tag{2.19}$$

$$\mathbf{P} + \mathbf{Q} = 1 \tag{2.20}$$

$$\mathbf{PQ} = 0 \tag{2.21}$$

To derive H_{eff} the Schrödinger equation in (2.14) is rewritten using equation (2.20):

$$H(\mathbf{Q}+\mathbf{P})\psi = E(\mathbf{Q}+\mathbf{P})\psi. \tag{2.22}$$

To move further, $\mathbf{Q}$ is applied to both sides of equation (2.22) above

$$\begin{aligned}(\mathbf{Q}H\mathbf{Q}+\mathbf{Q}H\mathbf{P})\psi &= E\mathbf{Q}\psi && (2.23)\\ (\mathbf{Q}H\mathbf{Q}-E)\mathbf{Q}\psi &= -\mathbf{Q}H\mathbf{P}\psi && (2.24)\\ \mathbf{Q}\psi &= -(\mathbf{Q}H\mathbf{Q}-E)^{-1}\mathbf{Q}H\mathbf{P}\psi. && (2.25)\end{aligned}$$

The expression for the $\mathbf{Q}$-projected eigenstates in equation (2.25) can then be inserted in equation (2.22)

$$(H - H(\mathbf{Q}H\mathbf{Q}-E)^{-1}\mathbf{Q}H\mathbf{P})\mathbf{P}\psi = E(\mathbf{P}+\mathbf{Q})\psi. \tag{2.26}$$

To achieve an eigenvalue problem for H_{eff}, $\mathbf{P}$ is applied to the left at both sides in equation (2.26)

$$(\mathbf{P}H\mathbf{P} - \mathbf{P}H(\mathbf{Q}H\mathbf{Q}-E)^{-1}\mathbf{Q}H\mathbf{P})\mathbf{P}\psi = E\mathbf{P}\psi. \tag{2.27}$$

Equation (2.27) is a Shrödinger equation of the same form as equation (2.15), describing the groundstate and the low energy excitations in the subspace S. Thus H_{eff} is given by:

$$\begin{aligned}H_{eff} &= \mathbf{P}H\mathbf{P} - \mathbf{P}H(\mathbf{Q}H\mathbf{Q}-E)^{-1}\mathbf{Q}H\mathbf{P} && (2.28)\\ &= \mathbf{P}H\mathbf{P} - \mathbf{P}H\mathbf{Q}\mathbf{Q}^{-1}(\mathbf{Q}H\mathbf{Q}-E)^{-1}\mathbf{Q}^{-1}\mathbf{Q}\mathbf{Q}H\mathbf{P} && (2.29)\\ &= \mathbf{P}H\mathbf{P} - \mathbf{P}H\mathbf{Q}(\mathbf{Q}H\mathbf{Q}-\mathbf{Q}E\mathbf{Q})^{-1}\mathbf{Q}H\mathbf{P}. && (2.30)\end{aligned}$$

For convenience H is written as: $H = H_K + H_U$
where $H_K = \sum_{\langle i,j\rangle\sigma} t_{ij}\left(c^\dagger_{i\sigma}c_{j\sigma} + h.c.\right)$ and $H_U = U\sum_i n_{i\uparrow}n_{i\downarrow}$.
$\mathbf{P}H\mathbf{P} = \mathbf{P}H_K\mathbf{P}$ because there are no double occupied sites in S.
To simplify H_{eff} it is expanded to the second order in t/U and to zeroth order in E/U.
Thus $\mathbf{Q}H\mathbf{Q}$ is replaced by U and E is replaced by 0, giving:

$$H_{eff} = \mathbf{P}\left(H_K - \frac{H_K\mathbf{Q}\mathbf{Q}H_K}{U}\right)\mathbf{P} \tag{2.31}$$

If $\mathbf{Q}H_K\mathbf{P}$ is not to be zero, H_K must connect the two subspaces S and D; thus, when $\mathbf{Q}H_K$ is applied to $\psi \in S$:

$$\begin{aligned}\mathbf{Q}H_K &= \left(1 - \prod_i (1 - n_{i\uparrow}n_{i\downarrow})\right)\left(\sum_{jj's} -t_{jj'}c^\dagger_{js}c_{j's}\right) && (2.32)\\ &= \sum_{ij's} t_{ij'}n_{i\uparrow}n_{i\downarrow}c^\dagger_{is}c_{j's}. && (2.33)\end{aligned}$$

The same argument is valid for $H_K\mathbf{Q}$, so

$$H_K\mathbf{Q}H_K = \sum_{lij'\sigma s} t_{li}t_{ij'}c^\dagger_{l\sigma}c_{i\sigma}n_{i\uparrow}n_{i\downarrow}c^\dagger_{is}c_{j's} \tag{2.34}$$

where $i \neq j'$ and $l \neq i$ to ensure that H_K connects the to subspaces S and D. Because $i \neq j'$ and $l \neq i$ equation (2.34) can be rewritten as:

$$= \sum_{lij'\sigma s} t_{li}t_{ij'}c^\dagger_{l\sigma}c_{j's}c_{i\sigma}n_{i\uparrow}n_{i\downarrow}c^\dagger_{is} \tag{2.35}$$

$$= \sum_{lij'\sigma s} t_{li}t_{ij'}c^\dagger_{l\sigma}c_{j's}c_{i\sigma}c^\dagger_{is}\left(\delta_{s\downarrow}n_{i\uparrow} + \delta_{s\uparrow}n_{i\downarrow} + n_{i\uparrow}n_{i\downarrow}\right) \tag{2.36}$$

$$= \sum_{lij'\sigma s} t_{li}t_{ij'}c^\dagger_{l\sigma}c_{j's}c_{i\sigma}c^\dagger_{is}n_i \tag{2.37}$$

where $n_i = n_{i\uparrow} + n_{i\downarrow}$.
To proceed, the following two identities are helpful:

$$c^\dagger_{l\sigma}c_{ls} = \delta_{\sigma s}\frac{n_{l\uparrow} + n_{l\downarrow}}{2} + \mathbf{S}_l \cdot \sigma_{s\sigma} \tag{2.38}$$

$$c_{i\sigma}c^\dagger_{is} = \delta_{\sigma s}\left(1 - \frac{n_{i\uparrow} + n_{i\downarrow}}{2}\right) - \mathbf{S}_i \cdot \sigma_{\sigma s} \tag{2.39}$$

For the case $l = j'$, equation (2.37) can be rewritten by applying the identities above:

$$= \sum_{li\sigma s} |t_{li}|^2\Big(\delta_{\sigma s}\frac{n_l}{2} + \mathbf{S}_l \cdot \sigma_{s\sigma}\Big)\left(\delta_{\sigma s}\left(1 - \frac{n_i}{2}\right) - \mathbf{S}_l \cdot \sigma_{\sigma s}\right)n_i \tag{2.40}$$

$$= \sum_{li\sigma s} |t_{li}|^2\Big(\frac{n_l}{2} - \frac{n_l n_i}{4} - \frac{n_l}{2}\mathbf{S}_i \cdot \sigma_{\sigma s} + \mathbf{S}_l \cdot \sigma_{s\sigma}\Big(1 - \frac{n_i}{2}\Big) - (\mathbf{S}_l \cdot \sigma_{s\sigma})(\mathbf{S}_i \cdot \sigma_{\sigma s})\Big)n_i$$

$$= \sum_{li\sigma s} |t_{li}|^2\Big(\frac{n_l}{2} - \frac{n_l n_i}{4} - (\mathbf{S}_l \cdot \sigma_{s\sigma})(\mathbf{S}_i \cdot \sigma_{\sigma s})\Big)n_i \tag{2.41}$$

$$= \sum_{li} |t_{li}|^2\Big(\frac{n_l n_i}{2}\Big) - \sum_{lis\sigma\alpha} |t_{li}|^2\left(S^\alpha_l\sigma_{s\sigma}S^\alpha_i\sigma_{\sigma s}\right) \tag{2.42}$$

$$= \sum_{li} 2\,|t_{li}|^2\Big(\frac{n_l n_i}{4} - \mathbf{S}_l \cdot \mathbf{S}_i\Big) \tag{2.43}$$

For the case $l \neq j'$, equation (2.37) can be rewritten as:

$$= \sum_{lij'\sigma s}^{l\neq j'} t_{li}t_{ij'}c^{\dagger}_{l\sigma}c_{j's}c_{i\sigma}c^{\dagger}_{is}n_i \tag{2.44}$$

$$= \sum_{lij'\sigma s}^{l\neq j'} t_{li}t_{ij'}c^{\dagger}_{l\sigma}c_{j's}(\delta_{\sigma s}(1-\frac{n_i}{2}) - \mathbf{S}_i\cdot\sigma_{\sigma s})n_i \tag{2.45}$$

$$= \sum_{lij'\sigma s}^{l\neq j'} t_{li}t_{ij'}\left(c^{\dagger}_{l\sigma}c_{j'\sigma}\frac{n_i}{2} - c^{\dagger}_{l\sigma}c_{j's}\mathbf{S}_i\cdot\sigma_{\sigma s}n_i\right) \tag{2.46}$$

Insertion of equations (2.43) and (2.46) in equation (2.31) gives the following expression for H_{eff}:

$$\begin{aligned} H_{eff} = \mathbf{P}\Bigg(&\sum_{ll'\sigma} -t_{ll'}c^{\dagger}_{l\sigma}c_{l'\sigma} + \sum_{li} 2\frac{-|t_{li}|^2}{U}\left(\frac{n_l n_i}{4} - \mathbf{S}_l\cdot\mathbf{S}_i\right) \\ &+ \sum_{lil'\sigma s}^{l\neq l'} \frac{-t_{li}t_{il'}}{U}\left(c^{\dagger}_{l\sigma}c_{l'\sigma}\frac{n_i}{2} - c^{\dagger}_{l\sigma}c_{l's}\mathbf{S}_i\cdot\sigma_{\sigma s}n_i\right)\Bigg)\mathbf{P} \end{aligned} \tag{2.47}$$

The t-J Model

The model in (2.47) is called the t-J model. It consists of four terms; the kinetic term $\sum_{ll'\sigma} -t_{ll'}c^{\dagger}_{l\sigma}c_{l'\sigma}$, the exchange term $J\sum_{li}\mathbf{S}_l\cdot\mathbf{S}_i$, the density-density term, $-J\sum_{li}\left(\frac{n_l n_i}{4}\right)$, and the three site term $\sum_{lil'\sigma s}^{l\neq l'} J_n\left(c^{\dagger}_{l\sigma}c_{l'\sigma}\frac{n_i}{2} - c^{\dagger}_{l\sigma}c_{l's}\mathbf{S}_i\cdot\sigma_{\sigma s}n_i\right)$, where $J = 2\frac{-|t_{li}|^2}{U}$ and $J_N = \frac{-t_{li}t_{il'}}{U}$.
The density-density term is neglected, because it is a constant at half-filling and, furthermore for finite doping numerical calculations have shown that the density-density term is almost constant[14]. The effect of the three-site term is proportional to δJ, so it is a factor δ less than the exchange term , and it is therefore also neglected. The final expression is:

$$H_{eff} = \mathbf{P}\left(\sum_{(ll')\sigma} -t_{ll'}c^{\dagger}_{l\sigma}c_{l'\sigma} + J\sum_{<li>}\mathbf{S}_l\cdot\mathbf{S}_i\right).\mathbf{P} \tag{2.48}$$

where summation over nearest and next nearest neighboring sites is denoted by (ij), and summation over nearest neighboring sites is denoted by $< ij >$.
Parameters typically used for the t-J model in the literature are: $t = 1$, $-t' \in [0.1, 0.3]$ and $J \in [0.2, 0.4]$. The scale of t is (0.3eV-0.4eV).

Chapter 3

RVB

3.1 The Resonating Valence-bond State

The exact groundstate for the t-J model in two dimensions is not known; but the undoped compound is expected to be in a Neel state. The latter is true because long-range AF-order is observed by NS experiments. However, the Neel state becomes frustrated upon doping as a consequence of the fact that the holes are mobile carriers and allowed to move, see figure 3.1 (a). The low dimension of the system and the frustration of the Neel state together should make it energetically favourable to "melt" the Neel state and a state of resonating singlet pairs is formed. This led P. W. Anderson to propose the resonating valens-bond (RVB) state as a trial state for the t-J model [12]. The variational state proposed by P. W. Anderson was a projected BCS state:

$$|\Psi\rangle = \mathbf{P}|\Psi_0\rangle_{BCS} \tag{3.1}$$

$$|\Psi_0\rangle_{BCS} = \prod_k (u_k + v_k c^\dagger_{k\uparrow} c^\dagger_{-k\uparrow})|0\rangle \tag{3.2}$$

where $|0\rangle$ is the vacuum state and u_k and v_k are the variational parameters which satisfies the normalization condition $|u_k|^2 + |v_k|^2 = 1$, and are given by

$$u_k = \sqrt{\frac{1}{2}\left(1 + \frac{\epsilon_k^{(0)} - \mu}{E_k}\right)}, \qquad v_k = \sqrt{\frac{1}{2}\left(1 - \frac{\epsilon_k^{(0)} - \mu}{E_k}\right)}, \tag{3.3}$$

where $E_k = \sqrt{(\epsilon_k^{(0)} - \mu)^2 + |\Delta_k|^2}$, and ϵ_k^0 is the non interacting particle energy dispersion given by

$$\epsilon_k^{(0)} = -2t(\cos k_x + \cos k_y) - 4t'(\cos k_x \cos k_y), \tag{3.4}$$

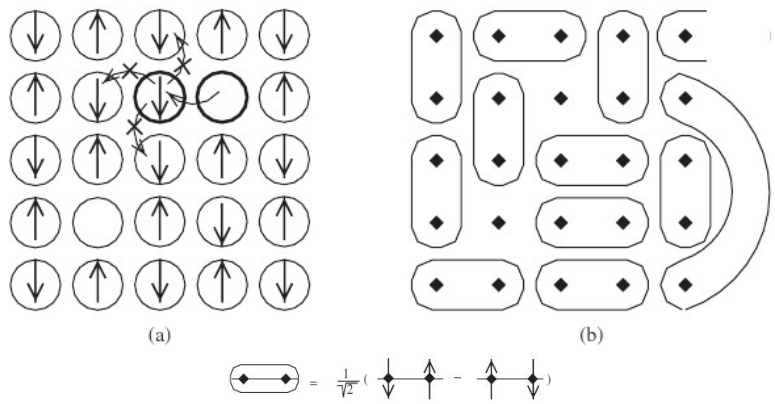

Figure 3.1: (a) In the half filled case the system experiences long range AF-order and the system is expected to be in a Neel state. However, upon doping, the antiferromagnetic Neel state becomes frustrated. (b) The low dimension of the system and the frustration of the Neel state together makes it energetically favourable to "melt" the Neel state, and a state of resonating singlet pairs is formed. Figure b is a snapshot of such a state. Figure adapted from [9].

and Δ_k is the superconducting order parameter, which for the d_{x-y}-wave superconductivity is given by $\Delta_k = \Delta(\cos k_x - \cos k_y)$.
The Fourier transformation of the projected BCS function is:

$$\begin{aligned}
\mathbf{P}|\Psi_0\rangle_{BCS} &= \mathbf{P}\prod_k (u_k + v_k c^\dagger_{k\uparrow} c^\dagger_{-k\downarrow})|0\rangle \\
&= \mathbf{P}(\prod_k u_k)\prod_k (1 + \frac{v_k}{u_k} c^\dagger_{k\uparrow} c^\dagger_{-k\downarrow})|0\rangle \\
&= \mathbf{P}(\prod_k u_k)\exp(\frac{v_k}{u_k} c^\dagger_{k\uparrow} c^\dagger_{-k\downarrow})|0\rangle \\
&= \mathbf{P}(\prod_k u_k)\exp(\sum_k a_k c^\dagger_{k\uparrow} c^\dagger_{-k\downarrow})|0\rangle \\
&= \mathbf{P}(\prod_k u_k)\exp(\sum_{ij} a_{ij} c^\dagger_{i\uparrow} c^\dagger_{j\downarrow})|0\rangle, \qquad (3.5)
\end{aligned}$$

where a_{ij} is defined by $a_{ij} \equiv \frac{1}{N}\sum_k a_k e^{ik(r_i - r_j)}$ with $a_k = \frac{v_k}{u_k} = \frac{\Delta_k}{\epsilon_k^{(0)} - \mu + \sqrt{(\epsilon_k^{(0)} - \mu)^2 + |\Delta_k|^2}}$.
$|\Psi_0\rangle_{BCS}$ is a grand canonical wavefunction, which means that the particle number is alloved to fluctuate, i.e. it is not an eigenstate of $\hat{N}$. To fix the total particle number a projection onto a fixed particle-number P_N is applied:

$$\mathbf{P}_N\mathbf{P}|\Psi_0\rangle_{BCS} = \frac{1}{(N/2)!}\mathbf{P}(\prod_k u_k)(\sum_{ij} a_{ij} c^\dagger_{i\uparrow} c^\dagger_{j\downarrow})^{\frac{N}{2}}|0\rangle. \qquad (3.6)$$

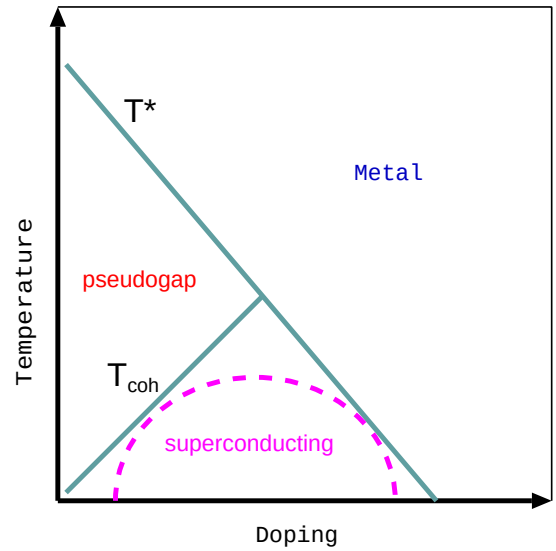

Figure 3.2: In the RVB picture the pseudogap is caused by the formation of the singlet pairs in the RVB state, which are formed below the temperature T^*. The superconducting state emerges when the preformed singlet pairs become coherent below the temperature T_{coh}. T_c are then the equal to the lower of T^* and T_{coh}.

The summation in (3.6) can be rewritten because a_k is an even function with respect to k and because $a_{ij} = a_{ji}$:

$$\sum_{ij} a_{ij} c^\dagger_{i\uparrow} c^\dagger_{j\uparrow} = \frac{1}{2} \sum_{ij} a_{ij} \left(c^\dagger_{i\uparrow} c^\dagger_{j\downarrow} - c^\dagger_{i\downarrow} c^\dagger_{j\uparrow} \right). \tag{3.7}$$

This illustrates that the wavefunction in (3.6) is a superposition of singlet bond configurations. Each valence bond is represented by $(c^\dagger_{i\uparrow} c^\dagger_{j\downarrow} - c^\dagger_{i\downarrow} c^\dagger_{j\uparrow})$ with amplitude a_{ij}; as in figure 3.1.

In the RVB picture the pseudogap is caused by the formation of the singlet pairs in the RVB state, which are formed below the temperature T^*. The superconducting state emerges when the preformed singlet pairs become coherent below the temperature T_{coh}. T_c is then equal to the lower of T^* and T_{coh} [16], see figure 3.2.

One of the early successes of the RVB picture was the prediction of d-wave superconductivity[17] and the disappearing of the superconductivity around 30% of doping, even before it was experimentally verified. The prediction was made from a variational calculation using the wavefunction in eq. (3.6) [34].

Chapter 4

The Gutzwiller Approximation

4.1 The Original Gutzwiller Approximation

To solve the t-J model the no double-occupation constraint has to be tackled. Using a Variational Mondocarlo (VMC) technique the constraint can be treated numerically exact. For inhomogeneous systems an alternative to the VMC method is desirable because VMC is numerically expensive, and thus makes calculations on inhomogeneous systems too heavy to compute. To solve it analytically, however, the constraint has to be approximated in some way. One possible method is the Gutzwiller approximation (GA). The GA agrees well with the VMC for homogeneous systems when a d-wave BCS function is assumed to be the ground state.

The idea behind the GA is to approximate the expectation value of an operator in the projected Hilbert space by multiplying the expectation value of the same operator in the preprojected Hilbert space by a statistical weight factor: $\langle \hat{O} \rangle = g^O \langle \hat{O} \rangle_0$ where:

$$\langle \hat{O} \rangle = \frac{\langle \Psi | \hat{O} | \Psi \rangle}{\langle \Psi | \Psi \rangle} \tag{4.1}$$

This statistical weight factor is called the Gutzwiller factor (GF). As the no double-occupation constraint forbids an electron to jump between two single occupied sites, the expectation value of the kinetic energy has a GF which is between 0 and 1; because, if every site is single occupied, jumping is completely suppressed and therefore $g^t = 0$; on the other hand, if there is only on electron present the no double-occupation constraint has no influence and $g^t = 1$. As the no double-occupation constraint also enhances the probability for a site to be single occupied, the GF for the exchange term is larger or equal to one; i.e. $g^s \geq 1$.

In the homogeneous paramagnetic case, an intuitive derivation of the Gutzwiller factor is provided by Zhang et. al. ref. [7]. The central result of ref. [7] is, that the GF for an operator $\hat{O}$ is given by the probability for the physical process described

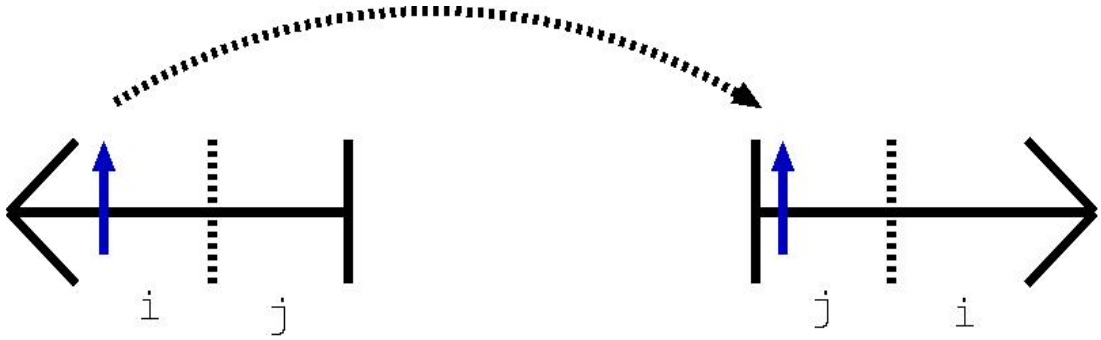

Figure 4.1: *Illustration of an spin-up hopping from site i to j. For $\psi \in S$ the probabilities for the configurations before and after hopping are: $\langle n_{i\uparrow}\rangle(1-\langle n_{j\uparrow}\rangle-\langle n_{j\downarrow}\rangle)$ and $\langle n_{j\uparrow}\rangle(1-\langle n_{j\uparrow}\rangle-\langle n_{j\downarrow}\rangle)$ respectively; while for $\psi_0 \in (S+D)$, the probabilities for the configurations before and after hopping are: $\langle n_{i\uparrow}\rangle_0(1-\langle n_{j\uparrow}\rangle_0)(1-\langle n_{j\downarrow}\rangle_0)$ and $\langle n_{j\uparrow}\rangle(1-\langle n_{j\uparrow}\rangle_0)(1-\langle n_{j\downarrow}\rangle_0)$ respectively.*

by the operator to occur in the projected Hilbert space divided by the probability for the same process to occur in the preprojected Hilbert space. By generalizing to the inhomogeneous case, Wing-Ho Ko et. al. ref. [3] supplemented the results of Zhang et. al. ref. [7]. The GA thus amounts to ascribe the probability for a physical process to occur to the probability for configurations, before and after the process, hence this method is referred to as the configuration counting method in the literature. The most widely used scheme is to take the site centered expectation values, ignoring inter-site correlations.

4.1.1 Example: The Hopping Operator

As an example consider the spin-up hopping operator $c^\dagger_{j\uparrow}c_{i\uparrow}$, which describes a process where a spin up electron hops from site-i to site-j, see figure 4.1 and 4.2. Before the hopping, an spin-up has to be situated on site-i; the Pauli exclusion principle demands no spin-up on site-j. After the hopping there has to be an spin-up on site-j and there is no longer an spin-up on site-i. This must be true in both the projected (S) and preprojected (S+D) Hilbert-space. In the projected space the no double occupation constraint forbids the presence of a spin-down, thus there is only one configuration which allows for the hopping to occur, as in figure 4.1. However, in the preprojected space there is no constraint other than the Pauli exclusion principle on the down-spins, thus giving four different configurations, the one in figure 4.1 and the three in figure 4.2. Summing-up all the allowed configurations, taking the ratio and including an overall square root, gives the GF:

$$g^t_{ij\uparrow} = \sqrt{\frac{\langle n_{i\uparrow}\rangle(1-\langle n_{j\uparrow}\rangle-\langle n_{j\downarrow}\rangle)\langle n_{j\uparrow}\rangle(1-\langle n_{j\uparrow}\rangle-\langle n_{j\downarrow}\rangle)}{\langle n_{i\uparrow}\rangle_0(1-\langle n_{j\uparrow}\rangle_0)\langle n_{j\uparrow}\rangle_0(1-\langle n_{i\uparrow}\rangle_0)}} \tag{4.8}$$

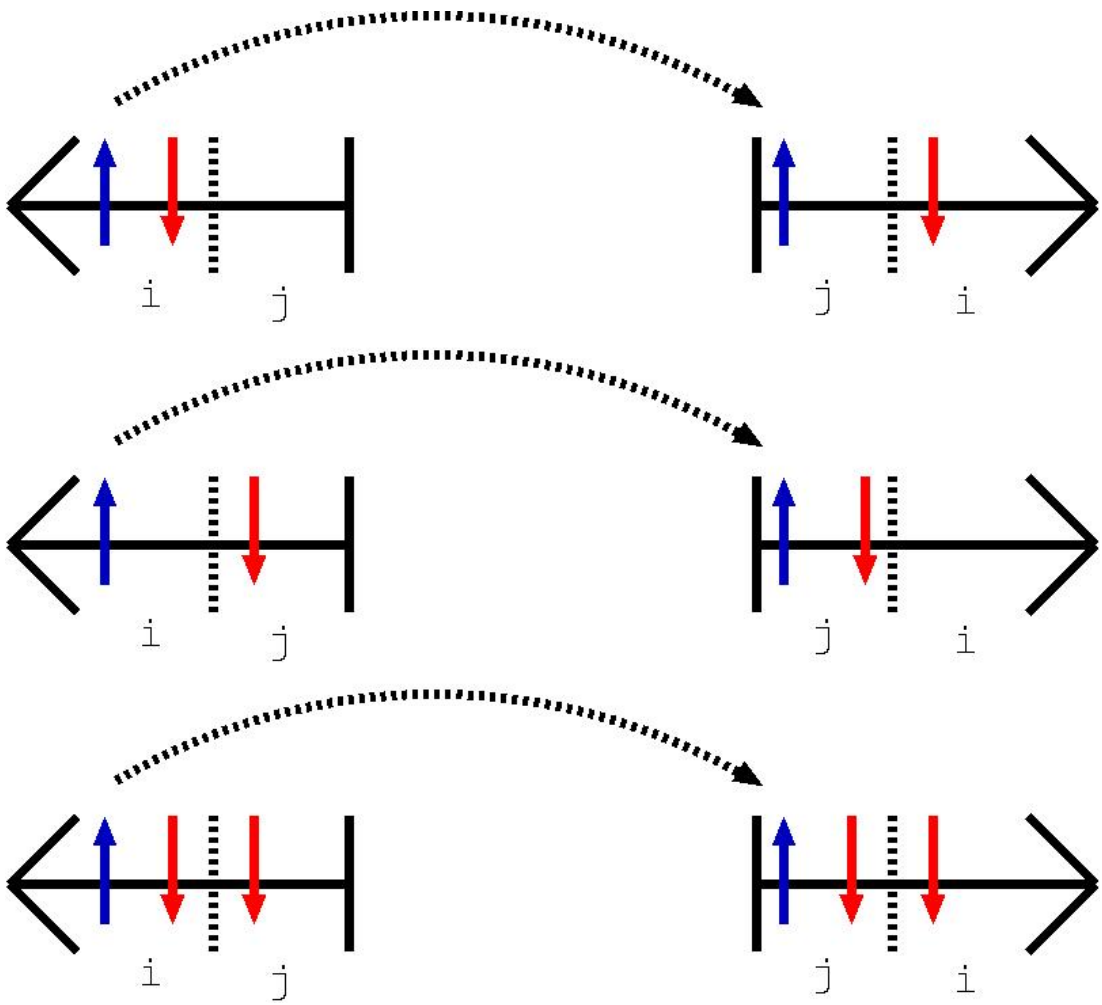

Figure 4.2: Illustration of three processes where an spin-up hops from site i to j, for $\psi_0 \in (S+D)$ the probabilities for the configurations before and after hopping are;

$$
\begin{aligned}
\textit{Before hopping} &= \langle n_{i\uparrow}\rangle_0 \langle n_{i\downarrow}\rangle_0 \left(1-\langle n_{j\uparrow}\rangle_0\right)\left(1-\langle n_{j\downarrow}\rangle_0\right) && (4.2)\\
\textit{After hopping} &= \left(1-\langle n_{i\uparrow}\rangle_0\right)\langle n_{i\downarrow}\rangle_0 \langle n_{j\uparrow}\rangle_0 \left(1-\langle n_{j\downarrow}\rangle\right) && (4.3)\\
\textit{Before hopping} &= \langle n_{i\uparrow}\rangle_0 \left(1-\langle n_{i\downarrow}\rangle_0\right)\left(1-\langle n_{j\uparrow}\rangle_0\right)\langle n_{j\downarrow}\rangle_0 && (4.4)\\
\textit{After hopping} &= \left(1-\langle n_{i\uparrow}\rangle_0\right)\left(1-\langle n_{i\downarrow}\rangle_0\right)\langle n_{j\uparrow}\rangle_0 \langle n_{j\downarrow}\rangle && (4.5)\\
\textit{Before hopping} &= \langle n_{i\uparrow}\rangle_0 \langle n_{i\downarrow}\rangle_0 \left(1-\langle n_{j\uparrow}\rangle_0\right)\langle n_{j\downarrow}\rangle_0 && (4.6)\\
\textit{After hopping} &= \left(1-\langle n_{i\uparrow}\rangle_0\right)\langle n_{i\downarrow}\rangle_0 \langle n_{j\uparrow}\rangle_0 \langle n_{j\downarrow}\rangle && (4.7)
\end{aligned}
$$

where $\langle n_{i\downarrow}\rangle_0\langle n_{j\downarrow}\rangle_0+\langle n_{i\downarrow}\rangle_0(1-\langle n_{j\downarrow}\rangle_0)+\langle n_{j\downarrow}\rangle_0(1-\langle n_{i\downarrow}\rangle_0)+(1-\langle n_{i\downarrow}\rangle_0)(1-\langle n_{j\downarrow}\rangle_0) = 1$ has been used.
For a canonical trial wavefunction the projection operator and the particle number operator commute, i.e. $\left[\hat{\mathbf{N}}, \mathbf{P}\right] = 0$. This means that $\hat{\mathbf{N}}\mathbf{P}|\Psi_0\rangle = N_e\mathbf{P}|\Psi_0\rangle$, i.e. the total number of electrons is the same before and after projection. For a homogeneous and paramagnetic trial wavefunction this leads to

$$\langle \hat{n}_\sigma\rangle = \langle \hat{n}_\sigma\rangle_0 = \frac{N_e}{2N} = \frac{n}{2}. \tag{4.9}$$

Thus in the homogeneous and paramagnetic case (4.8) becomes:

$$g^t = \frac{2\delta}{1+\delta} \tag{4.10}$$

where δ is the hole concentration, $\delta = 1 - n$.

4.1.2 Trial Wavefunction and Inhomogeneity

In a homogenous system VMC calculations can easily be preformed, because the number of variational parameters is limited. The GA, therefore, becomes more relevant when the system is inhomogeneous. However, the GF in eq. (4.10) is derived assuming homogeneity; so to get simple site dependent GFs most authors rewrite the GF in eq. (4.10) as:

$$g^t_{ij} = \sqrt{\frac{2\delta_i}{1+\delta_i}}\sqrt{\frac{2\delta_j}{1+\delta_j}}. \tag{4.11}$$

To rewrite eq. (4.10) as eq. (4.11) is not justified. However, with appropriate modification of the Gutzwiller projecter $\mathbf{P}$, eq. (4.11) proves to be correct. In this thesis in section 5.6 a similar rewriting of the extended GF is used.
To understand the effect of inhomogeneity on the GA, the GA can be perceived as an approximation to VMC. When doing VMC a trial wavefunction is assumed, and therefore the GA factors must depend on the choice of the trial function. For a general wavefunction, projecting down to a subspace where double occupation is forbidden can change both the total and local particle number. The change in total and local particle number depends on the assumed trial wavefunction. The most simple approach is to assume a canonical and uniform trial wavefunction; i.e. the total number of electrons (N_e) is fixed and the local electron density is given by $n_i = \frac{N_e}{N} = n$, as in eq. (4.9).

Then for an operator $\hat{O}$

$$\begin{aligned}\langle\hat{O}\rangle &= \frac{\langle\Psi_0|\mathbf{P}\mathbf{P}_N\hat{O}\mathbf{P}_N\mathbf{P}|\Psi_0\rangle}{\langle\Psi_0|\mathbf{P}\mathbf{P}_N\mathbf{P}_N\mathbf{P}|\Psi_0\rangle} \\ &\approx g_O\frac{\langle\Psi_0|\mathbf{P}_N\hat{O}\mathbf{P}_N|\Psi_0\rangle}{\langle\Psi_0|\mathbf{P}_N\mathbf{P}_N|\Psi_0\rangle} \\ &= g_O\frac{\langle\Psi_0|\hat{O}|\Psi_0\rangle}{\langle\Psi_0|\Psi_0\rangle} \end{aligned} \tag{4.12}$$

where P_N is a projection operator, which projects onto elements with a fixed particle number N in the Hilbert space, and thus makes $|\psi_0\rangle$ canonical. The first line in eq. (4.12) can be calculated numerically exact with VMC. As the particle number is fixed the GA can be used in the second line of eq. (4.12). The last equality in eq. (4.12) is only true if P_N projects onto elements with $N = N'$, where N' is the average particle number of $|\Psi_0\rangle$. Under this condition a transformation from a canonical to a grand canonical ensamble is valid in the preprojected Hilbert space [9].

If the trial wavefunction is not homogeneous then eq. (4.9) can not be assumed. Although the whole system is still canonical, each site can be seen as its own subsystem, which are allowed to exchange particles with the environment. This lead to the question of what happens if the trial state is grand canonical, and it is not projected to a fixed particle number?

In the grand canonical scheme the total number of particles fluctuates and the mean number of particles is given by :

$$\bar{N} = \sum_N N\rho_N \tag{4.13}$$

where

$$\rho_N = \frac{\langle\Psi|\mathbf{P_N}|\mathbf{\Psi}\rangle}{\langle\Psi|\Psi\rangle} \tag{4.14}$$

In the thermodynamic limit this distribution can be sharply peaked, however the Gutzwiller-projector will still change the mean particle number because states with a large number of particles will be more likely to have double occupied sites. B. Edegger et al. [10] calculated the particle-density after projection as a function of the particle-density before projection for the BCS state in eq. (3.2), see figure 4.3. Figure 4.3 clearly illustrates how the Gutzwiller-projection changes the particle density for. The change of particle density makes it necessary to relate $\langle n_{i\sigma}\rangle_0$ to $\langle n_{i\sigma}\rangle$ if the GA is to be used. The fact that there are different methods of relating $\langle n_{i\sigma}\rangle_0$ to $\langle n_{i\sigma}\rangle$ introduces an ambiguity; however a widely used assumption is to keep $\langle n_{i\sigma}\rangle_0 = \langle n_{i\sigma}\rangle = \frac{n_i}{2}$ in the paramagnetic case, and $\langle n_{i\sigma}\rangle_0 = \langle n_{i\sigma}\rangle = \frac{n_i}{2} + (-1)^i m$ in the case of AF-order. This can be enforced by including a local spin dependent fugacity factor in the projection operator:

$$\mathbf{P}' = \prod_i y_{i\uparrow}^{n_{i\uparrow}} y_{i\downarrow}^{n_{i\downarrow}}(1 - \hat{n}_{i\uparrow}\hat{n}_{i\downarrow}) \tag{4.15}$$

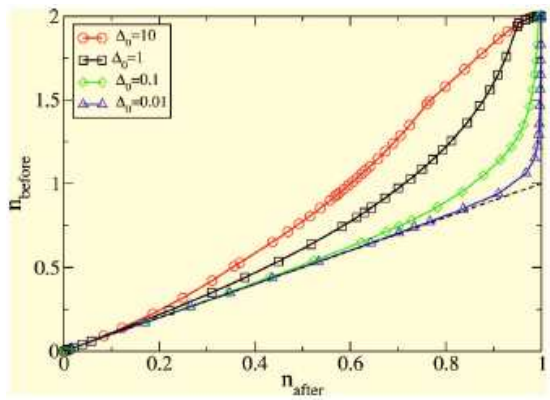

Figure 4.3: Particle density before the Gutzwiller projection n_{before} as a function of the particle density after projection n_{after} for different d-wave order parameters Δ_0. The dashed line indicates the Fermi liquid result $n_{before} = n_{after}$. Adapted from ref. [10].

.

The derivation and the role of the fugacity factors $y_{i\sigma}^{n_{i\sigma}}$ is not within the scope of this thesis. The interested reader is referred to ref. [3] and [10] for two distinct derivations. Thus, to be able to ensure the validity of the GA a fugacity factor has to be included in the Gutzwiller-projector, as in eq. (4.15). Thus

$$\langle \hat{O} \rangle = \frac{\langle \Psi_0 | \mathbf{P}' \hat{O} \mathbf{P}' | \Psi_0 \rangle}{\langle \Psi_0 | \mathbf{P}' \mathbf{P}' | \Psi_0 \rangle} \approx g_O \frac{\langle \Psi_0 | \hat{O} | \Psi_0 \rangle}{\langle \Psi_0 | \Psi_0 \rangle} \tag{4.16}$$

From eq. (4.12) and (4.16) it can be seen that

$$\frac{\langle \Psi_0 | \mathbf{P}' \hat{O} \mathbf{P}' | \Psi_0 \rangle}{\langle \Psi_0 | \mathbf{P}' \mathbf{P}' | \Psi_0 \rangle} \approx \frac{\langle \Psi_0 | \mathbf{P} \mathbf{P}_N \hat{O} \mathbf{P}_N \mathbf{P} | \Psi_0 \rangle}{\langle \Psi_0 | \mathbf{P} \mathbf{P}_N \mathbf{P}_N \mathbf{P} | \Psi_0 \rangle}, \tag{4.17}$$

i.e to obtain the same result in the canonical and grand canonical scheme different trial wavefunctions have to be assumed. To study a grand canonical wave function without including a fugacity it is necessary to include a fugacity factor in the preprojected wavefunction, this is shown by B. Edegger et al. in ref. [10]:

$$\frac{\langle \Psi_0 | \mathbf{P} \hat{O} \mathbf{P} | \Psi_0 \rangle}{\langle \Psi_0 | \mathbf{P} \mathbf{P} | \Psi_0 \rangle} \approx g_O \frac{\langle \Psi_0' | \hat{O} | \Psi_0' \rangle}{\langle \Psi_0' | \Psi_0' \rangle} \tag{4.18}$$

where $|\Psi_0'\rangle$ is a grand canonical wavefunction with an incorporated fugacity factor to ensure that the Gutzwiller projection does not change the mean particle number.

Another ambiguity with regard to the GA factors is the breaking of rotational invariance. The breaking of rotational invariance stems from the implicit choice of direction made during the configuration counting when deriving the GA factors[3]. This is evident from the GF for $\hat{\mathbf{S}}_l \cdot \hat{\mathbf{S}}_m$.

For an appropriate choice of fugacity factors $\langle n_{i\sigma}\rangle_0 = \langle n_{i\sigma}\rangle = \frac{n_i}{2}$, and for $\langle \hat{\mathbf{S}}_i \cdot \hat{\mathbf{S}}_j\rangle = g_{ij}^{s,xy}\langle S_i^+ S_j^- + S_i^- S_j^+\rangle_0 + g_j^{s,z}\langle S_i^z\rangle_0\langle S_j^z\rangle_0 + g_{ij}^{s,\uparrow}\langle \hat{c}_{j\uparrow}^\dagger \hat{c}_{i\uparrow}\rangle_0\langle \hat{c}_{j\uparrow}\hat{c}_{i\uparrow}^\dagger\rangle_0 + g_{ij}^{s,\downarrow}\langle \hat{c}_{j\downarrow}^\dagger \hat{c}_{i\downarrow}\rangle_0\langle \hat{c}_{j\downarrow}\hat{c}_{i\downarrow}^\dagger\rangle_0$ Wing-Ho Ko et al. [3] obtain the following GFs:

$$
\begin{aligned}
g_{ij}^{t} &= \sqrt{\frac{2\delta_i}{1+\delta_i}}\sqrt{\frac{2\delta_j}{1+\delta_j}} \\
g_{ij}^{s,xy} &= \sqrt{\frac{2}{1+\delta_i}}\sqrt{\frac{2}{1+\delta_j}} \\
g_{ij}^{s,z} &= g_{ij}^{s,\uparrow} = g_{ij}^{s,\downarrow} = 1
\end{aligned}
\tag{4.19}
$$

To restore rotational invariance most authors set $g_{ij}^{s,z} = g_{ij}^{s,\uparrow} = g_{ij}^{s,\downarrow} = g_{ij}^{s,xy}$.
This chapter illustrates some of the problems of the GA, where the most serious problem is how to make the GA site dependent. The rewriting leading to (4.11) imply the inclusion of a fugacity factor in the Gutzwiller projecter. The inclusion of a fugacity factor, however, only serves to give meaning to the rewriting, and there is no reason why the fugacity factor should be chosen to fulfill the relation $\langle n_\sigma\rangle_0 = \langle n_\sigma\rangle$ and not another relation. Thus the physics should not depend on the choice of fugacity factor.

Chapter 5

The Extended Gutzwiller Approximation

The former chapter discussed the original Gutzwiller approximation as introduced to HTSC by ref. [7]. This chapter will extend the GA following Ogata and Himeda in ref. [4]. The following derivation assumes a homogeneous system; however the extended Gutzwiller factors will be interpreted as site dependent in section 5.6, inspired by the site dependent original Gutzwiller factors in the former chapter. The idea behind the extension of the GA is to allow for not combinatorial correlations to influence the Gutzwiller factors. The most important consequence of the extension is the anisotropy between g^z and g^{xy}. The anisotropy between g^z and g^{xy} is necessary if AF-order is to be treated reliable within the GA. The Gutzwiller factors can be defined as:

$$g^{\hat{O}} = \frac{\langle \hat{O} \rangle}{\langle \hat{O} \rangle_0}. \tag{5.1}$$

From (5.1) the Gutzwiller factors can be calculated by VMC.This was done by Himeda and Ogata in ref. [8] and the result for zero doping can be seen in figure 5.1. From figure 5.1 the anisotropy is clear when AF-order is present.

5.1 The Original Gutzwiller Approximation

The method used by Ogawa et al. [1] to derive the original GA is straightforward to extend. In order to extend the GA the original GA is first derived following Ogawa et al.[1] and then extenden in the next section.
The expectation value of an operator $\hat{O}$ is given by:

$$\langle \hat{O} \rangle = \frac{\langle \Psi | \hat{O} | \Psi \rangle}{\langle \Psi | \Psi \rangle}. \tag{5.2}$$

The denominater, in (5.2), can be rewritten as follows:

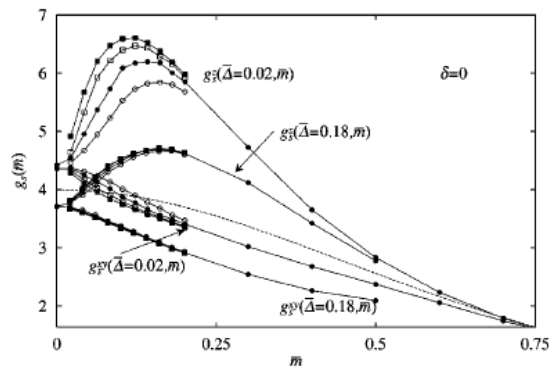

Figure 5.1: From ref. [8]. m-dependence at half filling of g_s^{xy} and g_s^z with delta fixed $\bar{\Delta} = 0.02, 0.18$. g_s^{xy} and g_s^z are calculated numerically using VMC results. Open circles are calculated on a 8X8 system, filled circles on a 10X10 system and filled squares on a 14X14 system. The broken line is the original g_s with AF order.

$$\begin{aligned}\langle\Psi|\Psi\rangle &= \langle\Psi_0|\mathbf{PP}|\Psi_0\rangle = \langle\Psi_0|\mathbf{P}|\Psi_0\rangle \\ &= \langle\Psi_0|\prod_i(1-n_{i\uparrow}n_{i\downarrow})|\Psi_0\rangle \\ &= \langle\Psi_0|\prod_i\left(n_{i\uparrow}(1-n_{i\downarrow})+n_{i\downarrow}(1-n_{i\uparrow})+(1-n_{i\uparrow})(1-n_{i\downarrow})\right)|\Psi_0\rangle \quad (5.3)\end{aligned}$$

$|\Psi_0\rangle$ can be written as a superposition of number-states and therefore the expansion in (5.3) can be rewritten as a sum of all possible configurations where each lattice site is occupied either by a single spin-up electron, a single spin-down electron, or is vacant:

$$\langle\Psi|\Psi\rangle = \sum_{config.}\langle\Psi_0|\prod_{i\in A}n_{i\uparrow}(1-n_{i\downarrow})\prod_{i\in B}n_{i\downarrow}(1-n_{i\uparrow})\prod_{i\in C}(1-n_{i\uparrow})(1-n_{i\downarrow})|\Psi_0\rangle \quad (5.4)$$

where A is the subset of lattice sites only occupied by a single spin up electron, B is the subset of lattice sites only occupied by a single spin down electron, and, finally, C is the subset of vacant lattice sites.
(5.4) can in principle be calculated exactly, using Wick's theorem. But in the original Gutzwiller approximation, only the site centered expectation values are taking in to account:

$$\sum_{config.}\prod_{i\in A}\langle n_{i\uparrow}(1-n_{i\downarrow})\rangle_0\prod_{i\in B}\langle n_{i\downarrow}(1-n_{i\uparrow})\rangle_0\prod_{i\in C}\langle(1-n_{i\uparrow})(1-n_{i\downarrow})\rangle_0 \quad (5.5)$$

Thus the denominator in (5.2) is given by

$$\langle\psi|\psi\rangle = \frac{N!}{N_A!N_B!N_C!}\omega_A^{N_A}\omega_A^{N_B}\omega_C^{N_C} \tag{5.6}$$

where the coefficient $\left(\frac{N!}{N_A!N_B!N_C!}\right)$ comes from counting the number og configurations. There are N sites, which gives $N!$ different configurations; however, swapping two sites with the same species of occupation leads to the same configuration. There are $N_A!$ ways to swap two up electrons, and the same applies to down electrons and empty sites. This leads to a total of $\frac{N!}{N_A!N_B!N_C!}$ different configurations. N_A (N_B) is the number of up (down) electrons and N_C is the number of empty sites;

and where ω_A in (5.6) is the weight of a site belonging to the subset A. Thus ω_A is defined by

$$\omega_A \equiv \langle n_{i\uparrow}(1-n_{i\downarrow})\rangle_0 = \frac{n}{2}(1-\frac{n}{2}) = \frac{1-\delta^2}{4} \tag{5.7}$$

n is the average electron density, $n = \frac{N}{N_e}$; and δ is the average hole density given by $\delta = (1-n)$. Likewise ω_B and ω_C are the weights of sites belonging to the subsets B and C respectably, where $\omega_B = \omega_A$ and $\omega_C = \left(1-\frac{n}{2}\right)^2 = \frac{(1+\delta)^2}{4}$.
For a two site operator $\hat{O}_{lm}$ [1] the nominator in (5.2) is given by:

$$\begin{aligned}
\langle\Psi_0|\hat{O}_{lm}\mathbf{PP}|\Psi_0\rangle &= \langle\Psi_0|\hat{O}_{lm}\prod_{i\neq l,m}\left(n_{i\uparrow}(1-n_{i\downarrow}) + n_{i\downarrow}(1-n_{i\uparrow}) + (1-n_{i\uparrow})(1-n_{i\downarrow})\right)|\Psi_0\rangle \\
&= \sum_{config.}\langle\hat{O}_{lm}\rangle_0\prod_{i\in A'}\langle n_{i\uparrow}(1-n_{i\downarrow})\rangle_0\prod_{i\in B'}\langle n_{i\downarrow}(1-n_{i\uparrow})\rangle_0\prod_{i\in C'}\langle(1-n_{i\uparrow})(1-n_{i\downarrow})\rangle_0 \\
&= \frac{(N-2)!}{N_{A'}!N_{B'}!N_{C'}!}\omega_A^{N_{A'}}\omega_B^{N_{B'}}\omega_C^{N_{C'}}\langle\hat{O}_{lm}\rangle_0
\end{aligned} \tag{5.8}$$

5.1.1 The Gutzwiller factor for $S_l^+S_m^-$

The Gutzwiller factor for $S_l^+S_m^-$ can now be calculated. As the material is not magnetic there has to be an equal amount of up and down spin electrons, thus $N_A = N_B = \frac{N_e}{2}$. The total number of electrons and holes must equal the total number of sites, which gives the relation $N_A + N_B + N_C = N$; thus $N_C = N - N_e$. The sites l and m contain one spin-op electron and one spin-down electron, thus $N_{A'} = N_{B'} = \frac{N_e}{2} - 1$ and $N_{C'} = N_C = N - N_e$. Insertion of these values in (5.8) gives the Gutzwiller factor below:

[1] In fact, it is for the operator $(1-n_{\uparrow l}n_{\downarrow l})(1-n_{\uparrow m}n_{\downarrow m})\hat{O}_{lm}(1-n_{\uparrow l}n_{\downarrow l})(1-n_{\uparrow m}n_{\downarrow m})$

$$
\begin{aligned}
g^{s,xy} &= \frac{\frac{(N-2)!}{N_{A'}!N_{B'}!N_{C'}}\omega_A^{N_{A'}}\omega_B^{N_{B'}}\omega_C^{N_{C'}}}{\frac{N!}{N_A!N_B!N_C}\omega_A^{N_A}\omega_A^{N_B}\omega_C^{N_C}} \\
&= \frac{N_A N_B \omega_A^{-1}\omega_B^{-1}}{N(N-1)} \\
&= \frac{\frac{N_e}{2}\frac{N_e}{2}}{N(N-1)}\frac{4*4}{(1-\delta^2)^2} = \frac{4(1-\delta)^2}{(1-\delta)^2(1+\delta)^2} = \frac{4}{(1+\delta)^2}
\end{aligned}
\tag{5.9}
$$

In the absence of AF-order the rotational invariance of the spin gives $g^{s,z} = g^{s,xy}$.

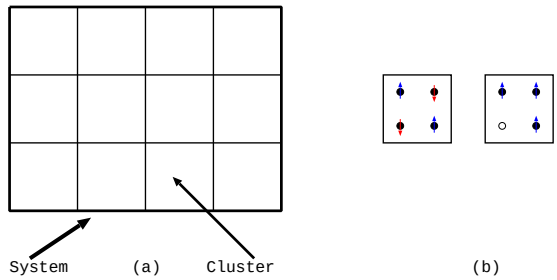

Figure 5.2: (a): The entire system contains N sites. The system is divided into clusters all containing N_c sites. Thus there are $\frac{N}{N_c}$ clusters in the system. (b): Each site in a cluster can be in 3 different states (occupied by an up/down spin electron or vacant), thus a cluster can be in $K = 3^{N_c}$ different states.

5.1.2 The Extended Gutzwiller Approximation

In the extendend Gutzwiller Approximation the none site diagonal expectation values are taken into account. This is done simply by a replication of the derivaton of the simple Gutzwiller Approximation, the difference being that the system is divided into clusters each containing N_c sites. This means instead of each site belonging to a subset depending on its occupation of an (up/down)-electron or a hole,
each cluster can now be in $K = 3^{N_c}$ different states. Each state is labelled by an index $i \in [1, K]$, and the number of clustters ind i'th state is labelled N_i. Thus in the extended Gutzwiller approximation the denominator in (5.2) is approximated as

$$\langle \Psi | \Psi \rangle = \sum_{config.} \prod_{i=1}^{K} \omega_i^{N_i}$$

where ω_i is the weight of a cluster in the i'th state. Explicitly the weight ω_i is defined as

$$\omega_i \equiv \langle \Psi_0 | \prod_{j \in A} n_{j\uparrow}(1 - n_{j\downarrow}) \prod_{j \in B} n_{j\downarrow}(1 - n_{j\uparrow}) \prod_{j \in C} (1 - n_{i\uparrow})(1 - n_{j\downarrow}) | \Psi_0 \rangle \qquad (5.10)$$

with j being the sites in the cluster.
The summing up is over all possible configurations of clusters in different states. Similar to the original Gutzwiller approximation, the summation is carried out by counting the number of configuratins.
There are $\frac{N}{N_c}$ clusters in the whole system; and there are $N_i!$ ways to swap two clusters in the same state. Thus there are $\frac{\frac{N}{N_c}!}{\prod_{i=1}^{K} N_i!}$ different configurations. N_i is only constrained by the demand, that the total number of up(down)-electrons

has to be $\frac{N_e}{2}$, where N_e is the total number of electons in the system, and the total number of holes has to be $N - N_e$.

$$\sum_{i=1}^{K} n_{\uparrow i} N_i = \frac{N_e}{2}, \quad \sum_{i=1}^{K} n_{\downarrow i} N_i = \frac{N_e}{2} \quad \text{and} \quad \sum_{i=1}^{K} n_{hi} N_i = N - N_e \tag{5.11}$$

where $n_{(\uparrow/\downarrow/h)i}$ is the number of up/down -electrons and holes in a cluster in the i'th state. Because the constraints are insufficient to determine N_i, a summing up over all possible values of N_i under the constraints (5.11) is still necessary

$$\sum_{\{N_i\}} \frac{\frac{N}{N_c}!}{\prod_{i=1}^{K} N_i!} \prod_{i=1}^{K} \omega_i^{N_i}. \tag{5.12}$$

The summation in (5.12) is heavy to compute. N is a very large number, thus the summation is well approximated by its largest term.
To find the largest term under the constraints (5.11), the Lagrange multipliers $\mu_\downarrow$, $\mu_\uparrow$ and λ are introduced in the function

$$\begin{aligned} f(N_i) &= ln\left(\frac{\frac{N}{N_c}!}{\prod_{i=1}^{K} N_i!} \prod_{i=1}^{K} \omega_i^{N_i}\right) - \mu_\downarrow \left(\sum_{i=1}^{K} n_{\downarrow i} N_i - \frac{N_e}{2}\right) \\ &\quad -\mu_\uparrow \left(\sum_{i=1}^{K} n_{\uparrow i} N_i - \frac{N_e}{2}\right) - \lambda \left(\sum_{i=1}^{K} n_{hi} N_i - (N - N_e)\right) \end{aligned} \tag{5.13}$$

The function $f(N_i)$ is then partial differentiated[2] with respect to N_i.

$$\begin{aligned} \frac{\partial f(N_i)}{\partial N_i} &= -\frac{\partial ln(N_i!)}{\partial N_i} + ln(\omega_i) - mu_\uparrow n_{\uparrow i} - mu_\downarrow n_{\downarrow i} - \lambda n_{hi} \\ &= -ln(N_i) + ln(\omega_i) - mu_\uparrow n_{\uparrow i} - mu_\downarrow n_{\downarrow i} - \lambda n_{hi} \end{aligned} \tag{5.14}$$

The largest term is then found by setting $\frac{\partial f(N_i)}{\partial N_i} = 0$. Thus the N_i that gives the largest term is given by:

$$\overline{N_i} = \omega_i exp(-\mu_\uparrow - \mu_\downarrow - \lambda_{nhi})$$

[2] Srinivasa Ramanujan showed

$$ln(n!) \approx ln(n)n - n + \frac{ln(n(1 + 4n(1 + 2n)))}{6} + \frac{ln(\pi)}{2}$$

and thus ignoring, that $n!$ is a step function and therefore not differentiable

$$\frac{\partial ln(n!)}{\partial n} = ln(n) + 1 - 1 + \frac{6(1 + 8n + 24n^2)}{n + 4n^2 + 8n^3} \approx ln(n)$$

Because a cluster has N_c sites, $n_{\uparrow i} + n_{\downarrow i} + n_{hi} = N_c$, and it is clear from the symmetry between up and down spins that $\mu_\uparrow = \mu_\downarrow$. Using this, $\overline{N_i}$ can be rewritten as:

$$\overline{N_i} = \omega_i e^{-\mu N_c} e^{(\mu-\lambda)n_{hi}}$$

It is convenient to introduce the new variables W and p

$$e^{-\mu N_c} \equiv \frac{N}{N_c}\frac{1}{W}, \quad e^{\mu-\lambda} \equiv p.$$

In terms of the variables W and p, $\overline{N_i}$ becomes

$$\overline{N_i} = \frac{N}{N_c}\frac{\omega_i}{W} p^{n_{hi}}.$$

The constraints in (5.11) are equivalent to

$$\sum_{i=1}^{K} \overline{N_i} = \frac{N}{N_c}, \quad \sum_{i=1}^{K} n_{hi}\overline{N_i} = N - N_c.$$

In terms of the variables W and p, the constraints in (5.11) can be rewritten as

$$\sum_{i=1}^{K} \frac{\omega_i}{W} p^{n_{hi}} = 1, \quad \sum_{i=1}^{K} n_{hi}\frac{\omega_i}{W} p^{n_{hi}} = 1. \tag{5.15}$$

It is also convenient to group all the possible states of a cluster by the number of holes they contain. For reference such subgroups are called j-hole sectors. The total weight of an j-hole sector is given by:

$$W_j \equiv \sum_{\text{i with j holes}} \omega_i.$$

Using W_j the constraints in (5.15) can be rewritten as

$$\sum_{j=0}^{N_c} \frac{W_j}{W} p^j = 1, \quad \sum_{j=0}^{N_c} j\frac{W_j}{W} p^j = \delta N_c. \tag{5.16}$$

The first of the constraints is equivalent to $W = \sum_j W_j p^j$, which shows that W represents the total weight.

The Numerator

In the extended Gutzwiller Approximation the numerator in (5.2) is evaluated in the same way as the denominator.
Consider an operator which operates on two sites inside a cluster in the i_0-th state, for reference this cluster is called the central cluster; then all of the configurations

of the remaining clusters are classified by N_i'. Equivalent to (5.12) $\langle\Psi|\hat{O}|\Psi\rangle$ can be rewritten as

$$\langle\Psi|\hat{O}|\Psi\rangle = \sum_{i_0}\sum_{\{N_i'\}} \frac{\left(\frac{N}{N_c}-1\right)!}{\prod_{i=1}^{K} N_i'!} \prod_{i=1}^{K} \omega_i^{N_i'} \langle\hat{O}\rangle_{i_0} \tag{5.17}$$

where $\langle\hat{O}\rangle_{i_0}$ means the expectation value of $\hat{O}$ together with the projection operator inside the cluster considered e.i.

$$\begin{aligned}\langle\hat{O}\rangle_{i_0} = & \\ & \langle\Psi_0|\prod_{j\in A} n_{j\uparrow}(1-n_{j\downarrow})\prod_{j\in B} n_{j\downarrow}(1-n_{j\uparrow})\prod_{j\in C}(1-n_{i\uparrow})(1-n_{j\downarrow})\hat{O}_{lm} \\ & \prod_{j\in A} n_{j\uparrow}(1-n_{j\downarrow})\prod_{j\in B} n_{j\downarrow}(1-n_{j\uparrow})\prod_{j\in C}(1-n_{i\uparrow})(1-n_{j\downarrow})|\Psi_0\rangle \end{aligned} \tag{5.18}$$

Becaus $\{N_i'\}$ represents the number of clusters in the i-th state, except for the central cluster, the constraints for $\{N_i'\}$ are modified accordingly, compared to the constraints for N_i in (5.11).

$$\begin{aligned}&\sum_{i=1}^{K} n_{\uparrow i}N_i' = \frac{N_e}{2} - n_{\uparrow i_0}, \quad \sum_{i=1}^{K} n_{\downarrow i}' N_i = \frac{N_e}{2} - n_{\downarrow i_0} \quad \text{and} \\ &\sum_{i=1}^{K} n_{hi}N_i' = N - N_e - n_{hi_0}\end{aligned} \tag{5.19}$$

The summation in (5.17) is over alle possible values of N_i', and is approximated by the largest term as was the case for the denorminator. Repetition of the same calculation, as with the denominator, gives the N_{i_0} which gives the largest term:

$$\overline{N_i'} = \frac{N}{N_c}\frac{\omega_i}{W'}p'^{n_{hi}}$$

W' and p' are slightly different from W and P due to the different constraints. Due to the constraints (5.19) $\overline{N_i'}$ fulfils the relations

$$\sum_{i}^{K} \overline{N_i'} = \frac{N}{N_c} - 1, \quad \sum_{i=1}^{K} n_{hi}\overline{N_i'} = N - N_e - n_{hi_0}.$$

Looking at the difference between $\overline{N_i'}$ and $\overline{N_i}$, $\Delta\overline{N_i'} = \overline{N_i'} - \overline{N_i}$, gives the relations

$$\sum_{i=1}^{K} \Delta\overline{N_i} = -1, \quad \sum_{i=1}^{K} n_{hi}\Delta\overline{N_i} = -n_{hi_0}$$

Using this relation the expectation value (5.2) can be calculated.

$$
\begin{aligned}
\langle \hat{O} \rangle &= \frac{\langle \Psi | \mathbf{P} \hat{O} \mathbf{P} | \Psi \rangle}{\langle \Psi | \mathbf{P}\mathbf{P} | \Psi \rangle} \\
&= \sum_{i_0} \frac{N_c}{N} \prod_{i=1}^{K} \frac{\overline{N_i}!}{\overline{N_i'}!} \prod_{i=1}^{K} \omega_i^{\overline{N_i'}-\overline{N_i}} \langle \hat{O} \rangle_{i_0} \\
&= \sum_{i_0} \frac{N_c}{N} \prod_{i=1}^{K} \left(\frac{\overline{N_i}}{\omega_i} \right)^{-\Delta \overline{N_i}} \langle \hat{O} \rangle_{i_0} \\
&= \sum_{i_0} \frac{N_c}{N} \prod_{i=1}^{K} \left(\frac{N}{N_c} \frac{p^{hi}}{W} \right)^{-\Delta \overline{N_i}} \langle \hat{O} \rangle_{i_0} \\
&= \sum_{i_0} \frac{N_c}{N} \left(\frac{N}{N_c} \frac{1}{W} \right)^{-\sum \Delta \overline{N_i}} \times p^{-\sum n_{hi} \Delta \overline{N_i}} \langle \hat{O} \rangle_{i_0} \\
&= \sum_{i_o} \frac{p^{hi_0}}{W} \langle \hat{O} \rangle_{i_0} \qquad (5.20)
\end{aligned}
$$

To summarise; In the last section a general formula for $\langle \hat{O} \rangle$ was derived and is stated (5.20). what is left is to evaluate p^{hi_0}, W and $\langle \hat{O} \rangle_{i_0}$. The first step is to evaluate ω_i given in (5.10) using Wick's Theorem, then W and p^{hi_0} can be found from the constraints in (5.15), and finally $\langle \hat{O} \rangle_{i_0}$ is also found using Wick's Theorem.

5.1.3 The Gutzwiller Factors at Half Filling

The derivation of the Gutzwiller Factors at half filling requires evaluation of W_0. This is done under the assumption that the correction to the original Gutzwiller factor, which only takes site-centered expectation values into account, is small. Considering the relative good agreement between VMT and the original Gutzwiller Approximation, especially without AF order, this is justifiable[34]. The nearest-neighbor expectation values that are going to be included are

$$\begin{aligned}\Delta_{ij\sigma} &= \sigma\langle\Psi_0|c_{i\sigma}c_{j\bar{\sigma}}|\Psi_0\rangle \\ \chi_{ij\sigma} &= \langle\Psi_0|c^\dagger_{i\sigma}c_{j\sigma}|\Psi_0\rangle.\end{aligned} \tag{5.21}$$

Both $\Delta_{ij\sigma}$ and $\chi_{ij\sigma}$ are treated as homogeneous; so $\chi_{ij\uparrow} = \chi_{ij\downarrow} = \chi$, and $\Delta_{ij\uparrow} = -\Delta_{ij\downarrow} = \Delta$. The sloppy notation $\Delta\Delta^* = \Delta^2$ will be used in the rest of the thesis. W_0 is given by:

$$\begin{aligned}W_0 &= \sum_{s \text{ with no holes}} \omega_s \\ &= \sum_s \langle \prod_{i\in A} \hat{n}_{i\uparrow}(1-\hat{n}_{i\downarrow}) \prod_{i\in B} \hat{n}_{i\downarrow}(1-\hat{n}_{i\uparrow})\rangle_0.\end{aligned} \tag{5.22}$$

The site centered expectation value gives:

$$\omega_i^0 = [r(1-w)]^{N_{right}}\,[w(1-r)]^{N_{wrong}} \tag{5.23}$$

where $N_{right}(N_{wrong})$ is the number of electrons with the right(wrong) direction of spin. The right(wrong) direction of spin is dependent on which of the two sublattices, 1 and 2, the electron is located on. The sublattices are distinguished by the presence of AF order. For sublattice 1 with positive magnetization m the quantities r and w are defined as:

$$\begin{aligned}r &\equiv \langle \hat{n_{i\uparrow}}\rangle_0 = \frac{n}{2} + m \\ w &\equiv \langle \hat{n_{i\downarrow}}\rangle_0 = \frac{n}{2} - m\end{aligned} \tag{5.24}$$

r and w are exchanged for sublattice 2. The magnetization is defined as, $m_i = \langle\Psi_0|\hat{S}_i^z|\Psi_0\rangle$

Thus summing over all the different states, with different numbers of right and wrong spins, the zero order contribution to W_0, with respect to Δ and χ, becomes:

$$W_0^0 = [r(1-w) + w(1-r)]^{N_c} \tag{5.25}$$

In the next order with respect to Δ and χ, expecation values of bonds in the cluster contribute to W_0. As an example, consider a bond connecting to neighboring

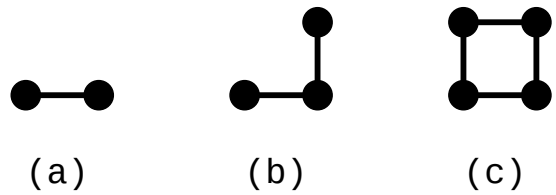

Figure 5.3: Real-space diagrams for the evalution of W_0. The diagram in (a) is taken into account, while the diagrams in (b) and (c) are neglected.

sites i and j (see figure 5.3.a) where both are occupied by a spin-up electron. The expectation value of this bond is then given by

$$P_{\uparrow\uparrow} = \langle (1-\hat{n}_{i\downarrow})\hat{n}_{i\uparrow}\hat{n}_{j\uparrow}(1-\hat{n}_{j\downarrow})\rangle_0.$$

For $P_{\sigma\sigma'}$ the convention, that the spin to the left is on sublattice 1 and that to the right is on sublattice 2, is used.
A calculation of $P_{\uparrow\uparrow}$ using Wick's theorem gives:

$$\begin{aligned} P_{\uparrow\uparrow} = {} & rw(1-r)(1-w) - (1-w)w\Delta^2 - (1-r)r\Delta^2 \\ & -(1-w)(1-r)\chi^2 - rw\chi^2 + (\chi^2+\Delta^2)^2 \end{aligned} \tag{5.26}$$

Besides $P_{\uparrow\uparrow}$, 3 more combinations contribute to W_0^1. $P_{\downarrow\downarrow}, P_{\uparrow\downarrow}$ and $P_{\downarrow\uparrow}$ are calculated the same way:

$$P_{\downarrow\downarrow} = P_{\uparrow\uparrow} \tag{5.27}$$
$$P_{\uparrow\downarrow} = r^2(1-w)^2 + 2r(1-w)\chi^2 + r^2\Delta^2 + (1-w)^2\Delta^2 + (\chi^2+\Delta^2)^2 \tag{5.28}$$
$$P_{\downarrow\uparrow} = w^2(1-r)^2 + 2w(1-r)\chi^2 + w^2\Delta^2 + (1-r)^2\Delta^2 + (\chi^2+\Delta^2)^2 \tag{5.29}$$

The sum of all these contributions gives:

$$P_{\uparrow\uparrow} + P_{\downarrow\downarrow} + P_{\uparrow\downarrow} + P_{\downarrow\uparrow} = (n-2rw)^2 + X \tag{5.30}$$

where

$$X = 2\delta^2(\Delta^2-\chi^2) + 8m^2(\chi^2+\Delta^2) + 4(\chi^2+\Delta^2)^2$$

and the relations $r = n/2 + m$ and $w = n/2 - m$ have been used. The first term in (5.30) belongs to W_0^0. Thus

$$W_0^1 = N_b X (n-2rw)^{N_c-2} \tag{5.31}$$

where N_b is the number of bonds in a cluster, X is the contribution from the bond, and $(n-2rw)^{N_c-2}$ is the contribution from the rest of the sites in the cluster. The contribution with 2 bonds is approximated as.

$$W_0^2 =_{N_b} C_2 X^2 (n-2rw)^{N_c-4} \tag{5.32}$$

where ${}_{N_b}C_2 = \frac{N_b!}{(N_b-2)!2!}$ is the number of ways to pick out two bonds of N_b bonds. In the same way the higher order terms are approximated

$$W_0 = \sum_{j=0}^{N_b} {}_{N_b}C_j X^j (n-2rw)^{N_c-2j} = (n-2rw)^{N_c}\left(1+\frac{X}{(n-2rw)^2}\right)^{N_b}$$

where the binomial theorem have been used to sum up the series. In the derivation of eq. (5.1.3) three assumptions are made; the contribution from the two diagrams (a) and (b) in figure 5.3 are expected to be small enough that they can be neglected[4]((b) is of the order $N_b\delta^2\chi^4$ or $N_b m^2\chi^4$ which is smaller than W_0^1 and (c) is of the order $X^2 N_b$, which is smaller than W_0^2 by a factor of $\frac{1}{N_b}$); and the number of bonds are not given by ${}_{N_b}C_j$ due to their overlapping, however the change for to bonds overlapping is small for $j >> N_b$ and X is of the order $\frac{1}{20}$, so for j large X^j keeps the error small.

The Gutzwiller Factor For $\langle S_l^+ S_m^- \rangle$ at Half Filling

The general formula (5.20) for the expansion of $\langle S_l^+ S_m^- \rangle$ gives

$$\langle S_l^+ S_m^- \rangle = \sum_{i_0} \frac{1}{W_0} \langle S_l^+ S_m^- \rangle_{i_0} \tag{5.33}$$

$\langle S_l^+ S_m^- \rangle_{i_0}$ is evaluated following the same scheme as for W_0. Hence the zero order and the first order term are given by.

$$\langle S_l^+ S_m^- \rangle_{i_0}^0 = (n-2rw)^{N_c-2} \langle S_l^+ S_m^- \rangle_0 \tag{5.34}$$

$$\langle S_l^+ S_m^- \rangle_{i_0}^1 = \tilde{N}_b X (n-2rw)^{N_c-4} \langle S_l^+ S_m^- \rangle_c \tag{5.35}$$

$\tilde{N}_b$ is the number of bonds not connected to the two sites l and m. For large enough clusters the possibility can be ignored for l and m situated on the edge. For later reference ignoring the possibility of a site situated on or near the edge is called "the large cluster approximation". Thus $\tilde{N}_b = N_b - 7$, as is evident from figure 5.4.
$\langle S_l^+ S_m^- \rangle_c$ is the connected expectation value; i.e., the expectation value of $S_l^+ S_m^-$ together with terms like $\hat{n}_{m'\sigma}(1-\hat{n}_{m'\bar{\sigma}})$ excluding the disconnected term, where m' is a nearest neighbour to m or l. But, since $\langle S_l^+ S_m^- \rangle_c \hat{n}_{m'\sigma}(1-\hat{n}_{m'\bar{\sigma}})\rangle_c = 0$ [3], then $\langle S_l^+ S_m^- \rangle_c = \langle S_l^+ S_m^- \rangle_0$, as will be shown later. This is the origin of the enhancment of $g^{s,z}$, because $\langle S_l^z S_m^z \rangle_c \neq \langle S_l^z S_m^z \rangle_0$.

[3] All contractions are of the type:

$$\langle c^\dagger_{m\sigma} c_{m\bar{\sigma}} c^\dagger_{m'\sigma'} c_{m'\sigma'} \rangle = \Delta_\sigma \delta_{\sigma\bar{\sigma'}} \Delta^*_{\bar{\sigma}} \delta_{\sigma\sigma'} - \chi_\sigma \delta_{\sigma\sigma'} \chi^*_{\bar{\sigma}} \delta_{\bar{\sigma}\sigma'} = 0$$

as the two delta functions can not be fulfiled at the same time in each term.

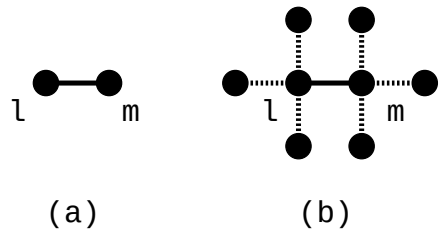

Figure 5.4: Real-space diagrams for the calculation of $\langle S_l^+ S_m^- \rangle$. (a) to zero order $\langle S_l^+ S_m^- \rangle_0$ contributes. (b) to first order the connected expectation value $\langle S_l^+ S_m^- \rangle_c$ contributes. The connected expectation value is here used as the expectation value of $S_l^+ S_m^-$ together with terms like $\hat{n}_{m'\sigma}(1-\hat{n}_{m'\bar{\sigma}})$ excluding the disconnected term, where m' is a nearest neighbour to m or l.

Analogues to W_0 the higher-order terms are approximated as

$$\langle S_l^+ S_m^- \rangle_{i_0}^2 =_{\tilde{N}_b} C_j X^j (n-2rw)^{\tilde{N}_c - 2j} \tag{5.36}$$

And thus summing up all the contributions

$$\begin{aligned}\sum_i \langle S_l^+ S_m^- \rangle_{i_0} &= \langle S_l^+ S_m^- \rangle_0 \left\{ (n-2rw)^{N_c} + \tilde{N}_b X (n-2rw)^{N_c-4} \dots \right\} \\ &= \langle S_l^+ S_m^- \rangle_0 (n-2rw)^{N_c} \left(1 + \frac{X}{(n-2rw)^2} \right)^{\tilde{N}_b}\end{aligned} \tag{5.37}$$

Then following (5.20)

$$\langle S_l^+ S_m^- \rangle = \frac{\langle S_l^+ S_m^- \rangle_0}{(n-2rw)^2} \left(1 + \frac{X}{(n-2rw)^2} \right)^{\tilde{N}_b - N_b} \tag{5.38}$$

And thus $g^{s,xy}$ is given by:

$$\begin{aligned} g^{s,xy} &= \frac{\langle S_l^+ S_m^- \rangle}{\langle S_l^+ S_m^- \rangle_0} = \frac{1}{(n-2rw)^2} \left(1 + \frac{X}{(n-2rw)^2} \right)^{\tilde{N}_b - N_b} \\ &= \frac{a^{\tilde{N}_b - N_b}}{(n-2rw)^2} \end{aligned} \tag{5.39}$$

where

$$a = \left(1 + \frac{X}{(n-2rw)^2} \right)$$

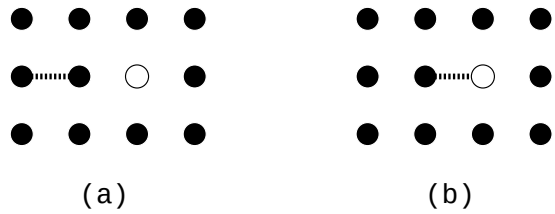

Figure 5.5: Real-space diagrams. To first order, where one bond present in each cluster, there are two possibilities: (a) the bond can connect two sites excluding the hole site or, (b) it can connect the hole site with a nearest-neighbor site

5.2 The Not Half Filled Case

In this section the calculation carried out for the half filled case is extended to the doped case. This calls for a calculation of W_i. This is done by first calculating the 1-hole sector and then generalising the result to the n-hole sector. The 1-hole sector is given by

$$W_1 = \sum_{\text{i with 1 hole}} \omega_i \tag{5.40}$$

In the lowest order of Δ and χ the 1-hole sector becomes

$$W_1 = N_c(1-r)(1-w)(n-2rw)^{N_c-1} \tag{5.41}$$

where $(1-r)(1-w)$ comes from the site diagonal weight of the hole, N_c comes from the number of different sites where the hole can be placed, and $(n-2rw)^{N_c-1}$ is just the site diagonal weight of the rest of the sites.
In the next order, where there is one bond present in each cluster, there are two possibilities. The bond can connect two sites excluding the hole site or it can connect the hole site with a nearest-neighbor site (see figure 5.5). In the first case the contribution to W_1^1 is given by:

$$N_c(1-r)(1-w)N_{B1}X(n-2rw)^{N_c-3} \tag{5.42}$$

where N_{B1} is the number of bonds not connected to the hole site. The contribution to W_1^1 from a bond connected to a hole site is given by:

$$\begin{aligned}&\langle(1-\hat{n}_{i\downarrow})(1-\hat{n}_{i\downarrow})(\hat{n}_{j\uparrow}(1-\hat{n}_{j\downarrow})+\hat{n}_{j\downarrow}(1-\hat{n}_{j\uparrow}))\hat{n}_{i\uparrow}\hat{n}_{j\uparrow}\rangle_0\\&=(n-2rw)(1-r)(1-w)+Y\end{aligned} \tag{5.43}$$

where i is the hole site and j is the nearest-neighbor site, and Y is given by:

$$Y = \delta(1+\delta)(\chi^2-\Delta^2) - 4m^2(\chi^2+\Delta^2) - 2(\chi^2+\Delta^2)^2. \tag{5.44}$$

Counting the possible configurations, the contribution to W_1^1 becomes

$$N_c(N_B - N_{B1})Y(n-2rw)^{N_c-2} \tag{5.45}$$

where the first term in (5.43) is absorbed into W_1^0. The higher-order terms are then approximated in the same way as was the case for W_0 in (5.32). Thus W_1 becomes:

$$\begin{aligned} W_1 &= N_c\left(\sum_j^{N_{1B}}(1-r)(1-w)X^j\frac{N_{B1}!}{(N_{1B}-j)!j!} + \sum_j^{\tilde{N}_{1B}}(N_B-N_{B1})YX^j\frac{\tilde{N}_{1B}!}{(\tilde{N}_{1B}-j)!j!}\right) \\ &= N_c\left((1-r)(1-w)(n-2rw)^{N_c-1}a^{N_{1B}} + (N_B-N_{B1})(n-2rw)^{N_c-2}Ya^{\tilde{N}_{1B}}\right) \end{aligned} \tag{5.46}$$

where $\tilde{N}_{1B}$ comes from the exclusion of possible position of X. Application of the large cluster approximation gives $\tilde{N}_{1B} = N_{1B} - 3$, thus

$$W_1 = N_C\left((1-r)(1-w) + \frac{(N_B-N_{B1})}{(n-2rw)}Ya^{-3}\right)(n-2rw)^{N_c-1}a^{N_{1B}}. \tag{5.47}$$

In the case of two holes in a cluster the same arguments as above leads to

$$W_2 =_{N_c} C_2\left((1-r)(1-w) + \frac{(N_B-N_{B1})}{(n-2rw)}Ya^{-3}\right)^2(n-2rw)^{N_c-2}a^{N_{2B}}. \tag{5.48}$$

where N_{2B} is the number of bonds not connected to the two hole sites. In (5.48) the terms where to holes are nearest neighbors, are negleced. It is clear from generalization of (5.47) and (5.48) that the case of j holes can be approximated as

$$W_j =_{N_c} C_j z^j(n-2rw)^{N_c-j}a^{N_{jB}}, \tag{5.49}$$

with

$$z = (1-r)(1-w) + \frac{(N_B-N_{B1})}{(n-2rw)}Ya^{-3} \tag{5.50}$$

W and p can now be determined from the constraints in (5.16). From the large cluster approximation $N_{jB} = N_B - j4$. Thus the constraints in (5.16) reads

$$\sum_j^{N_c}\frac{W_j}{W}p^j = \frac{1}{W}(n-2rw+pza^{-4})^{N_c}a^{N_B} = 1$$

$$\sum_j^{N_c}j\frac{W_j}{W}p^j = \frac{N_c}{W}pza^{-4}(n-2rw+pza^{-4})^{N_c-1}a^{N_B} = \delta N_c$$

thus giving the following expressions for W and p:

$$\begin{aligned} p &= \frac{\delta(n-2rw)}{nz}a^4 \\ W &= \left(\frac{n-2rw}{n}\right)^{N_c}a^{N_B} \end{aligned} \tag{5.51}$$

5.3 The Gutzwiller Approximaion For $\langle S_l^+ S_m^- \rangle$ In The Dopped Case.

The expectation value of $\langle S_l^+ S_m^- \rangle$ in the dopped case, is similar to the half-filled case given by the general formula in (5.20):

$$\langle S_l^+ S_m^- \rangle = \sum_{j=0}^{N_c-2} \frac{p^j}{W} \sum_{i_0 \text{ with j holes}} \langle S_l^+ S_m^- \rangle_{i_0}. \tag{5.52}$$

If the cluster considered has j holes the summation over different states of the cluster considered gives:

$$\begin{aligned} \sum_{i_0 \text{ with j holes}} \langle S_l^+ S_m^- \rangle_{i0} &= \sum_{i_0 \text{ with j holes}} \omega_i \langle S_l^+ S_m^- \rangle_0 \\ &= W_j \langle S_l^+ S_m^- \rangle_0 \\ &= {}_{N_c}C_j z^j (n-2rw)^{N_c-j} a^{N_{jB}} \langle S_l^+ S_m^- \rangle_0 \end{aligned} \tag{5.53}$$

Substituting p and W given in (5.51), as well as the summation given in (5.53), in the general formula given in (5.52) gives:

$$\begin{aligned} \langle S_l^+ S_m^- \rangle &= \sum_{j=0}^{N_c-2} \frac{p^j}{W} \sum_{i_0 \text{ with j holes}} \langle S_l^+ S_m^- \rangle_{i_0} \\ &= \frac{1}{W} (n - 2rw + pza^4)^{N_c-2} a^{\tilde{N}_B} \langle S_l^+ S_m^- \rangle_0 \\ &= \left(\frac{n}{n-2rw} \right)^2 a^{-(N_B - \tilde{N}_B)} \langle S_l^+ S_m^- \rangle_0 \end{aligned} \tag{5.54}$$

Since $N_B - \tilde{N}_B = 7$ the Gutzwiller factor $g^{s,xy}$ is:

$$g^{s,xy} = \frac{\langle S_l^+ S_m^- \rangle}{\langle S_l^+ S_m^- \rangle_0} = \left(\frac{n}{n-2rw} \right)^2 a^{-7} \tag{5.55}$$

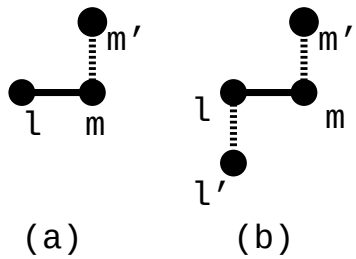

Figure 5.6: Real-space diagrams for the calculation of $\langle S_l^z S_m^z \rangle$. The connected expectation values of (a) and (b) give additional contributions to $g^{s,z}$ compared to $g^{s,xy}$.

5.4 The Enhancement of $g^{s,z}$ Compared to $g^{s,xy}$

$\langle S_l^z S_m^z \rangle$ is evaluated in the same manner as $\langle S_l^+ S_m^- \rangle$. The zero order contribution in Δ and χ is thus equivalent to (5.34)

$$\langle S_l^z S_m^z \rangle_{i_0}^0 = (n - 2rw)^{N_c - 2} \langle S_l^z S_m^z \rangle_0 \tag{5.56}$$

but in the next order the diagrams in figure 5.6 contribute to $\langle S_l^z S_m^z \rangle_{i0}$. Thus $\langle S_l^z S_m^z \rangle_{i_0} \neq \langle S_l^z S_m^z \rangle_0$ and $\langle S_l^z S_m^z \rangle_{i_0}$ is now given by:

$$\langle S_l^z S_m^z \rangle_{i_0} = \langle S_l^z S_m^z \rangle_0 + A_z + B_z \tag{5.57}$$

where A_z and B_z comes from the connected expectation value of the two diagrams in figure 5.6.
Calculating the connected expectation value of (a) in figure 5.6 gives:

$$\begin{aligned}
(a) &= \langle S_l^z S_m^z \big(\hat{n}_{m'\uparrow}(1 - \hat{n}_{m'\downarrow}) + \hat{n}_{m'\downarrow}(1 - \hat{n}_{m'\uparrow})\big)\rangle_c \\
&= \frac{\langle S_l^z \rangle}{2} \langle (\hat{n}_{m\uparrow} - \hat{n}_{m\downarrow}) \big(\hat{n}_{m'\uparrow}(1 - \hat{n}_{m'\downarrow}) + \hat{n}_{m'\downarrow}(1 - \hat{n}_{m'\uparrow})\big)\rangle_c \\
&= \frac{m}{2} \left(P_{\uparrow\uparrow} + P_{\downarrow\uparrow} - P_{\uparrow\downarrow} - P_{\downarrow\downarrow}\right) \\
&= -2m^2 X_2
\end{aligned} \tag{5.58}$$

where it has been assumed that l and m' are on sublattice 1. The contribution to $\sum_{i_0} \langle S_l^z S_m^z \rangle_{i_0}$ is

$$A_z = -4N_2 m^2 X_2 (1 - 2rw)^{N_c - 3} \tag{5.59}$$

where $N_2 = \frac{N_B - N_{B1-1}}{2}$ and is the number of bonds connected to the site m. The extra factor of two comes from the inclusion of a mirror image of diagram 5.6 (a) above. Likewise, the connected expectation value of the diagram in figure 5.6 (b) gives:

$$
\begin{aligned}
(b) &= \langle S_l^z \big(\hat{n}_{l'\uparrow}(1-\hat{n}_{l'\downarrow}) + \hat{n}_{l'\downarrow}(1-\hat{n}_{l'\uparrow})\big)\rangle_c \times \langle S_m^z \big(\hat{n}_{m'\uparrow}(1-\hat{n}_{m'\downarrow}) + \hat{n}_{m'\downarrow}(1-\hat{n}_{m'\uparrow})\big)\rangle_c \\
&= \frac{1}{4}\left(P_{\uparrow\uparrow} + P_{\downarrow\uparrow} - P_{\uparrow\downarrow} - P_{\downarrow\downarrow}\right)\left(-P_{\uparrow\uparrow} - P_{\downarrow\uparrow} + P_{\uparrow\downarrow} + P_{\downarrow\downarrow}\right) \\
&= -4m^2 X_2^2
\end{aligned} \tag{5.60}
$$

Since there are N_2^2 possible combinations of bonds connected to l and m, the contribution to $\sum_{i_0}\langle S_l^z S_m^z\rangle_{i_0}$ is

$$
B_z = -2N_2^2 m^2 X_2 (1-2rw)^{N_c-4}. \tag{5.61}
$$

The Higher-order terms are approximated and summed up following the same scheme as for $S_l^+ S_m^-$.

$$
\begin{aligned}
\langle S_l^z S_m^z\rangle = \frac{1}{W_0}\Big(&\langle S_l^z S_m^z\rangle_0 (n-2rw)^{N_c-2} a^{\tilde{N}_b} - 4N_2 m^2 X_2 (n-2rw)^{N_c-3} a^{\tilde{N'}_b} \\
&-2N_2 m^2 X_2 (n-2rw)^{N_c-4} a^{\tilde{N''}_b}\Big)
\end{aligned} \tag{5.62}
$$

$\tilde{N'}_b$ and $\tilde{N''}_b$ are the number of bonds that are not connected to the diagrams in figure 5.6 a and b. In the large cluster approximation, $\tilde{N'}_b$ and $\tilde{N''}_b$ are given by:

$$
\tilde{N'}_b = N_b - 10 \tag{5.63}
$$

$$
\tilde{N''}_b = N_b - 13. \tag{5.64}
$$

The Gutzwiller factor is defined as the ratio between the expectation value in the projected and preprojected Hilbert space, in this case however, they are not proportional to each other. Thus to obtain the Gutzwiller factor $g^{s,z}$ the preprojected expectation value is calculated:

$$
\langle S_l^z S_m^z\rangle_0 = -m^2 - \frac{X_2}{2}. \tag{5.65}
$$

Using this the Gutzwiller factor for $\langle S_l^z S_m^z\rangle$ becomes:

$$
g^{s,z} = g^{s,xy}\frac{1}{4m^2+2X_2}\left(1 + 4m^2\left(2X_2 + \frac{N_2 2X_2}{n-2rw}a^{-\tilde{N}_B-\tilde{N}'_B}\right)^2\right) \tag{5.66}
$$

where $\tilde{N}_B - \tilde{N}''_B = 2(\tilde{N}_B - \tilde{N}'_B)$ has been assumed.
In the large cluster approximation $N_B = 3$ and $\tilde{N}_B - \tilde{N}'_B = 3$, thus

$$
g^{s,z} = g^{s,xy}\frac{1}{4m^2+2X_2}\left(2X_2 + 4m^2\left(1 + \frac{6X_2}{n-2rw}a^{-3}\right)^2\right) \tag{5.67}
$$

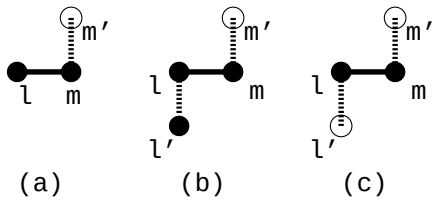

Figure 5.7: Real-space diagrams for the calculation of $\langle S_l^z S_m^z \rangle$ in the doped case. The connected expectation value of (a), (b) and (c) gives additional contributions to $g^{s,z}$ compared to $g^{s,xy}$.

5.5 The Gutzwiller Approximaion for $\langle S_l^z S_m^z \rangle$ in the Dopped Case.

In the doped case there are three new contributions to $\langle S_l^z S_m^z \rangle_0$. The contributions come from the connected expectation value of the diagrams in figure 5.7 where one of the neighbouring sites to l and/or m is occupied by a hole. The connected expectation value of S_i^z together with a neighbouring site occupied by a hole is:

$$\begin{aligned}
\langle S_i^z (1-\hat{n}_{i'\uparrow})(1-\hat{n}_{i'\downarrow})\rangle &= \frac{1}{2}\langle(\hat{n}_{i\uparrow}-\hat{n}_{i\downarrow})(1-\hat{n}_{i'\uparrow})(1-\hat{n}_{i'\downarrow}\rangle && (5.68)\\
&= \frac{1}{2}\Big(\langle\hat{n}_{i\uparrow}(1-\hat{n}_{i\downarrow})\hat{n}_{i'\downarrow}(1-\hat{n}_{i'\uparrow})\rangle && (5.69)\\
&\quad +\langle\hat{n}_{i\uparrow}(1-\hat{n}_{i\downarrow})\hat{n}_{i'\uparrow}(1-\hat{n}_{i'\downarrow})\rangle && (5.70)\\
&\quad -\langle\hat{n}_{i\downarrow}(1-\hat{n}_{i\uparrow})\hat{n}_{i'\downarrow}(1-\hat{n}_{i'\uparrow})\rangle && (5.71)\\
&\quad -\langle\hat{n}_{i\downarrow}(1-\hat{n}_{i\uparrow})\hat{n}_{i'\uparrow}(1-\hat{n}_{i'\downarrow})\rangle\Big) && (5.72)\\
&= \frac{1}{2}\Big(P_{\uparrow\uparrow}-P_{\downarrow\downarrow}-P_{\uparrow\downarrow}+P_{\downarrow\uparrow}\Big) = mX_2^2 && (5.73)
\end{aligned}$$

Thus the contribution from diagram (a) in figure 5.7 is m^2X_2 and the contribution from diagram (b) in figure 5.7 is $2m^2X_2^2$ and finally the contribution from diagram (c) in figure 5.7 is $-m^2X_2^2$.
Using these diagrams the 1-hole sector is:

$$\begin{aligned}
&\sum_{i_0 \text{ with 1 hole}} \langle S_l^z S_m^z \rangle \\
&= {}_{N_c-2}C_1 z(n-2rw)^{N_c-3} a^{\tilde{N}_{1B}} \\
&\quad -{}_{N_c-3}C_1 4N_2 m^2 X_2 z(n-2rw)^{N_c-4} a^{\tilde{N}_{1B}-3} \\
&\quad -{}_{N_c-4}C_1 4N_2^2 m^2 X_2^2 z(n-2rw)^{N_c-5} a^{\tilde{N}_{1B}-6} \\
&\quad +2N_2^2 m^2 X_2 (n-2rw)^{N_c-3} a^{\tilde{N}_B-3} \\
&\quad +4N_2^2 m^2 X_2 (n-2rw)^{N_c-4} a^{\tilde{N}_B-6} && (5.74)
\end{aligned}$$

And the two hole sector is:

$$
\begin{aligned}
&\sum_{i_0 \text{ with 1 hole}} \langle S_l^z S_m^z \rangle \\
&= {}_{N_c-2}C_2 z^2 (n-2rw)^{N_c-4} a^{\tilde{N}_{2B}} \\
&\quad - {}_{N_c-3}C_2 4 N_2 m^2 X_2 z^2 (n-2rw)^{N_c-5} a^{\tilde{N}_{2B}-3} \\
&\quad - {}_{N_c-4}C_2 4 N_2^2 m^2 X_2^2 z^2 (n-2rw)^{N_c-6} a^{\tilde{N}_{2B}-6} \\
&\quad + {}_{N_c-3}C_1 2 N_2^2 m^2 X_2 z (n-2rw)^{N_c-4} a^{\tilde{N}_{1B}-3} \\
&\quad + {}_{N_c-4}C_1 4 N_2^2 m^2 X_2 z (n-2rw)^{N_c-5} a^{\tilde{N}_{1B}-6} \\
&\quad \frac{N_2^2}{4} m^2 X_2^2 (n-2rw)^{N_c-4} a^{\tilde{N}_B-6}.
\end{aligned} \tag{5.75}
$$

Generalization to the to higher order contributions gives:

$$
\begin{aligned}
\langle S_l^z S_m^z \rangle &= \sum_{j=0}^{N_c-2} \frac{p^j}{W} \sum_{i_0 \text{ with j holes}} \langle S_l^z S_m^z \rangle_0 \qquad (5.76) \\
&= \frac{1}{W} \sum_{j=0}^{N_c-2} p^j \; {}_{N_c-2}C_j \langle S_l^z S_m^z \rangle_0 z^j (n-2rw)^{N_c-2-j} a^{\tilde{N}_{jB}} \\
&\quad - \frac{1}{W} \sum_{j=0}^{N_c-3} p^j \; {}_{N_c-3}C_j 2 N_2 m^2 2 X_2 z^j (n-2rw)^{N_c-3-j} a^{\tilde{N}_{jB}-3} \\
&\quad - \frac{1}{W} \sum_{j=0}^{N_c-3} p^j \; {}_{N_c-3}C_j 2 N_2 m^2 2 X_2 z^j (n-2rw)^{N_c-3-j} a^{\tilde{N}_{jB}-3} \\
&\quad - \frac{1}{W} \sum_{j=0}^{N_c-4} p^j \; {}_{N_c-4}C_j N_2^2 m^2 4 X_2^2 z^j (n-2rw)^{N_c-4-j} a^{\tilde{N}_{jB}-6} \\
&\quad + \frac{1}{W} \sum_{j=0}^{N_c-3} p^{j+1} \; {}_{N_c-3}C_j N_2 m^2 2 X_2 z^j (n-2rw)^{N_c-3-j} a^{\tilde{N}_{jB}-3} \\
&\quad + \frac{1}{W} \sum_{j=0}^{N_c-4} p^{j+1} \; {}_{N_c-4}C_j N_2^2 2 m^2 4 X_2^2 z^j (n-2rw)^{N_c-4-j} a^{\tilde{N}_{jB}-6} \\
&\quad - \frac{1}{W} \sum_{j=0}^{N_c-4} p^{j+2} \; {}_{N_c-4}C_j N_2^2 2 m^2 X_2^2 z^j (n-2rw)^{N_c-4-j} a^{\tilde{N}_{jB}-6} \\
&= \left(\frac{n}{n-2rw} \right)^2 a^{-(N_B-\tilde{N}_B)} \left[-\frac{X_2}{2} - m^2 \left\{ 1 + \frac{N_2 2 X_2 n}{n-2rw} \left(1 - \frac{p}{2} \right) a^{-3} \right\}^2 \right]
\end{aligned}
$$

Thus the Gutzwiller factor for $\langle S_l^z S_m^z \rangle$ is:

$$g^{s,z} = \frac{\langle S_l^z S_m^z \rangle}{\langle S_l^z S_m^z \rangle_0} = \frac{g^{s,xy}}{4m^2 + 2X_2} \left[2X_2 + 4m^2 \left\{ 1 + \frac{N_2 2X_2 n}{n - 2rw} \left(1 - \frac{p}{2} \right) a^{-3} \right\}^2 \right] \tag{5.77}$$

where it have been used that $\langle S_l^z S_m^z \rangle_0 = -m^2 - \frac{2X_2}{4}$. Further p, given in (5.51), is approximated by $p \approx 2\delta$. The approximation is obtained by setting a^4 equal to 1, z, given in (5.50), equal to $\frac{1}{4}$ and $\frac{\delta(n-2rw)}{nz}$ equal to $\frac{1}{2}$.

$$g^{s,z} = \frac{g^{s,xy}}{4m^2 + 2X_2} \left[2X_2 + 4m^2 \left\{ 1 + \frac{12X_2(1-\delta)^2}{1 - \delta^2 + 4m^2} a^{-3} \right\}^2 \right] \tag{5.78}$$

5.6 The Simplified Extended Gutzwiller Approximation

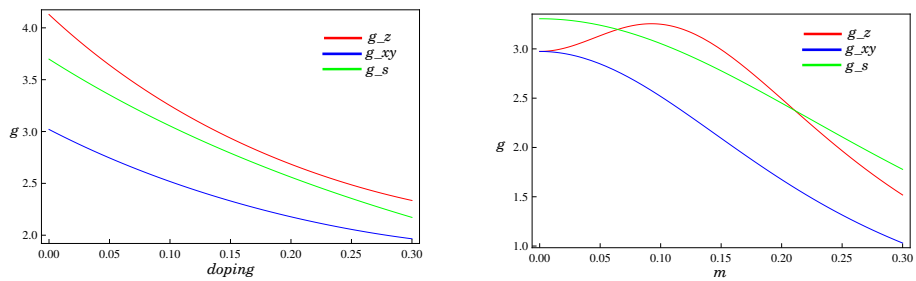

(a) *Typical doping-dependencies of* $g^{s,xy}$ *and* $g^{s,z}$ *for fixed values of,* $\Delta = 0.1$, $\chi = 0.19$ *and* $m = 0.1$. *For comparison the original GF extended to include AF-order* g^s *is also plotted for fixed* $m = 0.1$.

(b) *Typical m-dependencies of* $g^{s,xy}$ *and* $g^{s,z}$ *for fixed values of,* $\Delta = 0.1$, $\chi = 0.19$ *and* $\delta = 0.12$. *For comparison the original GF extended to include AF-order* g^s *is also plotted for fixed* $\delta = 0.12$.

Figure 5.8: Figure (a) and (b) show that the main effect of the extension of the GA is to introduce an anisotropy between $g^{s,xy}$ *and* $g^{s,z}$.

In the section above a set of extended Gutzwiller factors(EGFs) were derived following Ogata and Himeda in ref. [4]:

$$g^{s,xy} = \left(\frac{2(1-\delta)}{1-\delta^2+4m^2}\right)^2 a^{-7} \tag{5.79}$$

$$g^{s,z} = \frac{g^{s,xy}}{4m^2+2X_2}\left[2X_2 + 4m^2\left\{1+\frac{12X_2(1-\delta)^2}{1-\delta^2+4m^2}a^{-3}\right\}^2\right]$$

where

$$a = \left(1+\frac{X}{(n-2rw)^2}\right) \tag{5.80}$$

$$X = 2\delta^2(\Delta^2-\chi^2) + 8m^2(\chi^2+\Delta^2) + 4(\chi^2+\Delta^2)^2 \tag{5.81}$$

$$X_2 = \Delta^2 + \chi^2 \tag{5.82}$$

Ogata and Himeda [4] also derived the EGFs for the hopping operator, the superconducting order-parameter ($\Delta = g^{\Delta}\Delta_0$) and the magnetization ($m = g^m m_0$):

$$g^t = \frac{2\delta(1-\delta)}{1-\delta^2+4m^2}\frac{(1+\delta)^2-4m^2-2X_2}{(1+\delta)^2-4m^2} \tag{5.83}$$

$$g^{\Delta} = \frac{2\delta(1-\delta)}{1-\delta^2+4m^2}\frac{(1+\delta)^2-4m^2-2X_2}{(1+\delta)^2-4m^2}$$

$$g^m = \frac{2(1-\delta)}{1-\delta^2+4m^2}a^{-4}\left(1+\frac{6X_2(1-\delta)^2}{1-\delta^2+4m^2}a^{-3}\right)$$

The EGFs above take into account correlations beyond the combinatorial correlations included in the original GA. However, the EGFs above were derived assuming homogeneity; thus the EGFs remain to be interpreted in the non-homogeneous case. In the work done in this field where the EGFs above have been applied, different means of making the EGFs site-dependent have been used. In ref. [19] and ref. [20] the GFs are made site-dependent by the rewriting:

$$m \longmapsto \frac{1}{2}(m_i + m_j) \qquad \delta \longmapsto \frac{1}{2}(\delta_i + \delta_j) \tag{5.84}$$

$$\Delta \longmapsto \Delta_{ij} \qquad \chi \longmapsto \chi_{ij}; \tag{5.85}$$

and in ref. [18] δ is rewritten as $\delta \longmapsto \sqrt{\delta_i \delta_j}$ and m, Δ, χ are rewritten as above.

The Simplified Extended Gutzwiller Factors

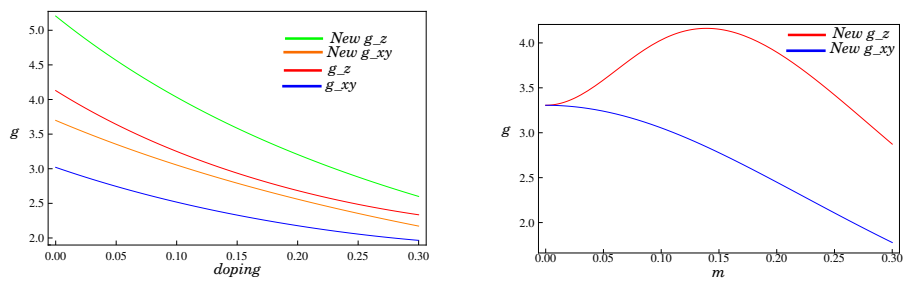

(a) *Typical doping-dependencies of the simplified New $g^{s,xy}$ and New $g^{s,z}$ for fixed values of, $\Delta = 0.1$ $\chi = 0.19$ and $m = 0.1$. For comparison the full EGFs are also plotted.*

(b) *Typical m-dependencies of the simplified New $g^{s,xy}$ and New $g^{s,z}$ for fixed values of $\Delta = 0.1$ $\chi = 0.19$ and $\delta = 0.12$.*

Figure 5.9: (a) shows that setting $a = 1$ overestimates the new simplified EGFs, However as seen from (a) and (b) the simplified EGFs have the correct dependencies on δ and m especially the anisotropy between $g^{s,xy}$ and $g^{s,z}$ is conserved.

In this thesis another rewriting has been used. The main motivation for the EGFs was the ambition to treat magnetism in the superconducting state in a reliable fashion. Thus in the absence of magnetic order it is reasonable to demand that the EGFs reduce to the orginal GFs. The EGFs have to be simplified in order to reduce to the original GF, thus a is set equal to one in $g^{s,xy}$ and $g^{s,z}$; and X_2 is omitted in g^t. To rewrite the simplified EGFs in a site dependent manner inspiration is taken from the original Gutzwiller approximation

$$g^t = \frac{2\delta}{1+\delta} \longmapsto \sqrt{\frac{2\delta_i}{1+\delta_i}}\sqrt{\frac{2\delta_j}{1+\delta_j}} \tag{5.86}$$

$$g^s = \frac{4}{(1+\delta)^2} \longmapsto \sqrt{\frac{4}{(1+\delta_j)^2}}\sqrt{\frac{4}{(1+\delta_j)^2}} \tag{5.87}$$

Thus the simplified EGFs are rewritten in the same manner as $g_{ij} = g_i g_j$ except for $g^{s,z}$ where the separation is not possible. The simplified EGFs depend on the local values of the magnetic and pairing order parameters, and the local kinetic energy and hole density defined as follows:

$$\begin{aligned} m_i &= \langle \Psi_0 | \hat{S}_i^z | \Psi_0 \rangle \\ \Delta_{ij\sigma} &= \sigma \langle \Psi_0 | c_{i\sigma} c_{j\bar{\sigma}} | \Psi_0 \rangle \\ \chi_{ij\sigma} &= \langle \Psi_0 | c_{i\sigma}^\dagger c_{j\sigma} | \Psi_0 \rangle \\ \delta_i &= 1 - \langle \Psi_0 | \hat{n}_i | \Psi_0 \rangle. \end{aligned} \tag{5.88}$$

Using the simplifications and the definitions above the simplified EGFs become

$$\begin{aligned} g_{ij\sigma}^t &= g_{i\sigma}^t g_{j\sigma}^t \\ g_{i\sigma}^t &= \sqrt{\frac{2\delta_i(1-\delta_i)}{1-\delta_i^2+4m^2} \frac{1+\delta_i+\sigma 2m_i}{1+\delta_i-\sigma 2m_i}} \\ g_{ij}^{s,xy} &= g_i^{s,xy} g_j^{s,xy} \\ g_{ij}^{s,xy} &= \frac{2(1-\delta_i)}{1-\delta_i^2+4m^2} \\ g_{ij}^{s,z} &= g_{ij}^{s,xy} \frac{2(\bar{\Delta}_{\langle ij \rangle}^2 + \bar{\chi}_{\langle ij \rangle}^2) - 4m_i m_j \mathbf{X}_{\langle ij \rangle}^2}{2(\bar{\Delta}_{\langle ij \rangle}^2 + \bar{\chi}_{\langle ij \rangle}^2) - 4m_i m_j} \\ \mathbf{X}_{ij} &= 1 + \frac{12(1-\delta_i)(1-\delta_j)(\bar{\Delta}_{ij}^2 + \bar{\chi}_{ij}^2)}{\sqrt{(1-\delta_i^2+4m_i^2)(1-\delta_j^2+4m_j^2)}} \end{aligned} \tag{5.89}$$

where $\bar{\Delta}_{\langle ij \rangle} = \sum_\sigma \frac{\Delta_{\langle ij \rangle \sigma}}{2}$,$\bar{\chi}_{\langle ij \rangle} = \sum_\sigma \frac{\chi_{\langle ij \rangle \sigma}}{2}$. Note that there in the simplified EGFs are allowed for $\Delta_\uparrow \neq \Delta_\downarrow$ and that g^t is naturally extended to hopping between two next-nearest neighbouring sites on the same sublattice by the inclusion of the factor $\frac{1+\delta_i+\sigma 2m_i}{1+\delta_i-\sigma 2m_i}$. The rewriting in eq. (5.89) of the EGFs was first done by Yang et al. in ref. [6].
Setting $a = 1$ overestimates the simplified EGFs as is evident from figure 5.9. The simplified EGFs are overestimated because a is close to, but always above one, and thus $a^{-7} \leq 1$ in eq. (5.80). However, as seen from figure 5.9(a) and 5.9(b) the simplified extended GFs have the correct dependencies on δ and m; especially the anisotropy between $g^{s,xy}$ and $g^{s,z}$ is conserved.

In this chapter a set of EGFs, $g^{s,xy}$ and $g^{s,z}$, was derived. The inclusion of inter-site correlations was seen to introduce anisotropy between $g^{s,xy}$ and $g^{s,z}$ in agreement with VMC calculations. Inspired by the site-dependent orginal GFs the EGFs were simplified and made site-dependent. The simplified EGFs were seen to have the right dependencies on δ and m as the EGFs, however, setting $a = 1$ led to an overall enhancement of the GFs.

Chapter 6

Renormalized Mean Field Hamiltonian

In this section a renormalized mean field Hamiltonian is derived using the simplified extended Gutzwiller approximation on the basis of the the t-J model in eq. (2.48). The first step in the derivation of a renormalized mean field Hamiltonian is to search for a projected state $\mathbf{P}|\Psi_0\rangle$, which minimizes the energy:

$$E_0 = \langle\ \Psi_0|H_{t-J}\mathbf{P}|\Psi_0\rangle \tag{6.1}$$

$$= \langle\ \Psi_0|\mathbf{P}\left(\sum_{ll'\sigma} -t_{ll'}c^{\dagger}_{l\sigma}c_{l'\sigma} + J\sum_{li}\mathbf{S}_l\cdot\mathbf{S}_i + \sum_i V_i\hat{n}_i\right)\mathbf{P}|\Psi_0\rangle. \tag{6.2}$$

The last term in eq. (6.2) comes from the inclusion of an onsite impurity-potential in the t-J model. To remove the Projection operator $\mathbf{P}$ the GA is applied to eq. (6.2):

$$\begin{aligned} E_0 = &-\sum_{(ij)\sigma} g^t_{i,j}\langle\ \Psi_0|\left(c^{\dagger}_{i\sigma}c_{j\sigma} + h.c\right)|\Psi_0\rangle \\ &+\sum_{<ij>} J\left[g^{s,z}_{ij}\langle\ \Psi_0|\hat{S}^{s,z}_i\hat{S}^{s,z}_j|\Psi_0\rangle + g^{s,xy}\langle\ \Psi_0|\left(\frac{\hat{S}^+_i\hat{S}^-_j + \hat{S}^-_i\hat{S}^+_j}{2}\right)|\Psi_0\rangle\right] \\ &+\sum_i V_i\langle\ \Psi_0|\hat{n}_i|\Psi_0\rangle. \end{aligned} \tag{6.3}$$

Per definition the impurity-term is not normalized because $n = n_0$ is assumed. The variational ground state may now be determined by searching for the state $|\Psi_0\rangle$, which minimizes the renormalized t-J Hamiltonian

$$
\begin{aligned}
H_{R\ t-J} = & -\sum_{(ij)\sigma} g^t_{i,j} t_{i,j} \left(c^\dagger_{i\sigma} c_{j\sigma} + h.c \right) \\
& + \sum_{<ij>} J \left[g^{s,z}_{ij} \hat{S}^{s,z}_i \hat{S}^{s,z}_j + g^{s,xy} \left(\frac{\hat{S}^+_i \hat{S}^-_j + \hat{S}^-_i \hat{S}^+_j}{2} \right) \right] \\
& + \sum_i V_i \hat{n}_i .
\end{aligned} \tag{6.4}
$$

The Hamiltonian in eq. (6.4) allows for several molecular fields, see eq. (5.88). However, a direct diagonalization of the mean field Hartree-Fock Hamiltonian obtained from (6.4), would not be sufficient, because the simplified EGFs also depend on the order-parameters. Instead, the energy has to be calculated from the mean field Hartree-Fock Hamiltonian and then minimized with respect to the unprojected wave function $|\psi_0\rangle$ under the two constraints: 1. the total electron density has to remain fixed, and 2. the wave function has to remain normalized:

$$
\sum_i n_i = N_e, \quad \langle \Psi_0 | \Psi_0 \rangle = 1. \tag{6.5}
$$

This is equivalent to minimizing the function:

$$
W = \langle \Psi_0 | H_{Rmf\ t-J} | \Psi_0 \rangle - \lambda(\langle \Psi_0 | \Psi_0 \rangle - 1) - \mu \left(\sum_i \hat{n} - N_e \right). \tag{6.6}
$$

The first step towards getting an expression for W is to write down the mean field Hartree-Fock Hamiltonian obtained from (6.4); for example the decoupling of the $\hat{S}^{s,z}_i \hat{S}^{s,z}_j$ gives:

$$
\begin{aligned}
\hat{S}^{s,z}_i \hat{S}^{s,z}_j \approx & \\
& \frac{1}{4} \Big(4 \left(\hat{S}^{s,z}_i \langle \hat{S}^{s,z}_j \rangle + \hat{S}^{s,z}_j \langle \hat{S}^{s,z}_i \rangle - \langle \hat{S}^{s,z}_i \rangle \langle \hat{S}^{s,z}_j \rangle \right) \\
& - c^\dagger_{j\sigma} c_{i\sigma} \langle c^\dagger_{i\sigma} c_{j\sigma} \rangle - c^\dagger_{i\sigma} c_{j\sigma} \langle c^\dagger_{j\sigma} c_{i\sigma} \rangle + \langle c^\dagger_{j\sigma} c_{i\sigma} \rangle \langle c^\dagger_{i\sigma} c_{j\sigma} \rangle \\
& c^\dagger_{i\bar{\sigma}} c^\dagger_{j\sigma} \langle c_{i\bar{\sigma}} c_{j\sigma} \rangle + c_{i\bar{\sigma}} c_{j\sigma} \langle c^\dagger_{i\bar{\sigma}} c^\dagger_{j\sigma} \rangle - \langle c_{i\bar{\sigma}} c_{j\sigma} \rangle \langle c^\dagger_{i\bar{\sigma}} c^\dagger_{j\sigma} \rangle \Big);
\end{aligned} \tag{6.7}
$$

thus the mean field Hartree-Fock Hamiltonian is given by:

$$
\begin{aligned}
& H_{Rmf\ t-J} = \\
& -\sum_{(ij)\sigma} g^t_{i,j} t_{ij} \left(c^\dagger_{i\sigma} c_{j\sigma} + h.c \right) + \sum_i V_i \hat{n}_i \\
& + \sum_{<ij>\ \sigma} \frac{J g^{s,z}_{ij}}{4} \Big(4 \left(2 \hat{S}^{s,z}_i m_j - m_i m_j \right) - (c^\dagger_{i\sigma} c_{j\sigma} \chi^*_{ij\sigma} + h.c.) - (c_{i\sigma} c_{j\bar{\sigma}} \Delta^*_{ij\sigma} + h.c). + \chi^2_{ij\sigma} + \Delta^2_{ij\sigma} \Big) \\
& + \sum_{<ij>\ \sigma} \frac{J g^{s,xy}_{ij}}{2} \Big(- (c^\dagger_{i\sigma} c_{j\sigma} \chi^*_{ij\bar{\sigma}} + h.c.) - (c_{i\sigma} c_{j\bar{\sigma}} \Delta^*_{ij\bar{\sigma}} + h.c.) + \chi_{ij\sigma} \chi^*_{ij\bar{\sigma}} + \Delta_{ij\sigma} \Delta^*_{ij\bar{\sigma}} \Big)
\end{aligned} \tag{6.8}
$$

Calculating the energy from eq. (6.8) gives:

$$
\begin{aligned}
E &= \langle \Psi_0 | H_{Rmf\ t-J} | \Psi_0 \rangle \\
&= -\sum_{(ij)\sigma} g^t_{i,j} t_{ij} \left(\chi_{ij\sigma} + h.c \right) - \sum_{<ij>} J \left(\frac{g^{s,z}_{ij}}{4} + \frac{g^{s,xy}_{ij}}{2} \frac{\Delta^*_{ij\bar{\sigma}}}{\Delta^*_{ij\sigma}} \right) \Delta^*_{ij\sigma} \Delta_{ij\sigma} \\
&\quad - \sum_{<ij>} J \left(\frac{g^{s,z}_{ij}}{4} + \frac{g^{s,xy}_{ij}}{2} \frac{\chi^*_{ij\bar{\sigma}}}{\chi^*_{ij\sigma}} \right) \chi^*_{ij\sigma} \chi_{ij\sigma} + \sum_{<ij>} g^{s,z}_{ij} J m_i m_j + \sum_i V_i n_i .
\end{aligned}
$$

Minimizing W with respect to $|\Psi_0\rangle$ gives:

$$
\begin{aligned}
0 &= \frac{\delta W}{\delta \langle \Psi_0 |} \\
&= \sum_{(ij)\sigma} \frac{\partial W}{\partial \chi_{<ij>\sigma}} \frac{\delta \chi_{ij\sigma}}{\delta \langle \Psi_0 |} + h.c. + \sum_{ij\sigma} \frac{\partial W}{\partial \Delta_{ij\sigma}} \frac{\delta \Delta_{ij\sigma}}{\delta \langle \Psi_0 |} + h.c. + \sum_{i\sigma} \frac{\partial W}{\partial \hat{n}_{i\sigma}} \frac{\delta \hat{n}_{i\sigma}}{\delta \langle \Psi_0 |} - \lambda |\Psi_0\rangle
\end{aligned}
\tag{6.9}
$$

The variation of the expectation value with respect to $|\Psi_0\rangle$ for an operator $\hat{O}$ with expectation value $O = \langle \Psi_0 | \hat{O} | \Psi_0 \rangle$, is given by:

$$
\frac{\delta \langle \Psi_0 | \hat{O} | \Psi_0 \rangle}{\delta \langle \Psi_0 |} = \hat{O} | \Psi_0 \rangle . \tag{6.10}
$$

Thus a Schrödinger equation $H_{mf} |\Psi_0\rangle = \lambda |\Psi_0\rangle$ is obtained where H_{mf} is given by:

$$
H_{mf} = \sum_{(ij)\sigma} \frac{\partial W}{\partial \chi_{ij\sigma}} \hat{c}^\dagger_{i\sigma} \hat{c}_{j\sigma} + h.c. + \sum_{<ij>\sigma} \frac{\partial W}{\partial \Delta_{ij\sigma}} \sigma \hat{c}_{i\sigma} \hat{c}_{i\bar{\sigma}} + h.c. + \sum_{i\sigma} \frac{\partial W}{\partial \hat{n}_{i\sigma}} \hat{n}_{i\sigma} \tag{6.11}
$$

6.1 Self Consistent Equations

The Hamiltonian in eq. (6.11) is the mean field Hamiltonian this thesis is going to use in the following calculations. The coefficients of H_{mf} are given by.

$$\begin{aligned}
\frac{\partial W}{\partial \chi_{(ij)\sigma}} &= -\delta_{(ij),<ij>} J_{<ij>} \left(\frac{g^z_{<ij>}}{4} + \frac{g^{xy}_{<ij>}}{2} \frac{\chi^*_{<ij>\bar{\sigma}}}{\chi^*_{<ij>\sigma}} \right) \chi^*_{<ij>\sigma} - g_{(ij)\sigma} t_{(ij)} \\
&\quad - \frac{J_{<ij>}}{4} \left(|\Delta_\uparrow|^2 + |\Delta_\downarrow|^2 + |\chi_\uparrow|^2 + |\chi_\downarrow|^2 - 4 m_i m_j \right) \frac{dg^z_{<ij>}}{d\chi_{<ij>\sigma}} \\
\frac{\partial W}{\partial \Delta_{<ij>\sigma}} &= -J_{<ij>} \left(\frac{g^z_{<ij>}}{4} + \frac{g^{xy}_{<ij>}}{2} \frac{\Delta^*_{<ij>\bar{\sigma}}}{\Delta^*_{<ij>\sigma}} \right) \Delta^*_{<ij>\sigma} \\
&\quad - \frac{J_{<ij>}}{4} \left(|\Delta_\uparrow|^2 + |\Delta_\downarrow|^2 + |\chi_\uparrow|^2 + |\chi_\downarrow|^2 - 4 m_i m_j \right) \frac{dg^z_{<ij>}}{d\Delta_{<ij>\sigma}} \\
\frac{\partial W}{\partial n_{i\sigma}} &= -\left(\mu - V_i \right) + \frac{1}{2} \sigma \sum_j g^z_{<ij>} J_{<ij>} m_j \\
&\quad - \frac{J_{<ij>}}{4} \left(|\Delta_\uparrow|^2 + |\Delta_\downarrow|^2 + |\chi_\uparrow|^2 + |\chi_\downarrow|^2 - 4 m_i m_j \right) \frac{dg^z_{<ij>}}{dn_{i\sigma}} \\
&\quad - \frac{J_{<ij>}}{2} \sum_\sigma \left(\left(\chi^*_{<ij>\bar{\sigma}} \chi_{<ij>\sigma} + \Delta^*_{<ij>\bar{\sigma}} \Delta_{<ij>\sigma} \right) \right) \frac{dg^{xy}_i}{dn_{i\sigma}} - \sum_\sigma t_{(ij)} g^t_j \frac{dg^t_i}{dn_{i\sigma}} \left(\chi_{(ij)\sigma} + \chi^*_{(ij)\sigma} \right)
\end{aligned} \tag{6.12}$$

The coefficients of H_{mf} above depend on the mean fields, however, the mean fields depend on the eigenvalues and eigenvectors of H_{mf}. Thus the system have to be solved self-consistently.

6.2 The Bogoliubov-de Gennes Transformation

The Hamiltonian in eq. (6.11) can be written in a matrix form because it is quadratic in creation and annihilation operators. $\hat{H} = \vec{C}^\dagger \bar{H} \vec{C}$, where $\vec{C}$ and $\bar{H}$ are given by:

$$\vec{C} = \begin{pmatrix} c_{1\uparrow} \\ \vdots \\ c_{N\uparrow} \\ c^\dagger_{1\downarrow} \\ \vdots \\ c^\dagger_{N\downarrow} \end{pmatrix}, \quad \bar{H} = \begin{pmatrix} \xi_\uparrow & \mathbf{\Delta} \\ \mathbf{\Delta}^* & -\xi_\downarrow \end{pmatrix} \tag{6.13}$$

where:

$$\xi_\sigma = \frac{\partial W}{\partial \chi_{(ij)\sigma}} + \frac{\partial W}{\partial n_{i\sigma}}, \qquad \mathbf{\Delta}_\sigma = \frac{\partial W}{\partial \Delta_{(ij)\sigma}}. \tag{6.14}$$

$\bar{H}$ can be diagonalized using the spin-generalized Bogoliubov-de Gennes(BdG) transformation. The spin-generalized BdG transformation is defined as:

$$c_{i\uparrow} = \sum_n u_{ni\uparrow}\hat{\gamma}_{n\uparrow} + v^*_{ni\uparrow}\hat{\gamma}^\dagger_{n\downarrow} \tag{6.15}$$

$$c^\dagger_{i\downarrow} = \sum_n u^*_{ni\downarrow}\hat{\gamma}^\dagger_{n\downarrow} + v_{ni\downarrow}\hat{\gamma}_{n\uparrow} \tag{6.16}$$

where $u_{ni\sigma}$ and $v_{ni\sigma}$ are complex numbers; and $\hat{\gamma}^\dagger_{n\sigma}$ and $\hat{\gamma}_{n\sigma}$ are a new set of creation and annihilation oprators. The $u_{ni\sigma}$s and $v_{ni\sigma}$s are determined by the constraint that the Hamiltonian is diagonal in $\hat{\gamma}^\dagger_{n\sigma}$ and $\hat{\gamma}_{n\sigma}$, i.e.:

$$H = E_g + \sum_{n\sigma} \epsilon_n \hat{\gamma}^\dagger_{n\sigma}\hat{\gamma}_{n\sigma} \tag{6.17}$$

where E_g is the ground state energy of the system, and ϵ_n is the positive energy of a non-interacting Fermionic BdG quasi-particle created (annihilated) by $\hat{\gamma}^\dagger_{n\sigma}$ ($\hat{\gamma}_{n\sigma}$). The non-interacting Fermionic BdG quasi-particles describe excitations above the system's ground state. The $u_{ni\sigma}$s and $v_{ni\sigma}$s are found by solving the matrix equation:

$$\begin{pmatrix} \xi_\uparrow & \mathbf{\Delta} \\ \mathbf{\Delta}^* & -\xi_\downarrow \end{pmatrix} \begin{pmatrix} u_n \\ v_n \end{pmatrix} = \epsilon_n \begin{pmatrix} u_n \\ v_n \end{pmatrix} \tag{6.18}$$

where for positive ϵ_n, $(u_n, v_n)^T$ corresponds to $(u_{n\uparrow}, v_{n\downarrow})^T$ and for negative ϵ_n, $(u_n, v_n)^T$ corresponds to $(v^*_{n\uparrow}, u^*_{n\downarrow})^T$. The matrix equation above is derived by computing the commutation relations $[H, c_{i\uparrow}]$ and $[H, c_{i\downarrow}]$ by two different methods. First by plugging in, and then by the use of the BdG transformation. Demanding that the same commutator gives the same result independent of method, leeds to eq. (6.18). For a detailed derivation see J. W. Harter ref. [21].

The Mean Fields In Terms of u and v

In terms of u and v the local values of the magnetic and pairing order parameters, and the local kinetic energy and hole density, are expressed as follows:

$$
\begin{aligned}
m &= \frac{1}{2}(n_{i\uparrow} - n_{i\downarrow}) \\
n_{i\sigma} &= \langle c^{\dagger}_{i\sigma} c_{i\sigma} \rangle = \sum_n \Big(|u_{n\sigma}|^2 \langle \hat{\gamma}^{\dagger}_{n\sigma} \hat{\gamma}_{n\sigma} \rangle + |v_{n\sigma}|^2 \langle \hat{\gamma}_{n\bar{\sigma}} \hat{\gamma}^{\dagger}_{n\bar{\sigma}} \rangle \Big) \\
&= \sum_n \big(|u_{n\sigma}|^2 f(\epsilon_{n\sigma}, T) + |v_{n\sigma}|^2 (1 - f(\epsilon_{n\bar{\sigma}}, T)) \big) \,, \qquad (6.19) \\
\Delta_{\sigma} &= \frac{\sigma}{2} \langle c_{i\sigma} c_{(ij)\bar{\sigma}} \rangle \qquad (6.20) \\
&= \sum_n u_{ni\sigma} v^*_{nj\bar{\sigma}} \hat{\gamma}_{n\sigma} \hat{\gamma}^{\dagger}_{n\sigma} + v^*_{ni\sigma} u_{ni\bar{\sigma}} \hat{\gamma}^{\dagger}_{n\bar{\sigma}} \hat{\gamma}_{n\bar{\sigma}} = \sum_n u_{ni\sigma} v^*_{ni\bar{\sigma}} (1 - f(\epsilon_{n\sigma}, T)) + v^*_{ni\sigma} u_{ni\bar{\sigma}} f(\epsilon_{n\bar{\sigma}}, T) \\
\chi_{ij\sigma} &= \langle c^{\dagger}_{i\sigma} c_{j\sigma} \rangle = \sum_n \Big(u_{ni\sigma} u^*_{nj\sigma} \langle \hat{\gamma}^{\dagger}_{n\sigma} \hat{\gamma}_{n\sigma} \rangle + v_{ni\sigma} v_{nj\sigma} \langle \hat{\gamma}_{n\bar{\sigma}} \hat{\gamma}^{\dagger}_{n\bar{\sigma}} \rangle \Big) \\
&= \sum_n \big(u_{ni\sigma} u^*_{nj\sigma} f(\epsilon_{n\sigma}, T) + v_{ni\sigma} v_{nj\sigma} (1 - f(\epsilon_{n\bar{\sigma}}, T)) \big) \qquad (6.21) \\
& \qquad (6.22)
\end{aligned}
$$

where $f(\epsilon_{n\sigma}, T)$ is the fermi distribution function for the non-interacting Bdg particles; and T is the temperature.

6.3 Density of states and STM

Besides the mean field parameters, the local density of states (LDOS) will also be calculated. The LDOS is defined as [22]:

$$LDOS(\omega, i) = \sum_{\sigma} -\frac{1}{\pi} \int_{\infty}^{\infty} Im \left[G^r_{i\sigma,i\sigma}(t,t') e^{i\omega(t-t')} \right]. \tag{6.23}$$

Using the BdG transformation, and the fact that the BdG quasi-particles are non-interacting, so their time evolution is given by $\gamma_n(t) = \gamma_n e^{-i\epsilon_n t}$, gives the following expression for LDOS:

$$LDOS(\omega, i) = \sum_{n\sigma} |u_{ni\sigma}|^2 \delta(\omega - \epsilon_n) + |v_{ni\sigma}|^2 \delta(\omega + \epsilon_n) \tag{6.24}$$

The LDOS is interesting to calculate because it is directly proportional to the differential conductance measured at site i by STM

$$\frac{dI}{dV}(\omega, i) \propto LDOS(\omega, i). \tag{6.25}$$

The total density of states is given as:

$$DOS(\omega) = \sum_{i} LDOS(\omega, i). \tag{6.26}$$

STM

In locally resolved electron-spectroscopy the tunneling current $I(V)$ is recorded, while the bias voltage is swept with the STM tip held in a fixed vertical position above the sample. If a positive bias voltage is applied, electrons tunnel from the tip into unoccupied sample states and in similar fashion if a negative bias voltage is applied, electrons tunnel from a filled sample state into the tip. To obtain the differential conduction the I-V curve is differentiated numerically[23]. The current is proportional to:

$$I_s \propto \int d\omega \left[f(\omega - eV) - f(\omega) \right] LDOS_{tip}(\omega - eV) LDOS_{sample}(\omega, i). \tag{6.27}$$

Assuming a structureless tip ($LDOS_{tip}(\omega - eV) = constant$) gives a differential conductance proportional to:

$$\sigma(i, V) \propto \int d\omega \left[-f'(\omega - eV) \right] LDOS_{sample}(\omega, i) \tag{6.28}$$

where f' is the derivative of the Fermi function. Thus STM measures the thermally smeared LDOS of the sample[23].

6.4 The c-Program

Most of the calculations in this thesis are done for systems containing 24*24 sites; for each system this calls for the diagonalization of a matrix of dimension 2*24*24=1152, furthermore the system must be solved self-consistently. Obviously this can not be done by hand; and therefore a program was written in c to do the job. This section gives a short description of the c-program.

The 1. step in the program is to ascribe values to the nearest neighbour hopping integral t, next nearest neighbour hopping integral t' and the exchange interaction J. t is set equal to 1, t' is set equal to -0.2 and J is set equal to 0.3.

The 2. step is to give an initial guess for Δ, χ, $n_\uparrow$, $n_\downarrow$ and μ.

The 3. step is to compute the elements of the matrix in eq. (6.18) using eq. (6.12).

the 4. step is to write the matrix in eq. (6.18) as:

$$
\begin{aligned}
&\text{if i=j:}\\
\bar{H}_{MF}[i][j] &= \frac{\partial W}{\partial n_{i,\uparrow}}\\
\bar{H}_{MF}[i+N^2][j+N^2] &= -\frac{\partial W}{\partial n_{i,\downarrow}}\\
&\text{if i and j nearest neighbors:}\\
\bar{H}_{MF}[i][j] &= \frac{\partial W}{\partial \chi_{<ij>,\uparrow}} + \left(\frac{\partial W}{\partial \chi_{<ji>,\uparrow}}\right)^*\\
\bar{H}_{MF}[i+N^2][j+N^2] &= -\frac{\partial W}{\partial \chi_{<ij>,\downarrow}} - \left(\frac{\partial W}{\partial \chi_{<ji>,\downarrow}}\right)^*\\
\bar{H}_{MF}[i+N^2][j] &= -\frac{\partial W}{\partial \Delta_{<ij>,\downarrow}} - \frac{\partial W}{\partial \Delta_{<ji>,\uparrow}}\\
\bar{H}_{MF}[i][j+N^2] &= -\left(\frac{\partial W}{\partial \Delta_{<ij>,\downarrow}} + \frac{\partial W}{\partial \Delta_{<ji>,\uparrow}}\right)^*\\
&\text{if i and j are next nearest neighbours:}\\
\bar{H}_{MF}[i][j] &= \frac{\partial W}{\partial \chi_{<ij>,\uparrow}} + \left(\frac{\partial W}{\partial \chi_{<ji>,\uparrow}}\right)^*\\
\bar{H}_{MF}[i+N^2][j+N^2] &= -\frac{\partial W}{\partial \chi_{<ij>,\downarrow}} - \left(\frac{\partial W}{\partial \chi_{<ji>,\downarrow}}\right)^*\\
&\text{else:}\\
\bar{H}_{MF}[i][j] &= 0\\
\bar{H}_{MF}[i+N^2][j+N^2] &= 0.
\end{aligned}
\tag{6.29}
$$

In the matrix above periodic boundary conditions are assumed.

The 5. step is to diagonalize the matrix above to obtain (u_n, v_n) as eigenvectors and ϵ_n as corresponding eigenvalues.

The 6. step is to compute Δ, χ, $n_\uparrow$ and $n_\downarrow$ using eq. (6.22)

The 7. step is to compare the output from step 6. $X_{new}(i)$ with the input from step 2. $X_{input}(i)$. If the difference between $X_{new}(i)$ and $X_{input}(i)$ is less than 10^{-5} fol all sites i, i.e if.

$$|X_{new}(i) - X_{input}(i)| < 10^{-5} \text{ for all sites } i \tag{6.30}$$

the system is said to be converged.

The 8. step only apply if the system is not converged. The 8. step is to give new input. The new input, $X_{New-input}(i)$ is given as below:

$$X_{New-input}(i) = (1-a)X_{input}(i) + aX_{new}(i) \tag{6.31}$$

The method to give new input above in eq. (6.31) is called simple mixing and a is called the mixing parameter[1]. In order to achieve convergense the value of the mixing parameter must not exceed 0.1. The reason for this limitation of the mixing parameter is the term $\frac{dg^t_{(ij)}}{dn_{i\sigma}}$ in eq. (6.12). The role of $\frac{dg^t_{(ij)}}{dn_{i\sigma}}$ is to work against disorder, see figure 6.1. However, for a mixing parameter above 0.1 $\frac{dg^t_{(ij)}}{dn_{i\sigma}}$is doing the job too well, making the electron density oscillate as a forced pendula.

The 9. step is to update the chemical potential by: $\mu_{new} = \mu_{old} + 0.5(1 - \delta - n_{average})$, where $n_{average}$ is the average electron density calculated in step 6. and δ is the doping level which is to be considered.

The steps above are repeated until the condition in eq. (6.30) is fulfilled.

The final step is to print out Δ, χ n and m; and calculate the DOS and the LDOS for selected sites.

Calculation of DOS and LDOS

The LDOS and DOS are calculated using eq. (6.23) and eq. (6.26) respectively. However, the number of discrete eigenvalues are only $2N^2$ for a system of size

[1]Another more advanced method called the generalized second Broyden method [24] was tried. It takes into account some of the past iterations to give a better $X_{New-input}(i)$. However the generalized second Broyden method was found to slow the convergence speed down.

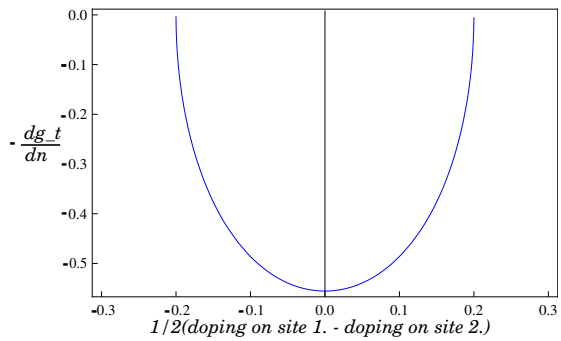

Figure 6.1: Plot of $\frac{dg^t}{dn}(0.5(\delta_1 - \delta_2))$ *for two neighbouring sites. The average doping is held fixed:* $0.5(\delta_1 + \delta_2) = 0.2$. *From the plot it is evident that the role of* $\frac{dg^t}{dn}$ *is to work against disorder.*

N*N. This means that for a system of limited size, e.g. 24*24, the finite size effects are substantial. To achieve a smooth LDOS two modifications are made. The first modification is to replace the delta functions in (6.23) with the function:

$$-\frac{1}{\pi} im \left[\frac{1}{\epsilon_n - \omega + i\eta} \right] \tag{6.32}$$

where η is the broadening factor.
The second modification is to use the method of "super cells". In the method of "super cells" the original (N*N) system is first solved self-consistently, and is afterwards replicated to give a system of (M*M) replicas of the original system. The periodic boundary condition for the original system is replaced with a periodic boundary condition for the (M*M) system. The periodic boundary condition for the (M*M) system means that an electron moving from the left side of the (M*M) system all the way to the right, comes back to the same side. This means that going from one of the (N*N) systems to the next, the electron picks up a phase of $\exp(ik_x r_x)$, where $k_x = \frac{2\pi}{NM}$, and where r_x is equal to N or $-N$, where the sign depends on whether the electron is moving forward or backward. So moving all the way from the left to right the electron picks up a phase of $\exp(ik_x r_x)^M = \exp(i2\pi) = 1$. The same is the case for the y-direction.
To summarize instead of solving a system of size $(M * M * N * N)$, it is only necessary to solve $(M * M)$ almost identical systems of sizes (N*N). The (N*N) systems only differ by the different block wave boundary conditions:

$$\bar{H}_{MF}[i][j] * e^{ik \cdot r} \tag{6.33}$$

where k runs over the first brilliant zone: $(-\frac{\pi}{M} < k_x < \frac{\pi}{M}), (-\frac{\pi}{M} < k_y < \frac{\pi}{M})$.
The method of "super cells" saves a lot of memory space and cpu-time. However, new information about the system is not gained, it only serves to smoothen the

LDOS.

In the next chapter the results from self-consistent calculations, using the c-program described above, will be presented.

Chapter 7

Results

This chapter presents results obtained by the use of the program described in the former chapter.

7.1 V Shaped LDOS

As mentioned in the introduction impurities are inevitably introduced into the HTCSs materials when they are doped. However, unlike s-wave superconductors where Andersons theorem insures insensitivity to small potential scattering, d-wave superconductivity has zero superconducting gap in the nodal direction; and furthermore, even weak impurities can be poorly screened by the electrons around them because the cuprates are quasi-two-dimensional metals. However, experiments indicate that despite the two former arguments the cuprates are robust against disorder [26]. One indication of the robustness against disorder, is the clear V shape of the local density of states (LDOS) at low energy measured by STM on underdoped and nearly optimal doped $Bi_2Sr_2CaCu_2O_{8+\delta}$, see figure 7.1

7.1.1 Reproduction of Garg

The clear V shape of the LDOS has been treated in the framework of strong correlations by A. Garg et al. [27], Fukushima et al. [26], and B. M. Andersen and H. J. Hirschfeld [30]. Below a reproduction of the results of A. Garg et al. [27] is presented.
The model used in this sub-section and the model used in the rest of the thesis differ in three ways: 1. the density-density term is retained in the t-J model, 2. the GFs used are the simple original GFs, and 3. the energy is not minimized as

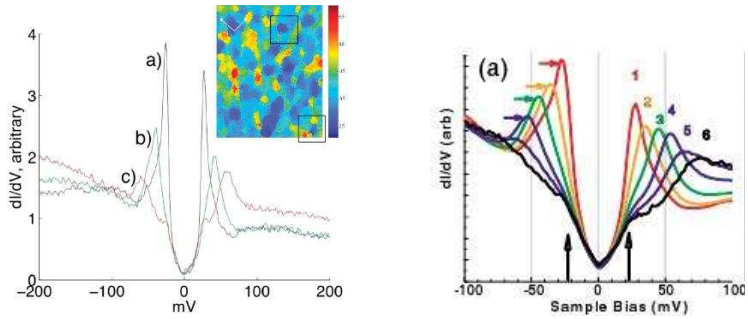

(a) *STM studies on nearly optimally doped* $Bi_2Sr_2CaCu_2O_{8+\delta}$. *Spectra in a (a) small-, (b) average-, and (c) large-gap region Adapted from ref. [28]*

(b) *STM studies on underdoped* $Bi_2Sr_2CaCu_2O_{8+\delta}$, *Each curve is obtained by averaging the spectra in the region that exhibit a given local gap value. Adapted from ref. [29]*

Figure 7.1:

opposed to eq. (6.9). This leads to the model also used by A. Garg et al. [27]:

$$H = \sum_{(li)\sigma} -g^t_{li} t_{li} c^\dagger_{l\sigma} c_{l'\sigma} + \sum_{<li>\sigma} \left[J \frac{3g^s_{li}+1}{4} (c^\dagger_{l\uparrow} c^\dagger_{i\downarrow} - c^\dagger_{l\downarrow} c^\dagger_{i\uparrow}) \Delta^*_{li} + H.C. \right] + \sum_{<li>\sigma} \left[J \frac{3g_s - 1}{4} c^\dagger_{l\sigma} c_{i_\sigma} \chi_{il\bar{\sigma}} + H.C. \right] + \sum_l (V(l) - \mu)\, n_l \tag{7.1}$$

where $g^t_{li} = \sqrt{\frac{2\delta(l)}{1+\delta(l)}}\sqrt{\frac{2\delta(i)}{1+\delta(i)}}$ and $g^s_{li} = \frac{4}{(1+\delta(l))(1+\delta(i))}$.
To see the effect of the strong correlations a comparison is made between the full model in (7.1) and a pure d-wave superconductor, i.e. the same model but with $g^t_{li} = g^s_{li} = 1$. To make a meaningful comparison all the parameters are chosen to be the same except for J which is chosen to give the same gap in the absence of disorder. The spatially averaged DOS is then calculated for different concentrations of weak (V=1t) impurities using eq. (6.26). The results and the choice of parameters are seen in figure 7.2.
For a clean system both the case with and without correlations shows a clear V shape behaviour in the low energy DOS ($DOS(\omega) \approx |\omega|$). However, as the impurity concentration increases the case with correlations maintain the V shape while the case without correlations does not, see figure 7.2.

However, as mentioned above, the model in eq. (7.1) ignores that the GFs themselves depend on the electron density and it is therefore not an adequate model for describing the strong correlations. Furthermore it was shown by Fukushima et al. [26], that the result obtained above, which is in agreement with the results by A. Garg et al. [27], only maintains the V shape as a result of averaging over

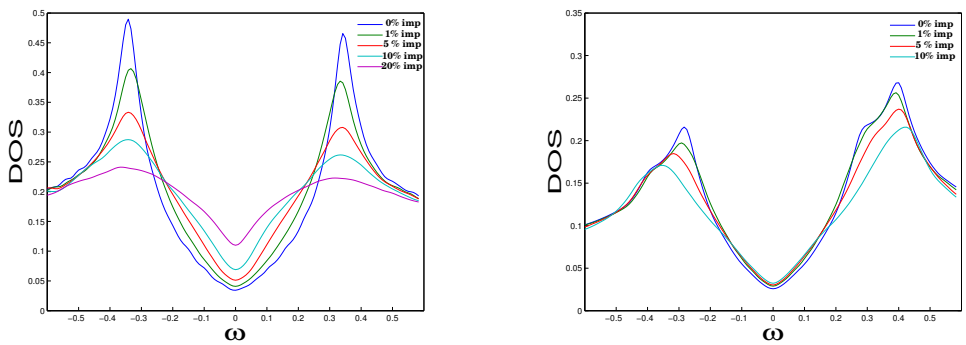

(a) *No correlations: Spartially averaged DOS for different impuritie concentrations (0%-20%) impurities. The calculation is done on 10*10 super-cells of 20*20 arrays, and averaged over 10 impurity configurations. And* $\eta = 0.025$ *is used to get smooth curves.*$(t = 1, t' = -0.25, j = 1.1)$

(b) *With correlations: Spatially averaged DOS for different impuritie concentrations(0%-10%) impurities. The calculation is done on 10*10 super-cells of 20*20 arrays, and averaged over 10 impurity configurations. And* $\eta = 0.025$ *is used to get smooth curves.*$(t = 1, t' = -0.25, J = 0.33)$

Figure 7.2: figure (a) and figure (b) are a reproduction of the main result in A. Garg et al. [27] and are in full agreement with ref. [27]

asymmetric LDOS and therefore do not reflect a V shaped LDOS.

Therefore, for the rest of this thesis the model used by A. Garg et al. [27] is abandoned and instead the model in eq. (6.11) is used. The model in eq (6.11) is an improvement compared eq. (7.1) because it includes a "local chemical potential" μ_i by:

$$\begin{aligned}\mu_i = & - \frac{J_{<ij>}}{4}\left(|\Delta_\uparrow|^2 + |\Delta_\downarrow|^2 + |\chi_\uparrow|^2 + |\chi_\downarrow|^2 - 4m_i m_j\right)\frac{dg^z_{<ij>}}{dn_{i\sigma}} \\ & - \frac{J_{<ij>}}{2}\sum_\sigma\left(\left(\chi^*_{<ij>\bar{\sigma}}\chi_{<ij>\sigma} + \Delta^*_{<ij>\bar{\sigma}}\Delta_{<ij>\sigma}\right)\right)\frac{dg^{xy}_i}{dn_{i\sigma}} \\ & - \sum_\sigma t_{(ij)} g^t_j \frac{dg^t_i}{dn_{i\sigma}}\left(\chi_{(ij)\sigma} + \chi^*_{(ij)\sigma}\right) \qquad (7.2)\end{aligned}$$

The μ_i originates from the minimizing of the energy in eq. (6.9), and as will be evident later it plays a central role in the "renormalization" of the impurity potential. The model in eq. (6.11) is also an improvement compared to the model used by Fukushima et al. [26] because it allows for magnetic order, which is known to play a large role in the underdoped and to some extent also in the optimally doped compounds.

7.1.2 V shaped LDOS in the Improved Model

This section presents an improvement of results obtained in the former section. The DOS(ω) was calculated for a system with an impurity concentration of 20% weak ($V = 1t$) impurities using the model in eq. (6.11), the result can be seen in figure 7.3(a). Figure 7.3(a) shows a clear V shape. Figure 7.3(b) shows the LDOS on the impurity site (site(13,13)) and the nearby sites for a system containing a single impurity. From figure 7.3(b) it is evident that also the LDOS shows a clear V shape as opposed to A. Garg et al. [27], according to [26].

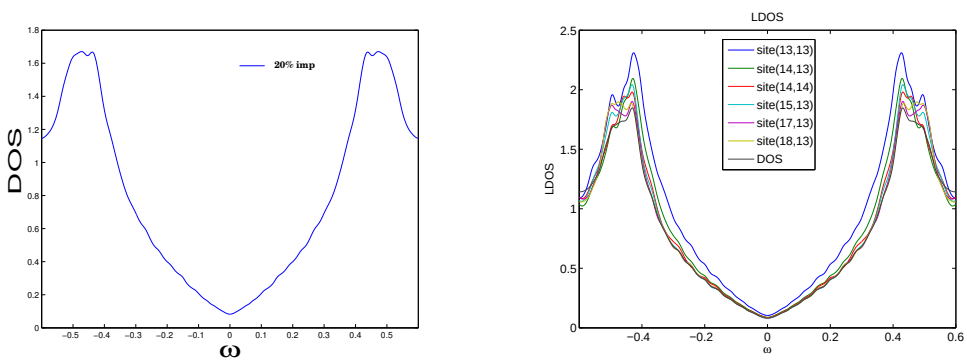

(a) (b)

*Figure 7.3: (a) The DOS for a system containing 20% weak ($V_i = 1t$) impurities. (b) The LDOS for a system containing a single weak (V=1t) impurity at site (13,13).(δ = 20%, t=1, t'=-0.2, J=0.3 and system size=24 × 24). The calculations were done for 10*10 super-cells and an $\eta = 0.016$ was used to get smooth curves.*

To understand why the DOS and LDOS are insensitive to the impurity potential the sum $\mu_i + V_i$ is shown in figure 7.4(b). From figure 7.4(b) it can be seen how the μ_i works against the impurity potential. The size of the impurity potentials are $V_i = 1t$, however, the difference between $max(\mu_i + V_i)$ and $min(\mu_i + V_i)$ is only $0.5t$; thus the effective potential, felt on a impurity site, is only half the original impurity potential. Furthermore the potential is smeared out making the local environment more homogeneous. This can also be seen from the electron density in figure 7.4(a), where the electron density next to an impurity site also is slightly suppressed.

Figure 7.5 shows a comparison between the gap Δ_0 obtained in this thesis, see figure 7.5(a), for a impurity concentration of 20%; and the gap published by A. Garg et al. [27],see figure 7.5(b), for a impurity concentration of only 1%. Figure 7.5(a) shows a gap which does not vary more than 30% between the maximum and minimum, while the gap in figure 7.5(b) almost disappears at

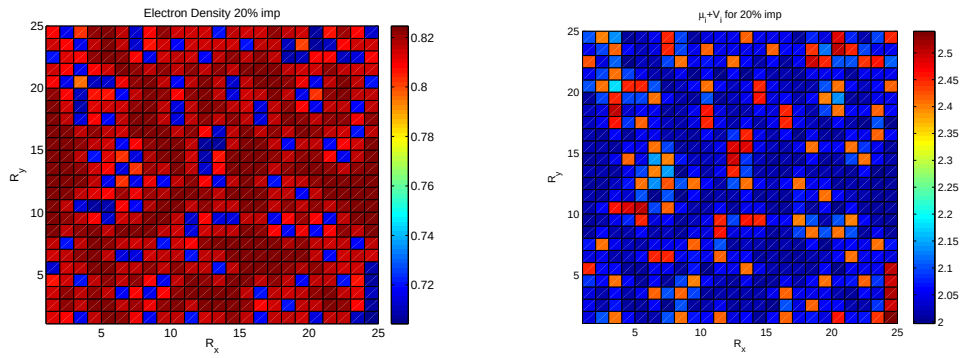

(a) (b)

Figure 7.4: (a) The electron density and (b) the sum of the local chemical potential μ_i and the impurity potential V_i, for a system containing 20% weak impurities (V=1t). ($\delta = 20\%$, t=1, t'=-0.2 and J=0.3)

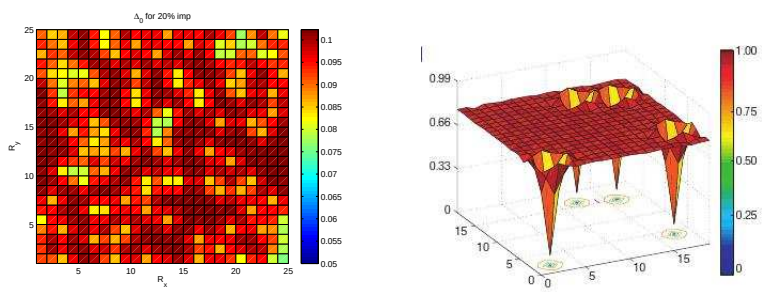

(a) (b)

Figure 7.5: (a) Δ_0 for a system containing 20% weak impurities (V=1t) and for $\delta = 20\%$, t=1, t'=-0.2 and J=0.3. (b) The Δ_0 obtained by A. Garg et al. [27] for for a system containing 1% weak impurities (V=1t) and for ($\delta = 20\%, t = 1, t' = -0.25, J = 0.33$)

the impurity sites. If the picture is adopted that the impurities stem from the dopants, then this picture implies that an overdoped compound would have an impurity concentration of around 20%; and according to the figure 7.5(b) this would lead to a disappearing gap in 20% of the sites; this is in disagreement with experimental observations [29][28].

To summarize, the strong correlations, treated in the GA, affect the impurity potential in two ways:

1. the suppression of the electron density at the impurity site i enhances the effective hopping integral $t_{eff} = g^t_{ij} t$; this can be seen as a healing of the damage done by the impurity by the following logic: the impurity lowers the possibility for an electron to hop on to site i, thus the impurity could have been modelled as a lowering of t_{ij} and it is this lowering of t_{ij} which is healed by g^t.

2. The electron density redistributes to minimize the energy because the Gutzwiller factors themselves depend on the electron density. The redistribution of the electron density is enforced by the local chemical potential. The local chemical potential tends to work against the impurity potential.

7.2 Impurity Induced Magnetism

This section presents results of impurity induced-magnetism. The undoped mother compound of all cuprates exhibits AF order, which has led to speculations of an intimate relation between superconductivity and magnetism. Neutron scattering experiments have shown evidence of coexistence of superconducting and magnetic order in LSCO [32][33]; as opposed to $Y_{1-\delta}CaBa_2Cu_3O_{6+\delta}$ (YBCO) where the spin-glass phase is believed to be minimal compared to LSCO [31]. One of the differences between LSCO and YBCO is the way the dopants enter the material. In LSCO the strontium dopants distribute randomly giving rise to a weak out-of-plane impurity potential; while in YBCO the O dopants order in the CuO chains located further away from the CuO_2 planes, making YBCO the cleanest of the cuprate HTSCs. This difference between LSCO and YBCO makes it plausible that it is the impurities which are responsible for the incommensurate ordering wave vector evident by a quartet of peaks surrounding (π, π) revealed in the NS experiments on LSCO.

Impurity induced magnetism have been studied by the Hubbard model treated in an unrestricted Hartree-Fock approximation [31]. However, a mean field treatment of the Hubbard model does not capture the band narrowing due to the strong correlations near half filling. Therefore in a simple mean field treatment of the Hubbard model, the Hubbard U has to be adjusted by hand when different doping levels are considered. The onset of magnetic order depends heavily on the choice of U. To move beyond the phenomenological treatment offered by the mean field treatment of the Hubbard model and to eliminate the freedom in the choice of U, this section presents results of impurity-induced magnetism studied by the t-J model using the site dependent simplified extended GA. i.e. the model given in eq. (6.11).

7.2.1 Weak Impurities (V=1t)

Figure 7.6 shows the local magnetization m_0[1] for a system with $\delta = 14\%$ and a impurity concentration of 14% weak (V=1t) point impurities. If the system experience AF-order the fourier transformed magnetization will show a single peak in (π, π), however, as seen in figure 7.6 the fourier transformed magnetization shows a ring surrounding (π, π), and six peacks. Two in the diagonal right next to (π, π) and a quartet on the ring. The deviation from what is to be expected for AF or-

[1] m_0 is the local magnetization in the pre-projected space; to get the physical magnetization a GA is applied $m = g^m m_0$. However, it is not clear what is the correct choice of g^m in the case of the site dependent simplified extended GA. However, m and m_0 have the same sign. For simplicity $g^m = 1$ is assumed.

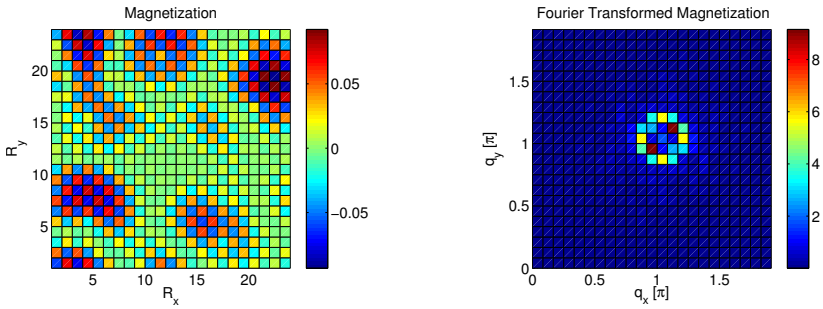

Figure 7.6: The magnetization in real and reciprocal space for a system containing 14% weak impurities (V=1t). ($\delta = 14\%$, t=1, t'=-0.2 and J=0.3)

der indicates the existence of some non-trivial magnetic order. Calculations were made for three other impurity configurations all showing a non-trivial magnetic order. A calculation was also done for a clean system and here no magnetization was found. To give any conclusive offer on the magnetic order a larger number of different impurity configurations are needed and preferably also a larger system size.

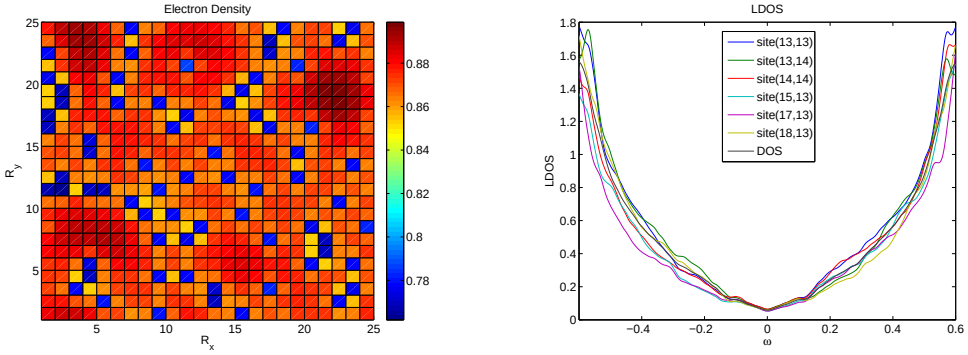

(a) (b)

*Figure 7.7: (a) The electron density for a system containing 14% weak impurities (V=1t). The impurities are situated at the blue sites. (b) The LDOS for some of the sites, for the same system as (a).($\delta = 14\%$, t=1, t'=-0.2, J=0.3 and system size=24×24). The calculations was done for 10*10 super-cells and an $\eta = 0.016$ was used to get smooth curves.*

Figure 7.7(a) shows the electron density where the impurities are located at the blue sites. The same impurity configuration is used for the figures 7.7(a), 7.7(b) and 7.6. From figure 7.7(a) is it evident that the electron density clusters together away from the impurity sites. A comparison between figure 7.7(a)and figure 7.6

shows the remarkable fact that the impurity induces magnetism away from the impurity sites. The impurity induced magnetism away from the impurity sites is in contrast to what was found by B. M. Andersen el al. [31]. The course of the magnetism is the redistribution of the electron density caused by the impurities. The electron density locally exceeds the threshold for which magnetic order is energetic favorable in the bulk system, because the electron density clusters together away from the impurities.
Figure 7.7(b) shows the DOS and for some of the sites the LDOS. Figure 7.7(b) shows how the low energy DOS and LDOS show a clear V shape. However, the higher energy LDOS seems to be more affected by the impurities.

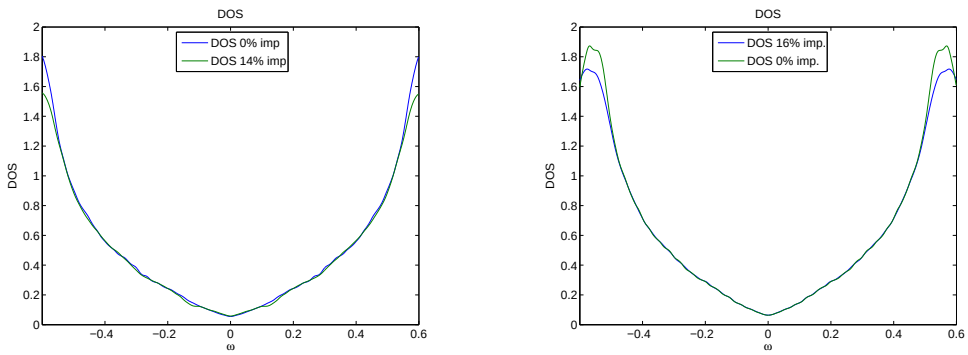

(a) (b)

*Figure 7.8: (a) The DOS for a clean system (0%imp.) and the DOS for a system with 14% impurities both at the doping level $\delta = 14\%$. (b) The DOS for a clean system (0%imp.) and the DOS for a system with 16% impurities both at the doping level $\delta = 16\%$. For both (a) and (b): t=1, t'=-0.2, J=0.3 and system size $= 24 \times 24$. The calculations was done for 10*10 super-cells and an $\eta = 0.016$ was used to get smooth curves.*

Figure 7.7(b) exhibits a small shoulder around $\omega = \pm 0.1t$. Figure 7.8(a) show the DOS averaged over three different impurity configurations compared with the DOS for a clean system. The small shoulder are also visible in the DOS for the disorder system but are missing in the clean system. For comparison the DOS for a system with doping level $\delta = 16\%$ and a impurity concentration of 16% is shown in figure 7.8(b) together with the DOS of the clean system. There are no shoulder in 7.8(b). The DOS in figure 7.8(b) experiences more disorder, however, as evident from figure 7.9(b) the disorder does not lead to a magnetic order. Thus the shoulder in figure 7.7(b) and figure 7.8(a) originates from the magnetic order[35] seen in figure 7.6.

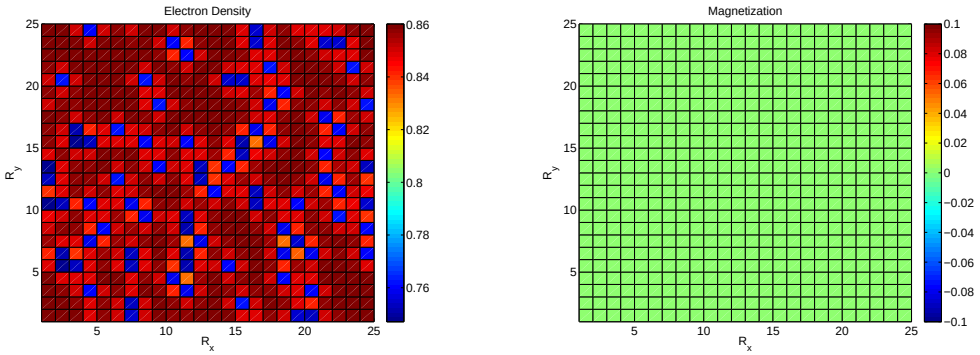

(a) aa (b) bb

Figure 7.9: (a) The electron density and (b) The magnetization for a system containing 16% weak impurities (V=1t). ($\delta = 16\%$, t=1, t'=-0.2 and J=0.3)

7.2.2 Strong Impurities (V=100t)

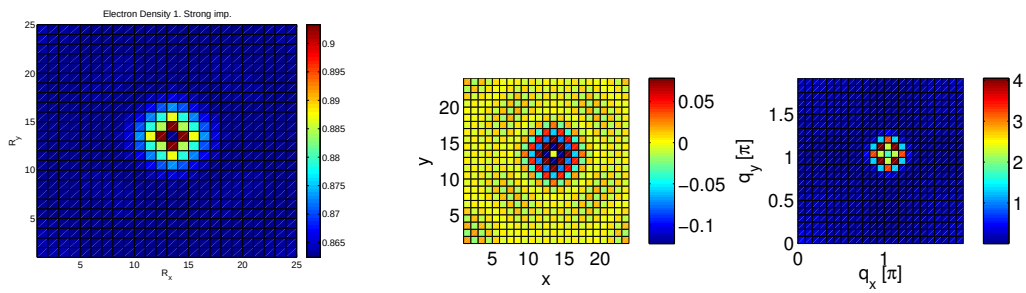

(a) aa (b) bb

Figure 7.10: (a) The electron density for a system containing a single strong impurity (V=100t) at site (13,13). The electron density is equal to zero at the impurity site. (b) The magnetization in real and reciprocal space. ($\delta = 13.7$, t=1, t'=-0.2 and J=0.3)

This section discusses the magnetization induced by strong impurities (V=100t). As mentioned in the structure section a strong impurity is typically an in-plane impurity as for instance when a Zn ion substitutes a Cu ion in the $Cu-O$ plane. The energy cost for occupying the Zn site is large, because Zn has a full outer shell.

The main difference between the strong and the weak impurity case is that one strong impurity can induce magnetism, while impurity induced magnetism in the weak impurity case is a pure many-impurity phenomenon. Figure 7.10(b) shows the magnetization induced by a single strong impurity for an average doping level of $\delta = 13.7\%$. It is evident from figure 7.10(a) that the electron density rises on the sites next to the impurity.

Figure 7.11 shows the electron density for a system containing 2% strong impurities (V=100t). The inclusion of more than one impurity reduces the doping threshold for impurity induced magnetism, because, the electrons removed from the impurity sites lowers the doping level on the rest of the sites, and furthermore two impurities close to each other can interfere constructively making a local environment where the electron density is above the threshold for magnetic order.
Figure 7.12 shows the magnetism induced by the 2% strong impurities. Similar to it was the case for the magnetization induced by weak impurities, the fourier transformed magnetization exhibits a deviation from the single peak in (π, π) expected from pure AF-order. However one impurity configuration is not enough to give any conclusive offer on the magnetic order in real systems.

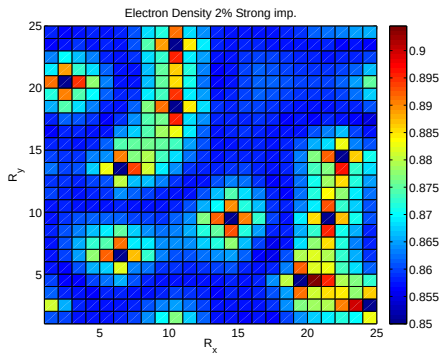

Figure 7.11: The electron density for a system containing 2% strong impurities (V=100t). The electron density is equal to zero at the impurity sites (the deep blue sites). ($\delta = 13.7$, t=1, t'=-0.2 and J=0.3)

Figure 7.13 shows the electron density and the magnetization for a system containing 3% strong impurities and has an average doping level of $\delta = 20\%$. As seen from figure 7.13(b) the strong impurities can not induce magnetic order at this doping level, except for a single site where two impurities makes a single magnetic droplet.

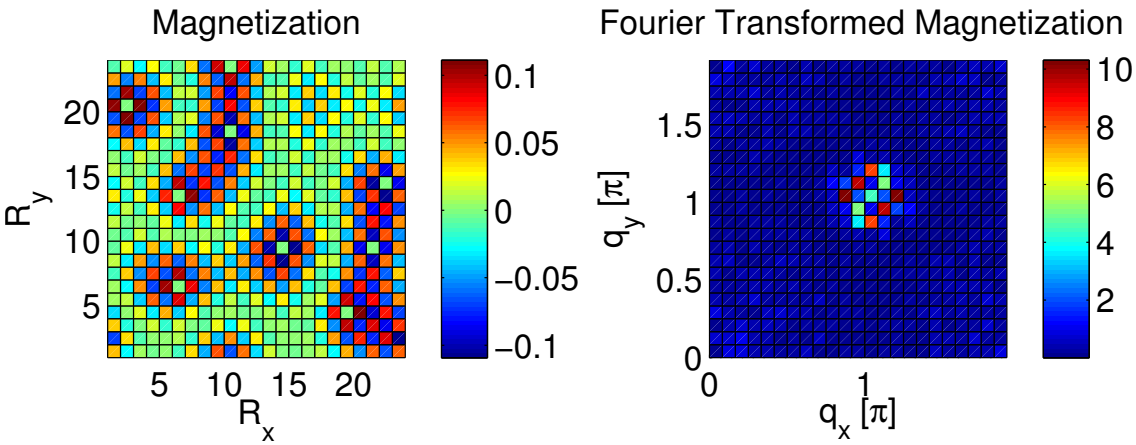

Figure 7.12: The magnetization in real and reciprocal space for a system containing 2% strong impurities (V=100t). ($\delta = 15\%$, t=1, t'=-0.2 and J=0.3)

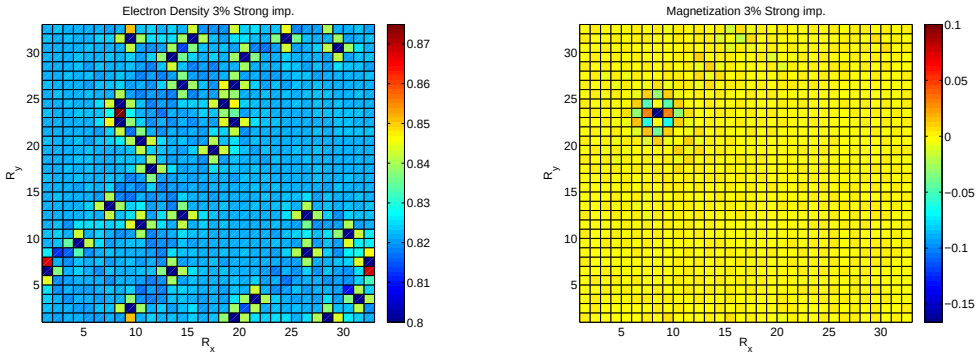

(a) (b)

Figure 7.13: (a) The electron density and (b) The magnetization for a system containing 3% strong impurities (V=100t). The electron density is equal to zero at the impurity sites (the deep blue sites). ($\delta = 20\%$, t=1, t'=-0.2 and J=0.3)

7.3 One Impurity For Different Scattering Strengths

In this section results for a single impurity are presented. The strength of the impurity potential is varied to get a better understanding of the difference between a "strong" and a "weak" impurity. The average doping level is fixed to ($\delta = 13.5$), by adjusting the chemical potential μ. The clean system does not exhibi any magnetic order for ($\delta = 13.5$); however, a single strong impurity is able to induce magnetism. Eight different values for the strength of the impurity potential are used: $V = 1t$, $V = 2t$, $V = 4t$, $V = 7t$, $V = 8t$, $V = 9t$, $V = 10t$ and $V = 50t$.

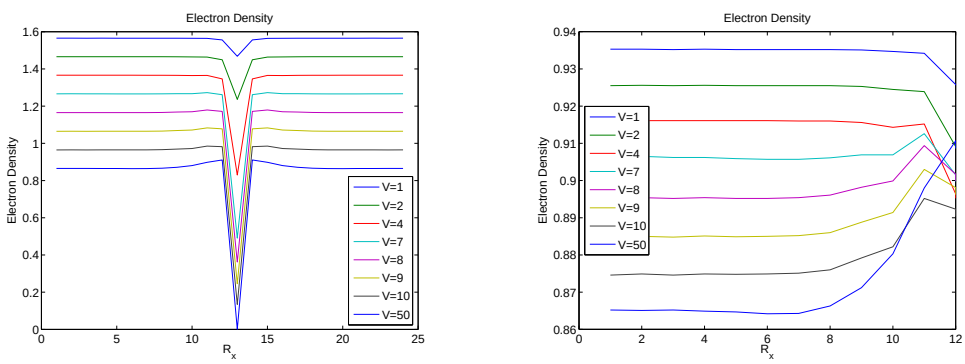

(a) (b)

Figure 7.14: (a) The electron density in the R_x direction for a system containing a single impurity. The impurity is situated at site=13. Each curve represents different impurity potentials V. The different curves are shifted upward by 0.1 with respect to each other for clarity. ($\delta = 13.5$, t=1, t'=-0.2 and J=0.3). (b) The same as (a) but cut off right before the impurity site.

Figure 7.14(a) shows the electron density in the R_x direction for a system containing a single impurity. The impurity is situated at site=13. Figure 7.14(a) illustrates how the electron density is gradually suppressed at the impurity site as the impurity potential is increased. However, as evident from figure 7.14(b) the electron density at the neighboring sites varies from being suppressed to being increased depending on the impurity strength. A system with a weak impurity prefers to suppress the electron density on the neighboring sites while a system containing a strong impurity prefers to increase the electron density on the neighbouring sites.

Figure 7.15 shows the local chemical potential μ_i for different impurity potentials. It is clear from figure 7.15(a) that μ_i works against the impurity potential on the impurity site, the larger V the smaller μ_i. However, the renormalization of the impurity potential by μ_i has the largest impact on weak impurity poten-

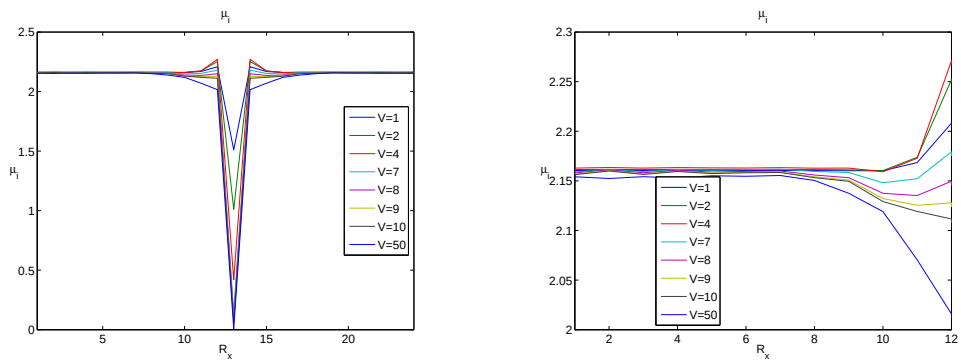

(a) (b)

Figure 7.15: (a) The local chemical potential μ_i in the R_x direction for a system containing a single impurity. Each curve represents different impurity potentials V. The impurity is situated at site=13. ($\delta = 13.5$, t=1, t'=-0.2 and J=0.3). (b) The the same as (a) but cut off right before the impurity site.

tials because μ_i take values in the range $[0, 2.2]$. Figure 7.15(b) illustrates how μ_i varies for the neighbouring sites depending on the impurity potential. For weak impurities μ_i spreads out the impurity potential, while for large impurity potentials μ_i attracts electrons to the neighbouring sites.

Figure 7.16 reveals how a single impurity for a large enough impurity potential can induce magnetization. The amplitude of the magnetization depends on the strength on the impurity. The amplitude at the edge seems not correlated with the impurity strength, probably do to finite size effects and the periodic boundary conditions of the system.

Figure 7.17 shows the LDOS on the impurity site and the nearest neighbouring site. The LDOS maintains the V shape on the impurity site and the nearest neighbouring site for $V \leq 4$, however, for $V \geq 7$ the V shape is destroyed.

To summarise, for all values of V, the electron density is suppressed on the impurity sites; however, for $V \geq 7$ the electron density has a maximum on the nearest neighbouring or next nearest neighbouring sites. For $V \geq 7$ the impurity induces magnetic order while for $V \leq 4$ the magnetic order is absent. For $V \geq 7$ the V shaped LDOS is destroyed on the nearest and the next nearest neighbouring site to the impurity site while for $V \leq 4$ the V shape is maintained. Thus there are two different regimes of impurity strengths. A strong regime for $V \geq 7$ where it is energetic favourable for the electron density to pile up around the impurity and where magnetic order is induced around the impurity and the V shaped LDOS is destroyed; and a weak regime for $V \leq 4$ where the electron density is pushed away from the impurity and the V shaped LDOS is maintained.

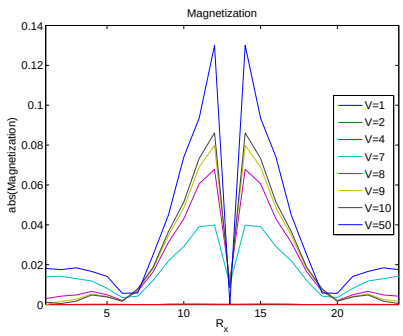

Figure 7.16: The amplitude of the magnetization $|m_i|$ in the R_x direction for a system containing a single impurity. Each curve represents different impurity potentials V. The impurity is situated at site=13. ($\delta = 13.5$, t=1, t'=-0.2 and J=0.3).

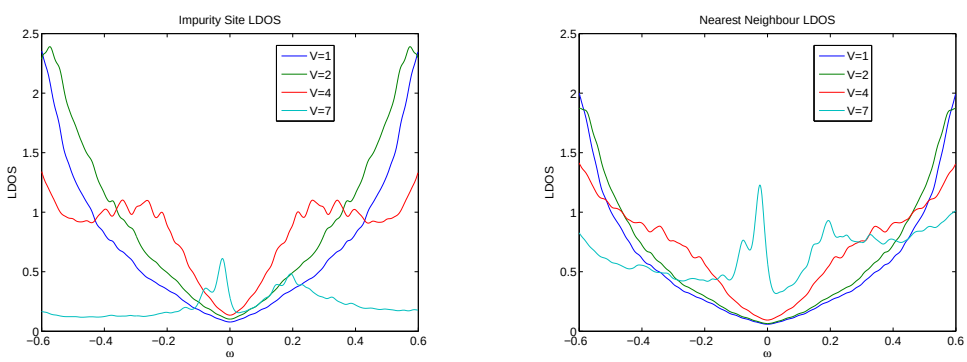

(a) (b)

*Figure 7.17: (a) The LDOS on the impurity site. (b) The LDOS on the nearest neighbour site to the impurity site. Each curve represents different impurity potentials V For both (a) and (b). ($\delta = 13.5\%$, t=1, t'=-0.2, J=0.3 and system size=24×24). The calculations were done for 10*10 super-cells and an $\eta = 0.016$ was used to get smooth curves.*

Chapter 8

Conclusion

In this thesis the effects of impurities in HTSCs has been discussed. They have been treated by the t-J model using an extended Gutzwiller approximation. First, the V shaped LDOS in the over doped compound was considered, here the inclusion of the local chemical potential μ_i was shown to be crucial in order to avoid that the gap vanish at the impurity sites and to maintain the V shape of the LDOS.

The study in the overdoped case was extended to the optimal/under-doped case; where the low energy LDOS also maintained the V shape despite the inclusion of weak impurities. Furthermore, the impurities were found to induce magnetic order. The magnetic order was shown to originate from the redistribution of the electron density. The redistribution of the electron density is enforced by μ_i. μ_i redistribute the electron density in order to minimize the total energy of the system as a consequence of the fact that the effective hopping integral ($t_{eff} = g^t_{ij} t$) and the effective exchange interaction ($J_{eff} = g^s_{ij} J$) depend on the electron density themselves.

The magnetism induced by weak impurities is a many-impurity phenomenon, because a single weak impurity cannot induce magnetism. The magnetism induced by weak impurities appears away from the impurity sites, in contrast to earlier findings [30]. The induced magnetic order results in a small shoulder in the LDOS. In contrast to the weak impurity case a single strong impurity is able to induce magnetism in an underdoped compound and furthermore the magnetism is induced around the impurity site. Both the magnetism induced by weak and strong impurities shows signs of non-trivial magnetic order, however, to give any conclusive offer on the magnetic order calculations for larger number of impurity configurations are needed, and preferably also a larger system sizes.

The case of a single impurity was considered for different scattering strengths at a doping level ($\delta = 13.5\%$), not far before bulk long-range order enters. It was found that there are two different regimes of impurity strengths. A strong regime for $V \geq 7t$ where it is energetic favourable for the electron density to pile up around the impurity and where magnetic order is induced around the impurity

and the V shaped LDOS is destroyed; and a weak regime for $V \leq 4t$ where the electron density is pushed away from the impurity and the V shaped LDOS is maintained.

In conclusion the treatment of impurity induced states in high temperature superconductors studied in the RVB picture using an extended Gutzwiller approximation is able to explain why the V shape of the low energy LDOS is insensitive to disorder, and how impurities can induce magnetic order. Furthermore the system exhibits the right doping dependence because the Gutzwiller factors are taking the band narrowing due to the strong correlations near half filling into account. For weak impurities the strong correlations lead to the remarkable result that the magnetic order is induced away from the impurity sites.

Acknowledgment

First and foremost, I would like to thank Brian M. Andersen for excellent guidance, enlightening discussions and inspiration throughout the last year. I would also like to thank all the people in the Nano Theory group for a pleasant working environment. Last but not least my thanks also befalls Uni Beck for kind help and proof reading.

Bibliography

[1] T. Ogawa, K. Kanda and T. Masubara: Prog. Theor- Phys. **53** (1975) 614.

[2] J.G. Bednorz and K.A. Müller, Z. Phys. **64** 189 (1986)

[3] Wing-Ho Ko, Cody P. Nave, and Patrick A. Lee, Phys. Rev. B **76**, 245113 (2007)

[4] Ogata M and Himeda A 2003 J. Phys. Soc. Japan 72 374-91

[5] Masao Ogata and Hidetoshi Fukuyama, Rep. Prog. Phys. **71** (2008) 036501

[6] Kai-Yu Yang, Wei Qiang Chen, T M Rice, M Sigrist and Fu-Chun Zhang New Journal of Physics 11 (2009) 055053

[7] F. C. Zhang, C. Gros, T. M. Rice, and H. Shiba, Supercond. Sci. Technol. **1**, 36 (1988)

[8] A. Himeda and M. Ogata: Phys. Rev. B **60** (1999) R9935

[9] B. Edegger, V. N. Muthukumar and C. Gros, Andvances in Physics, Vol. 56, No 6, November-December 2007, 927-1033

[10] B. Edegger, N. Fukushima, C. Gros, And V. N. Muthukumar, Phys. Rev. B **72**, 134504, (2005)

[11] The picture to the left is taken from http://www.physics.ubc.ca/ bercium/RESEARSH/ and the picture to the right is the same picture modified in inkscape

[12] P. W. Anderson Science **235**, 1196 (1987)

[13] F.C. Zhang and T.M. Rice, Phys. Rev. B **37**, 3759 (1988)

[14] Yokoyama H and Ogata M 1996 J. Phys. Soc. Japan **65** 3615

[15] Paramekanti A, Randeria M and Trivedi N 2001 Phys. Rev. Lett. **87** 217002

[16] Paramekanti A, Randeria M and Trivedi N 2001 Phys. Rev. B **70** 054504

[17] C. Gros, Phys. Rev. B **38** 931 (1988).

[18] Hiroki Tsuchiura, Yukio Tanaka, Masao Ogata, and Satoshi Kashiwaya Phys. Rev. B **64**, 140501(R) (2001)

[19] Hiroki Tsuchiura, Masao Ogata, Yukio Tanaka, and Satoshi Kashiwaya Phys. Rev. B **68**, 012509 (2003)

[20] H. Tsuchiura And M. Ogata Journal of Physics: Conference Series **150** (2009) 052272

[21] John W. Harter, Thesis: Numerical modeling of impurity-induced magnetic behavior in cuprate superconducters, April 2006

[22] A. V. Balatsky, I. Vekhter and Jian-Xin Zhu, Rev. Mod. Phys. **78** April-June 2006

[23] Øystein Fischer, Martin Kugler, Ivan Maggio and Christophe Berthod, Rev. Mod. Phys. **79** January-March 2007

[24] V. Eyert, Journal of computational physics **124**, 271-285 (1996)

[25] Brian Møller Andersen, Ph.D. thesis, Ørsted Laboratory, Niels Bohr Institute, University of Copenhagen 2004

[26] Noboru Fukushima, Chung-Pin Chou, and Ting Kuo Lee: Phys. Rev. B **79**, 184510 (2009)

[27] Arti Garg, Mohit Randeria and Nandini Trivedi: Nature physics **4**, 762 (2008)

[28] A. C Fang, L. Capriotti, D. J. Scalapino, S. A. Kivelson, N. Kaneko, M. Greven and A. Kapitulnik: Phys. Rev. Lett. **96**, 017007 (2006)

[29] K. McElroy, D.-H Lee, J. E. Hoffman, K. M. Lang, J. Lee, E. W. Hudson, H. Eisaki, S. Uchida, and J. C. Davis Phys. Rev. Lett. **94**, 197005 (2005)

[30] B. M. Andersen and H. J. Hirschfeld: Phys. Rev. Lett. **100**, 257003 (2008)

[31] B. M. Andersen and H. J. Hirschfeld: Phys. Rev. Lett. **99**, 147002 (2007)

[32] B. Lake et al., Nature (London) **415**, 299 (2001)

[33] S. Wakimoto et al., Phys. Rev. B **63**, 172501 (2001)

[34] P. W. Anderson, P. A. Lee, M Randeria, T M Rice, N Trivedi and F. C. Zhang J. Phys.: Condens Matter **16** (2004) R755-R769

[35] B. M. Andersen and H. J. Hirschfeld: Phys. Rev. B **79**, 144515 (2009)